Abstract

LUCIER, GREGORY W. Evaluation of MMFX Steel for Concrete Bridge Decks. (Under the direction of Dr. Sami Rizkalla.)

Commercially available Micro-Composite, Multi-Structural, Formable (MMFX) steel reinforcing bars are a proprietary product claiming to provide both high tensile strength and excellent corrosion-resistance when compared to conventional Grade 60 steel. Use of MMFX steel reinforcement could potentially lead to significant cost savings due to these unique characteristics. Recently, many state transportation departments, including the North Carolina Department of Transportation (NCDOT), have begun to use MMFX steel as a direct replacement for conventional steel in reinforced concrete bridge decks. However, the behavior of bridge decks reinforced with MMFX steel bars was previously undocumented. In light of this fact, a research program was commissioned by the NCDOT in which three concrete bridge decks, each having a span-to-depth ratio of 12.5, were constructed and tested to failure under simulated truck wheel loads. Two of the decks were constructed with identical reinforcement ratios, one utilizing conventional Grade 60 steel and the other MMFX steel. The third bridge deck was also reinforced with MMFX steel, but was reinforced with 33 percent less steel in an attempt to utilize the higher tensile strength offered by MMFX.

The results of the experimental program demonstrate that taking advantage of lowered reinforcement ratios by utilizing the higher strength of MMFX steel is a definite possibility in reinforced concrete bridge decks. The bridge deck reinforced with 33 percent less MMFX steel developed the same load-carrying capacity as the deck reinforced with conventional Grade 60 steel. In addition, the same deck showed the same deflections at service load as the deck reinforced with Grade 60 steel.

Evaluation of MMFX Steel for Concrete Bridge Decks

by

GREGORY W. LUCIER

A thesis submitted to the graduate faculty of

North Carolina State University

in partial fulfillment of the

requirements for the degree of

Master of Science

CIVIL ENGINEERING

Raleigh, NC

May, 2006

Approved By:

Dr. Sami Rizkalla (Chair) 

Dr. Emmett Sumner 

Dr. Paul Zia 

Biography

Gregory Lucier began his study of engineering in August, 2000 as an undergraduate student in the Construction Engineering and Management program at North Carolina State University. During his undergraduate program, he gained valuable onsite experience by spending several summers as an intern with a commercial construction company. Gregory graduated summa cum laude in May of 2004, and subsequently enrolled in the graduate program at NC State to pursue a Master of Science degree in Civil Engineering with a concentration in structures. He has been involved in several research projects focused primarily on shear and torsion in reinforced concrete. He especially enjoys structural testing, and hopes to continue working on large-scale projects.

Acknowledgements

I would like to take this opportunity to acknowledge the North Carolina Department of Transportation for their generous support in sponsoring this research. In addition, I would like to thank MMFX Technologies Corporation for supplying the MMFX steel, SteelFab of Charlotte, NC for donating the structural steel sections used in the testing frames, and C.C. Mangum, Inc. of Raleigh, NC for their assistance in casting the three bridge decks.

Next, I would like to extend my sincere gratitude to the members of my committee, Dr. Emmett Sumner, Dr. Paul Zia, and Dr. Sami Rizkalla, for their guidance and wisdom throughout the course of my studies at NC State. Special thanks are due to my advisor, Dr. Rizkalla, for his generous, continuous, and steadfast support.

I am greatly indebted to the entire staff at the Constructed Facilities Laboratory – Jerry Atkinson, Bill Dunleavy, Lee Nelson, and Amy Yoni, for their help with all aspects of this project. Their assistance was invaluable in dealing with the details of laboratory testing, and with the intricacies of the administrative requirements. In addition, special thanks are due to fellow graduate student Mina Dawood for his advice and encouragement over the course of my time at the Constructed Facilities Laboratory.

I would also like to thank my family for their support, guidance, and encouragement throughout my life and my studies.

Finally, I would like to extend a heartfelt thank you to my good friend and partner on this project, Hatem Seliem. Hatem's extensive engineering knowledge and advanced analytical skills were a tremendous asset to this research. His hard work and dedication did not go unnoticed, and I was very fortunate to have learned such a great deal from working with him. It was truly a joy to work with someone having such compassion, commitment, and professional skill.

Table of Contents

List of Tables

List of Figures

Chapter 3

Chapter 4

Appendix A

Appendix B

Appendix C

1. Introduction

1.1. Background

Corrosion of steel reinforcement is undoubtedly one of the leading causes of deterioration in concrete bridges. A well-publicized study recently conducted by the American Society of Civil Engineers estimates that nearly 30% of the nation's bridges are structurally deficient or obsolete, requiring repair or replacement (ASCE, 2005). Corrosion-related problems are responsible for a huge number of these structural deficiencies.

Concrete bridge decks are a prime example of bridge components typically subjected to severe environmental conditions during service. Factors such as the presence of moisture, numerous freeze-thaw cycles, thin or deteriorated concrete cover, and cracking all facilitate the corrosion of reinforcing steel embedded in concrete decks. In many instances, chlorides leaching into the deck only exacerbate the corrosion problem. Chloride exposure may come from natural sources such as seawater, or may be applied to the deck in the form of de-icing compounds that are used in many regions (Emmons, 1993).

There are two main problems with having corroded steel reinforcement in concrete, the first of which is that corrosion reduces the effective cross-sectional area of a steel bar, thereby reducing its strength. The second problem with corroded reinforcing bars is that they occupy a larger volume of space in the corroded state than they did originally. This expansion causes internal pressures to develop in the concrete, and often leads to cracking, spalling, and deterioration. Cracking provides

a conduit for moisture, oxygen, and chlorides to more easily reach the embedded steel, and the rate of corrosion only tends to increase. Ultimately, corrosion problems can lead to failure of the structure (Emmons, 1993).

Over the last few decades, various technologies have been developed in an attempt to mitigate this expensive corrosion problem. Such technologies include cathodic protection systems, chemical corrosion inhibitors, high-performance concretes, epoxy-coated bars, non-metallic reinforcement, and corrosion-resistant steels. While these technologies represent significant advances in preventing corrosion of concrete reinforcement, there are certainly drawbacks to many of these systems, and the corrosion problem is by no means solved. As an example, consider that the use of fiber reinforced polymer (FRP) bars is limited due to the lack of information on the long term performance of those materials under field conditions, and the use of epoxy-coated bars has been restricted by several states and by some countries due to unsatisfactory behavior. Many of the other technologies are too expensive for common usage, or are difficult to implement.

The recent development of a high strength, highly corrosion-resistant steel, commercially known as Micro-composite Multi-Structural Formable (MMFX) steel, is a promising option for reducing corrosion of steel bars embedded in concrete. According to the manufacturer (MMFX Technologies Corporation), this new steel offers corrosion resistance approaching that provided by stainless steel, but at a fraction of the cost. In addition, MMFX steel claims to offer a high tensile strength while providing superior mechanical properties and enhanced ductility over other high-strength steels. High corrosion resistance is provided without the use of the

coating technologies, and is achieved through proprietary alteration of the steel composition and microstructure. Use of MMFX steel in place of traditional Grade 60 steel has the potential to lead to significant cost savings if reinforcement ratios can be reduced, and service lives increased, by taking advantage of the higher strength and increased corrosion resistance.

Recently, many state transportation departments have begun to use MMFX steel as a direct replacement for conventional Grade 60 steel in concrete bridge decks. MMFX steel has been used as reinforcement in new bridge deck projects by the Iowa DOT, the Kentucky DOT, and the Pennsylvania DOT. Also, it has been used as shear reinforcement in bridge girders by the Oklahoma DOT. Most pertinent to this research program, however, is a bridge constructed in 2004 by the NCDOT in Johnston County, NC. The concrete bridge deck on this project was reinforced exclusively with MMFX steel bars which were substituted directly for conventional Grade 60 reinforcement.

Despite these field applications, however, the behavior of reinforced concrete flexural members, and especially the behavior of deck slabs, which are constructed using MMFX steel as main longitudinal reinforcement is not well documented. Given this fact, the North Carolina Department of Transportation commissioned this research program to evaluate the usage of MMFX steel reinforcement in cast-in-place concrete bridge decks.

1.2. Objectives

The objectives of the research program are two-fold. First, it is desired to examine the performance and evaluate the effectiveness of using MMFX steel reinforcing bars as the main flexural reinforcement for concrete bridge decks. Second, the research aims to develop an approach to take advantage of the higher strength offered by MMFX steel, so as to provide a safer and more economical design for reinforced concrete bridge decks in North Carolina.

1.3. Scope

In order to meet the objectives outlined above, the following tasks were pursued:

1. A comprehensive state-of-the-art literature review was conducted on MMFX steel reinforcement. The review includes all published reports and articles on completed research pertinent to the use of MMFX steel in concrete decks.

2. The fundamental mechanical properties of MMFX steel bars reported in literature were evaluated, and were verified with material testing.

3. Design requirements for the use of MMFX steel bars as reinforcement for concrete bridge decks were evaluated.

4. An experimental testing program was developed in which three full-scale reinforced concrete bridge decks were built and tested in the laboratory.

5. The behaviors of the three test specimens were observed and evaluated including the behaviors prior to cracking, post-cracking, at yielding, and at ultimate. The modes of failure in each case were examined.

6. Analytical modeling was conducted to develop an in-depth understanding of the behavior of concrete bridge decks reinforced with MMFX steel bars. The behavior of decks reinforced with Grade 60 steel was modeled for comparison purposes. The analytical modeling was not conducted by this author and is not covered in this thesis.

7. The experimental results were compared to predictions calculated using three common design codes. The ability of the code equations to predict bridge deck strength was investigated for decks reinforced with MMFX steel.

8. The effects of bending on the tensile strength of MMFX steel bars were evaluated. Four small test specimens were developed to test bent stirrups that would typically be used as transverse reinforcement. This portion of the research is not covered in this thesis.

9. The rate of corrosion of MMFX steel bars in comparison to conventional Grade 60 steel was examined. This portion of the research project is still ongoing, and will not be discussed in this thesis.

10. The results from this research were synthesized into recommendations for the NCDOT. In order to transfer the results to the Department, various technical papers discussing the results of the research were submitted to several journals and conferences for publication. In addition, a seminar is scheduled with NCDOT personnel to review and discuss the results of the project.

2. Literature Review

2.1. Introduction

This chapter provides a general review of the behavior of concrete bridge decks, and examines the punching shear capacity of bridge deck slabs. Review of the current code provisions for predicting shear capacity of concrete slabs is also included. In addition, background is given related to corrosion of steel and to the problem of corrosion in embedded steel reinforcement. The documented mechanical properties of Micro-composite Multi-Structural Formable (MMFX) steel are also presented. It should be noted that 'concrete bridge decks', 'concrete deck slabs', 'concrete decks', and 'concrete slabs' will be used interchangeably throughout this section, since all of this different terminology appears throughout the relevant literature.

2.2. Corrosion in Highway Bridges

As was mentioned in the introduction, the problem of corrosion in embedded steel reinforcement is immense. Reinforced concrete bridge components are especially vulnerable to corrosion problems since they are typically subjected to very harsh environmental conditions. It has been reported that 27.1% of the nearly 600,000 bridges in the United States are structurally deficient or obsolete, and need to be repaired or replaced (ASCE, 2005). A huge percentage of these deficiencies can be attributed to corrosion problems, as is documented by a Federal Highway

Administration report which estimates the annual direct cost of corroded highway bridges in the United States at $8.3 billion (FHA, 2001).

2.3. Corrosion and MMFX Steel

Corrosion is an electrochemical process in which electrons travel from an anode to a cathode through an electrode. In a reinforced concrete structure, the concrete matrix makes an excellent electrode when it is moist. The embedded steel serves as both the anode and the cathode since electrical potential can develop between ferrite (the anode) and iron-carbide (the cathode). As the reaction progresses, micro-galvanic cells are created, leading to an increase in volume, and to the formation of ferrous oxide $Fe(OH)_x$, or rust. In a well-designed structure constructed with quality concrete, the corrosion process will proceed very slowly (Emmons, 1993).

There are two major causes of accelerated steel corrosion in concrete, namely carbonation of the concrete and chloride-attack. There is also the potential for rapid corrosion when dissimilar metals are placed in close proximity within a concrete structure. In a typical situation, embedded steel is protected from corrosive attack by a thin, passive film that forms on the steel surface. This layer develops as a result of the high alkalinity of the concrete pore water, which typically has a pH value around 12.5. If this passive layer remains undisturbed, corrosion will not occur (Hunkler, 2005).

Carbonation of concrete is a process in which the calcium hydroxide dissolved in the concrete reacts with carbon dioxide in the air to reduce the pH of the concrete

over time. This lowered pH level allows the passive layer covering the reinforcing steel to deteriorate, and the corrosion reaction will dramatically accelerate. The carbonation reaction requires wet-dry cycles and high levels of available carbon dioxide (Emmons, 1993). Bridge decks are obviously subjected to wet-dry cycles, and can be subjected to elevated carbon dioxide levels due to motor-vehicle exhaust.

While carbonation can potentially pose a problem for any structure subjected to wet-dry cycles, chloride-attack is the most significant corrosion-inducing process for structures exposed to a chloride source. Sources are frequently external to the concrete, such as de-icing salts or a marine climate. In addition, chlorides can come from within the concrete itself if salt-contaminated aggregates, chloride-containing chemical admixtures, or salty mixing water are used.

Over time, available chlorides will penetrate the layer of concrete covering the reinforcing steel. The rate of this penetration depends on a variety of factors including the amount and concentration of available chloride ions, the depth of the concrete layer, the permeability and condition of the concrete, and the amount of moisture present. When chloride ions reach the passive protective layer, this layer is destroyed, and corrosion of the steel reinforcement will develop at a rapid rate if moisture and oxygen are present (Emmons, 1993).

The advantage that MMFX steel has over traditional black steel with respect to corrosion-resistance is that MMFX steel is virtually carbide free (less than 1% carbon content), and has a high chromium content (8-10% chromium). This lack of carbide inhibits the formation of microgalvanic cells, and accounts for the superior corrosion-

resistance of MMFX steel. In addition, chromium is an element which aids in the formation of the passive layer. Typically, higher chromium contents indicate higher corrosion resistance (MMFX, 2002).

Field observations along with results from non-standard, short-term accelerated chloride threshold tests support the claim that MMFX steel offers dramatically improved corrosion resistance over conventional steel. However, it is cautioned that results from a short-term corrosion study cannot necessarily be extended to long-term behavior. There is a lack of long-term experimental data verifying the long-term corrosion–resistance of MMFX steel (CIAS, 2003). A long-term corrosion study is currently in progress as part of the overall research program for the NCDOT. Results from this corrosion study are not yet available.

2.4. Mechanical Properties of MMFX Steel

The mechanical properties of MMFX steel relevant to structural engineering are well documented. The engineering stress-strain curve of MMFX steel starts out as linear with a modulus of elasticity of 29,000 ksi (200 GPa), matching that of traditional black steel. The curve becomes nonlinear at a proportional limit of roughly 90 ksi (620 MPa), and does not have a well-defined yield plateau. Ultimate tensile stress of MMFX bars has been reported in the range of 165 to 175 ksi (1140 – 1200 MPa), which is more than double the ultimate stress typically achieved from testing traditional grade 60 reinforcing bars. Ultimate strains for MMFX steel have been reported in the range of at least 0.05, so the material still displays significant ductile capacity. If the ASTM 0.2% offset method is used to determine an equivalent

yield point, it can be determined that MMFX steel will 'yield' at roughly 120 ksi (830 MPa) with a corresponding strain of over 0.006 (El-Hacha, 2002).

2.5. General Behavior of Bridge Decks

In general, the behavior of concrete bridge decks is governed by three critical parameters: the amount of steel reinforcement (reinforcement ratio), the span-to-depth ratio, and the degree of lateral restrain at the edges of the deck. Consequently, the potential failure modes of concrete decks can be classified into three categories: pure flexural failure, pure punching shear failure, and ductile shear failure. Bridge decks having a small span-to-depth ratio (< 18) will fail primarily due to punching shear under a truck wheel load. These decks will exhibit small deflections prior to failure. Conversely, bridge decks having a large span-to-depth ratio will behave mainly in flexure, exhibiting substantial deflections prior failure, but will ultimately fail at lower loads than similar decks with small span-to-depth ratios. In addition, laterally restraining the edges of a bridge deck will significantly enhance its punching shear capacity due to the formation of compressive membrane forces, a phenomenon known as "arching action" (Marzouk and Hussein, 1991). These various categories of bridge deck behavior will be discussed in detail in the following sections.

2.6. Effect of Reinforcement ratio

As would be logically expected, both the load-carrying capacity and the punching shear strength of concrete bridge decks (or concrete slabs in general) tend to increase with the addition of steel reinforcement. Due to this fact, many researchers included the reinforcement ratio as a variable in their research programs, especially between the 1930's and 1970's (Dilger et al., 2005).

Marzouk and Hussein (1991) examined the behavior of two-way slabs through experimental testing. Based on their experimental results, a mechanical model was adopted and developed for high-strength concrete slabs. They reported that the ultimate punching shear load increased as the reinforcement ratio was increased. They also concluded that the degree to which yielding spread in the reinforcement varied with the reinforcement ratio. For slabs with a high reinforcement ratio, yielding of the reinforcement occurred at a high load, but was localized to the column stub. On the other hand, for lightly reinforced slabs, yielding initiated at the column stub and gradually spread throughout the whole length of tension reinforcement.

Kuang and Morely (1992) experimentally tested 12 concrete slabs with different reinforcement ratios, different span-to-depth ratios, and different degrees of edge restraint. With respect to the influence of steel reinforcement, they concluded that reinforcement ratio has an important effect on the punching shear strength for slabs that are lightly reinforced, but has less effect for those that are heavily reinforced.

Khanna et al. (2000) tested a full-scale bridge deck model that was divided into four segments. The first segment was reinforced with orthotropic steel reinforcement arranged in two layers. The second segment contained only the

bottom layer of steel reinforcement. The third segment contained only bottom transverse steel bars (transverse bars run perpendicular to the direction of supporting girders, longitudinal bars run parallel to traffic flow), and the fourth segment contained only bottom transverse Glass Fiber Reinforced Polymer (GFRP) bars. It was concluded that only the bottom transverse reinforcement affects the load-carrying capacity of the concrete bridge deck. Moreover, Khanna concluded that the stiffness of the bottom transverse reinforcement has a larger effect on the load-carrying capacity of the slab than does the strength of that reinforcement.

Hassan et al. (2000) investigated the effect of reinforcement ratio on bridge deck capacity by using an analytical model which was verified by a two-way slab model experimentally tested at Ghent University, Belgium. The analytical results indicated that the failure load increased with increases in reinforcement ratio. Hassan et al. also concluded that the use of top reinforcement does not affect the ultimate capacity of bridge deck slabs. This finding is in agreement with the conclusions of Khanna et al. (2000) and with those of Kuang and Morely (1992).

Dilger et al. (2005) conducted a statistical evaluation of the experimental results obtained by many researchers to demonstrate the effect of reinforcement ratio on the punching shear strength of concrete slabs. From the test series of Vanderbilt (1972), Marzouk and Hussien (1991), and Hallgren (1996), they concluded that as the flexural reinforcement ratios are increased, the stresses along the punching shear cone increase, and hence, the load-carrying capacity of the concrete slab increases. They also reported that an explanation of this behavior was originally given by Richart (1948) who found that significant yielding of the flexural

reinforcement produces large cracks, thereby reducing the effective concrete area resisting shear. Since the crack width and depth are controlled by the amount of flexural reinforcement, it was concluded that the reinforcement ratio significantly influences the punching shear strength of concrete slabs.

2.7. Effect of Lateral Restraint

With the presence of lateral restraint, a bridge deck is capable of forming in-plane compressive forces due to an internal arching action mechanism that develops. Lateral restraint in bridge decks is commonly provided by longitudinal supporting beams, adjacent slab sections, or the surrounding slab area, (Hon et al., 2005).

Taylor and Hayes (1965) tested 22 plain and reinforced square concrete slabs which were simply supported around their perimeters. The slabs were then loaded in the center by means of a hydraulic jack. The effect of lateral restraint on punching shear strength was obtained by testing matched pairs of slabs. One slab in each pair was unrestrained while the other was restrained by means of a surrounding steel frame. Direct comparison of the failure loads of the pairs of slabs was used to evaluate the extent of influence provided by the lateral restraint. Even an unreinforced, plain concrete slab with edge restraint could withstand significant loading, as premature collapse was prevented since the load could be carried to the supports through arching action or membrane action. Restraint of the edges of slabs with low reinforcement ratio (1.57 percent) had little effect on the early behavior, where crack widths and deflections of unrestrained slabs were similar to restrained slabs. However, the presence of edge restraint affected the later stage

behavior and increased the ultimate punching failure load by 16-60 percent. For slabs with a high reinforcement ratio (3.14 percent), the punching failure load was increased by only 15 percent. Slabs having a low reinforcement ratio that were approaching flexural failure at their point of collapse derived the greatest benefit from the presence of lateral restraint.

Kuang and Morely (1992) reported an increase in punching shear capacity of 46 percent for thin concrete slabs and of 64 percent for thick concrete slabs due to edge restraint. This increase in the load-carrying capacity reveals that edge restraint has a significant effect on the ultimate punching load of reinforced concrete slabs. Kuang and Morely also noted that lateral restraint results in enhanced shear resistance, and will effectively increase the load-carrying capacity.

Hassan et al. (2000) tested two full-scale models in addition to their analytical model. Their test results revealed that laterally restraining the bridge deck increased the load-carrying capacity by 20 percent. Also, adding additional stiffening in the form of steel sections bolted top and bottom to the outer edges of the slab increased the ultimate capacity of the slab by an additional 12 percent.

Hon, et al. (2005) presented a design method which aims to assess the restraint stiffness that exists for a slab. The method provides a technique for evaluating the strength enhancement due to compressive membrane action provided for by the restraint stiffness. The method was developed based on experimental testing of concrete slabs and through the use of non-linear finite element modeling. Hon et al. found that the strength of the slabs in both flexure and punching shear was enhanced due to the presence of edge restraint.

Appreciation of the internal arching system that develops in bridge decks led to the development of fiber-reinforced concrete (FRC) deck slabs which do not include any internal tensile reinforcement, a type of concrete slabs known as the steel-free deck. Mufti et al. (1993) demonstrated through experimental testing that deck slabs void of steel reinforcement can develop the same load-carrying characteristics as conventional deck slabs, provided that the supporting girders are connected with sufficient transverse steel straps that are properly spaced. The steel-free deck concept utilizes the transverse steel straps to laterally restrain the supporting girders, and to ensure that the deck slab develops the required arching forces. The concept utilizes the synthetic fibers in the fiber reinforced concrete to control cracking in the concrete, which could develop due to temperature and shrinkage effects shortly after the initial setting of the concrete.

2.8. Punching Shear of Concrete Slabs

Punching shear, also known as two-way action shear, is the typical mode of failure for concrete slabs subjected to concentrated loads. Common examples of this behavior are slab-column connections in flat-slab buildings, and bridge decks having relatively low span-to-depth ratios which are subjected to heavy truck wheel loads. The most pertinent rational model that has been proposed by researchers to both describe and quantify possible punching shear failures in concrete slabs is given in this section. In addition, current code provisions for predicting the punching shear strength are presented in the following section.

Kinnunen and Nylander (1960) conducted an extensive experimental and theoretical study which dealt with the punching strength of slabs without shear reinforcement. They derived a detailed model from the results of their study. Several circular concrete slabs, uniformly supported along the circumference and loaded by a column stub at the center, were tested to failure. Several types of reinforcement were tested including tangential only, radial and tangential, and orthogonal. For each type of reinforcement, the amount of flexural reinforcement used in each slab was varied.

Kinnunen and Nylander's test results and theoretical approach can be summarized as follows. At a load corresponding to between 45 and 75 percent of the ultimate punching load, the first shear crack was observed forming a circle out from the base of the column stub. Outside of this primary shear crack, only radial cracks were observed. In addition, deflection measurements showed that deflections outside of the shear crack varied linearly towards the edge of the slab. Given these results, it was surmised that the portion of the slab outside of the primary shear crack be treated as a rigid body which rotates around the root of the shear crack. The area inside the shear crack, attached to the column stub, was idealized as compressed conical shell. It was proposed that it is this conical shell carries the outer portion of the slab until the tangential compressive concrete strain on the loaded face of the slab reaches a value at which embedment of the shell is compromised.

Kinnunen and Nylander's model has served as the basis of many models developed thereafter by others. Marzouk and Hussein (1991) reported that the

model developed by Kinnunen and Nylander still provides the best account of the punching behavior of concrete slabs. Mufti and Newhook (1998) deployed the Kinnunen and Nylander model with a modification to the failure strain.

2.9. Code Provisions

This section presents common design code provisions currently used to predict the punching shear capacity of reinforced concrete slabs. Three different codes are presented with appropriate symbols and units defined for each. The approaches taken by these three codes are very similar, and are rooted in the concepts originally proposed by Kinnenun and Nylander. Obviously, before using any of the following equations for design purposes, the code-appropriate strength reduction factors, load multipliers, or other code-specific modifiers would have to be applied. The details of using the following equations for structural design are not presented here.

American Concrete Institute (ACI 318-05)

Equations for predicting the punching shear strength of concrete slabs are found in section 11.12.2.1 of ACI 318-05. For two-way action in nonprestressed slabs and footings, the nominal shear resistance, V_c (in pounds), shall be the lesser of the following three equations:

$$V_C = 4\sqrt{f_c'}\,b_o d \qquad \text{Equation (1)}$$

$$V_C = \left(2 + \frac{4}{\beta_c}\right)\sqrt{f_c'}\,b_o d \qquad \text{Equation (2)}$$

$$V_C = \left(2 + \frac{\alpha_s}{b_0}\right)\sqrt{f_c'}\, b_o d \qquad \text{Equation (3)}$$

Where:

V_c = the predicted punching shear capacity of the deck in kips

β_c = the unit-less ratio of the length of the long side of the loading plate to the short side of loading plate

f_c' = the concrete compressive strength in pounds per square inch

b_o = the perimeter of the critical section taken at a distance d/2 from the edges of the loading plate in inches

d = the effective section depth of the concrete slab in inches

α_s = a unitless constant defined as 40 for interior columns or loads, 30 for edge columns or loads, and 20 for corner columns or loads

Again, these equations are valid only for nonprestressed slabs and footings subjected to a concentrated load or reaction, frequently from a column. A separate equation, which is not presented here, would be used if prestressing forces were present.

All of the equations in the set of three are based on the idea of determining shear strength by multiplying the shear area, defined as the critical perimeter multiplied by the slab depth, by a concrete shear strength expressed as a multiplier times the square root of concrete strength. In the first equation, four roots of concrete compressive strength are taken as the shear strength. This equation is likely to be sufficient for square and circular column sections. However, testing has shown that

four roots of compressive strength will sometimes under-estimate concrete shear strength when dealing with columns or bearing areas having rectangular shapes (ACI, 2005).

The second equation in the set accounts for the influence of a rectangular shaped loading area. This equation varies the concrete shear strength linearly between two and four roots of the compressive strength depending on the ratio of the long side of the loaded area to the short side of the loaded area.

Finally, testing has also shown that concrete shear strength decreases as the ratio of critical perimeter to slab depth increases (ACI, 2005). This observation is accounted for by the third equation, which also varies the concrete shear strength linearly between two and four roots of the compressive strength. This equation makes use of the ratio between slab depth and critical section perimeter, and also includes a factor to account for the location of the column, reaction, or concentrated load with respect to the edges of the slab. This α_s term adjusts punching shear capacity for interior, edge, and corner locations. Punching failure in all cases will occur along a truncated conical shell which develops underneath the applied force, as reported by Kinnenun and Nylander (1960) among others.

In the case of an interior column, reaction, or load, the conical failure plane will extend into the slab on all sides of the column. For an edge column or load, the truncated shear cone will only be able to extend outward from three of the four column faces, as would happen for a column located on the edge of slab or slab opening. Finally, a corner column, reaction, or load is located on an exterior slab corner, and the shear cone can only exist on two of the four column faces. In the

case of a bridge deck subjected to a concentrated truck wheel load, the interior case would almost always apply, as a truck wheel would typically rest well away from any unsupported slab edge. An exception to this case could be an edge loading situation where the bridge deck was cantilevered over the outermost supporting girder.

In addition to checking punching shear capacity at column-to-slab connections and concentrated reactions, it is also important to examine any locations where the slab thickness changes. While this is not especially relevant to concrete bridge decks, it is very common in cast-in-place buildings that use drop panels or column capitals. In such cases, there would be two critical sections to check, one at a distance d/2 from where the column meets the drop panel and another at a distance d/2 from where the drop panel transitions to the thinner slab depth.

It should also be noted that ACI 318 also has a provision for checking wide-beam action, or one-way shear action, in elevated slabs. In the case of one-way shear, a critical section is taken at a distance d/2 from the supports. This section would extend across the entire width of the slab. While one-way shear action will seldom govern in reinforced concrete bridge deck designs, it should be checked in all cases to ensure that the shear strength of the concrete is not exceeded.

AASHTO LRFD (2004)

The equations used by the American Association of State Highway Transportation Officials for predicting punching shear capacity are the same as those presented by ACI, except the constants have been modified to reflect a

change in units. In addition, AASHTO only utilizes a set of two equations, excluding the equation accounting for the ratio of critical perimeter to slab depth and load location. For sections of two-way action without transverse reinforcement, the nominal shear resistance of the concrete, V_c, in units of kips and inches, is taken as the lesser of:

$$V_C = 0.126\sqrt{f_c'}\,b_o d \qquad \text{Equation (4)}$$

$$V_C = \left(0.063 + \frac{0.126}{\beta_c}\right)\sqrt{f_c'}\,b_o d \qquad \text{Equation (5)}$$

Where:

V_c = the predicted punching shear capacity of the deck in kips

β_c = the unitless ratio of the length of the long side of the loading plate to the short side of loading plate

f_c' = the concrete compressive strength in kips per square inch

b_o = the perimeter of the critical section taken at a distance d/2 from the edges of the loading plate in inches

d = the effective section depth of the concrete slab in inches

The AASHTO LRFD Design Code also specifies standard truck loadings for highway bridges. The single-axle design load for a standard design truck can be as high as 32 kips per axle. In the case of tandem axles, loading is specified as a design tandem, defined as a pair of 25 kip axles spaced 4 feet apart longitudinally and 6 feet apart transversely.

Ontario Highway Bridge Design Code (OHBDC-1991)

The nominal shear strength, V_c, of concrete slabs in two-way action is given by the following equation using units of Newtons and millimeters:

$$V_C = \left(0.6 f_r + 0.25 f_{pc}\right) b_o d + 0.9 V_p \qquad \text{Equation (6)}$$

Where:

V_c = the predicted punching shear capacity of the deck Newtons

f_r = the concrete tensile strength in MPa

f_{pc} = compressive stress at the concrete centroid due to prestressing in MPa

b_o = the perimeter of the critical section taken at a distance d/2 from the edges of the loading plate in millimeters

d = the effective section depth of the concrete slab in millimeters

V_p = the component of effective prestressing force in direction of applied shear in Newtons

The equation presented by the Ontario code is very similar to an equation given by ACI for prestressed slab and footings. If the terms in this equation related to prestressing forces are neglected for a situation where there is no prestressing present, the equation takes the familiar form of a concrete shear strength multiplied by a shear area (critical section perimeter multiplied by slab depth). If the modulus of rupture of the concrete, f_r, is taken as 6 roots of compressive strength, the Ontario equation reduces to 3.6 roots of the compressive strength multiplied by the shear area with compressive strength in

pounds per square inch. (The Ontario Code specifies that rupture strength be taken as 0.5 roots of compressive strength in megapascals when no better information is available. This equates to 6 roots of compressive strength when the units are converted to match the other codes presented here). For many situations, especially those with square loading areas, this formulation is somewhat more conservative than the ACI or AASHTO approach.

3. Experimental Program

3.1. Introduction

Despite the availability of advanced and powerful computing techniques, experimental testing remains a reliable and necessary tool for understanding and evaluating the inelastic behavior of reinforced concrete structures. The following section describes an experimental testing program conducted at the Constructed Facilities Laboratory (CFL) of North Carolina State University in Raleigh, NC, USA.

3.2. Overview

In this testing program, it was desired to evaluate the performance of MMFX steel used as longitudinal reinforcement for cast-in-place concrete bridge decks. Three full-size bridge deck sections were tested to failure in order to evaluate their response. All three bridge decks consisted of two spans and two cantilevers supported in composite action by three post-tensioned concrete girders. All three decks were identical except for the type and amount of reinforcement used in each. The first deck was reinforced with MMFX steel, while the second deck was reinforced with Grade 60 steel in exactly the same configuration. The third deck was reinforced with MMFX steel at a significantly reduced ratio in an attempt to take advantage of the high strength offered by MMFX steel.

The dimensions of the decks were chosen to match the dimensions of a bridge constructed using MMFX steel in Johnston County, NC. The configuration of the MMFX reinforcement used in the first test deck exactly replicated the reinforcement scheme used in the actual bridge.

3.3. Material Tests

Accurate determination of the material properties of the concrete and steel used to construct the three bridge deck specimens was a necessity for effectively evaluating and comparing bridge deck response. Concrete and reinforcing steel samples were taken from each deck, and were tested as described below.

Testing of Steel Reinforcement

In order to determine the actual stress-strain characteristics of the reinforcing steel used in each deck, samples were tested in accordance with ASTM A370. Samples of #4 (No. 13) and #5 (No. 16) MMFX bars were taken from the supply used to construct the first and third bridge decks. Samples of the #5 (No. 16) Grade 60 bars used to construct the second bridge deck were also tested.

For each steel type and bar size, five specimens were tested using an MTS universal tension-compression testing machine with hydraulic grips and a 220-kip capacity. Grip sizes were selected to match the bar sizes being tested. Data were recorded on three channels using an electronic Optim data acquisition system. Test load and stroke from the testing machine were monitored and recorded, and the strain reading was recorded from an MTS extensometer attached to each bar.

The diameter of each tested sample was measured to the nearest 0.001 inches using a digital caliper to verify the nominal cross-sectional area. Instantaneous measurements of the cross-sectional area were not made during testing, because only the engineering properties were desired.

Each of the tested samples were prepared with an 8 inch gage length for measuring the total elongation at failure. The gage length was marked on each specimen, and elongation measurements were made over this length. The center of the gage length was aligned with the center of the specimen along its length. Each bar sample was sized to accommodate the 8 inch gage length, at least two bar diameters between each end of the gage length and the grips of the testing machine, and an additional length to fill both 5 inch grips of the tension testing machine. An MTS axial-mechanical extensometer that measures the change in length over a 2-in gage length was attached to each test specimen at mid-height to measure the deformation during loading, as shown in Figure 3-1.

Figure 3-1: Extensometer Attached to a #5 MMFX Bar in the Testing Machine

Each specimen was subjected to a gradually increasing uniaxial load until failure took place. Load was applied at a rate of 0.001 inches displacement per second. When the applied load necessary to produce additional strain began to decrease, the test was paused, and the MTS extensometer was removed to prevent damage at rupture. Loading was then continued until fracture of the specimen.

After failure, each specimen was removed from the testing machine, the broken pieces were aligned, and the fractured ends were fit together. The elongated gage length was then measured using a digital caliper to an accuracy of within 0.5%, as is specified by ASTM A370. The recorded data taken during the test were combined with the gage length measurements and the nominal cross-sectional areas to develop engineering stress-strain curves and to determine key properties for the tested reinforcing bars.

Testing of Concrete Cylinders

Concrete cylinders were produced each time concrete was cast. This was done so that the material properties of the concrete used to construct the three bridge deck specimens could be determined. Cylinders were made in accordance with ASTM C31 *Making and Curing Concrete Test Specimens in the Field* using 4” x 8” plastic molds. The cylinders cast with a particular bridge deck were cured alongside that deck so as to obtain the most accurate estimate possible of in place properties. Ten cylinders were cast with each deck so that one extra cylinder would be available after breaking three each at 7 days, 14 days, and 28 days (or the day of bridge deck testing).

Cylinders were tested in a 500-kip capacity Forney compression-testing machine in accordance with ASTM C39 *Compressive Strength of Cylindrical Concrete* at a rate of 35 psi / second. Prior to testing, the top and bottom surfaces of each cylinder were ground smooth with a stationary rotary-polishing machine to ensure an even distribution of pressure between the loading surfaces of the testing machine and the cylinder surfaces. The applied load was monitored during the test, and the maximum load achieved was used to calculate the ultimate stress of each cylinder.

3.4. Full Scale Bridge Decks

Test Specimens

The three bridge decks specimens evaluated in the experimental program were identical in all respects except for the type and amount of steel reinforcement used in each. Each bridge deck consisted of two spans and two cantilevers, supported in composite action by three precast post-tensioned concrete girders. Each end of the girders rested on a concrete support block. An isometric rendering of a bridge deck specimen, the three composite girders, and six support blocks is shown in Figure 3-2.

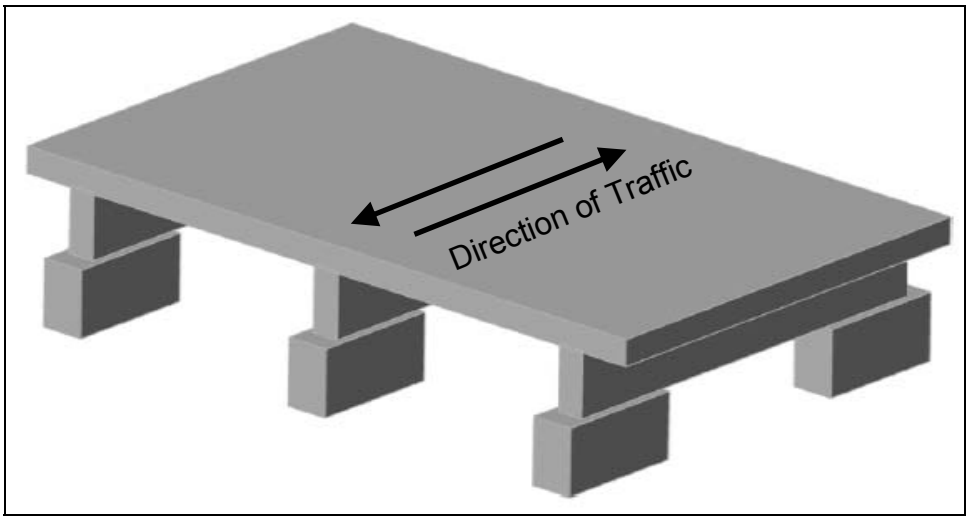

Figure 3-2: Sketch of Deck, Girders, and Blocks

. The overall dimensions of each deck were 21’-10” by 13’-2” (6655 x 4013 mm). The center to center span between girders measured 9 feet (2743 mm). The thickness of each deck was 8⅝” (220 mm), providing a span to depth ratio of 12.5. Since each test specimen models a section of a real bridge, traffic would flow in lanes running parallel to the girders. Thus, the longitudinal direction of the test specimens is defined as the direction running parallel to the girders, and the transverse direction is defined as that perpendicular to the girders. Load was applied simultaneously at the center of each span to a 10” by 20” (254 by 508 mm) loading plate, the long dimension of the plate oriented along the transverse direction of the bridge deck. A plan view of a typical test specimen, showing the dimensions of the deck and the longitudinal and transverse directions, is given in Figure 3-3. The figure also gives a reference direction of North which will be used to orient future figures.

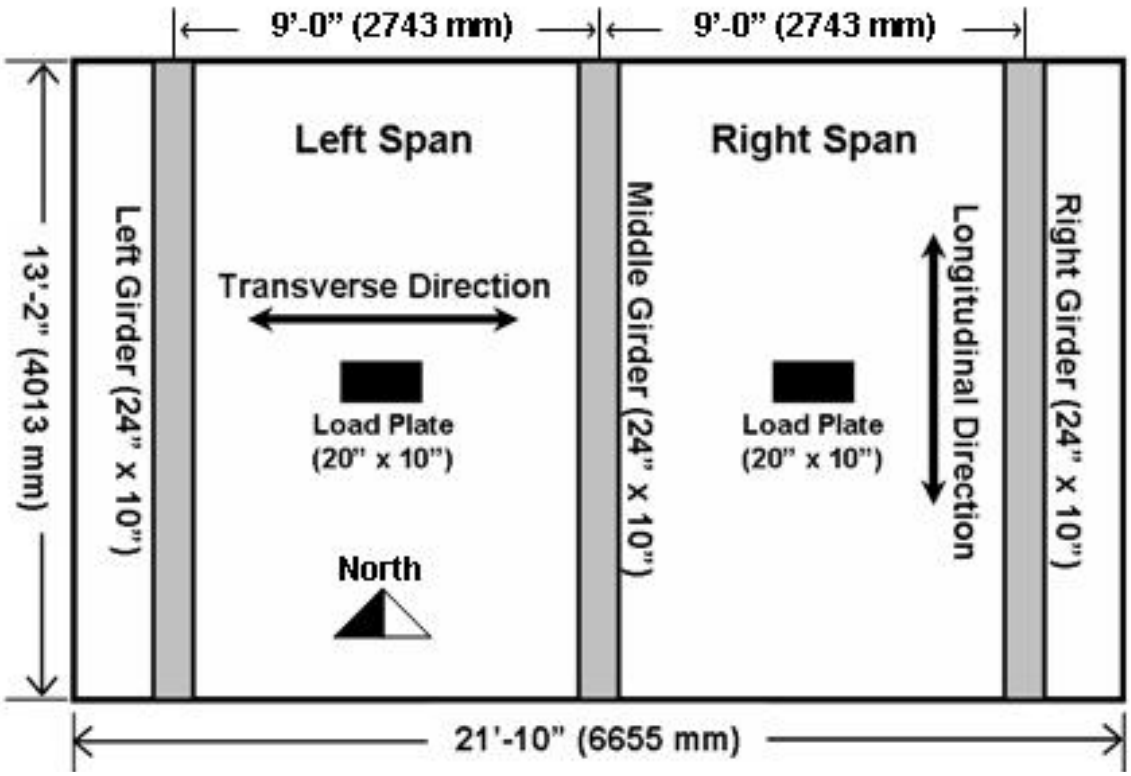

Figure 3-3: Plan View of Typical Test Specimen

The precast, prestressed girders supporting each deck had cross-sectional dimensions of 24" by 10" (610x254 mm), and were cast integrally into the slab. The girders were oriented with their 10" dimension horizontally. Each girder had stirrups protruding from the top surface which, when cast into the deck, allowed for composite action to develop between the slab and the girders. The design of these prestressed concrete girders was critical because the deck of the Johnston County Bridge is supported by steel girders. Unfortunately, the cost of steel girders was prohibitive for this testing program, and prestressed concrete girders were used instead. In order to ensure that the modeled behavior was as realistic as possible, the concrete girders were carefully designed to have a torsional rigidity equal to matched that of the steel girders used in the actual bridge. Torsional stiffness of the

supporting girders plays a significant role in the load-carrying capacity of a bridge deck.

To ensure matching torsional stiffness between the concrete and steel girders, both the actual bridge and the proposed test models were analyzed with the non-linear finite element programs *ANACAP* and *SAP2000*. Once the torsional properties of the actual bridge girders were determined, several concrete girder cross-sections and spans were evaluated.

A prestressed concrete girder having cross-sectional dimensions of 24” by 10” (610x254 mm) and a span of 96” (2438 mm) was found to have a torsional stiffness matching the steel girders on the actual bridge. Since the bridge deck models were set at 13’-2” (4013 mm) wide, concrete support blocks were used to create the required 96” (2438 mm) span. The supporting girders and the concrete blocks were designed and detailed according to ACI 318-05, and were produced by a local precast supplier. Nine girders and six blocks were produced. Three girders were used for each test, and the six support blocks were reused for all tests.

Post-tensioning of the concrete girders was done by using threaded prestressing bars having a 1 inch (25 mm) diameter and an ultimate strength of 150 ksi (1034 MPa). Each girder was cast with four ducts spaced concentrically about the centroid of the cross-section. The four prestressing bars used for each girder provided a total prestressing force of 360 kips (1601 KN) per girder. Prestressing was applied prior to casting the deck to ensure that the total prestressing forces were resisted by the girders only. Sufficient jacking force was applied to account for relevant elastic, seating, and relaxation losses.

The reinforcement for all specimens was configured in two orthogonal mats running continuously in both directions throughout all three bridge decks. The first and third bridge decks were reinforced with MMFX steel, while the second bridge deck was reinforced with conventional Grade 60 steel for comparison purposes. Internal reinforcement was the only variable in the test program. The test matrix is given in Table 1, and the reinforcement details for all three bridge decks are shown in Figure 3-4. Note that the reinforcement details of the first and second bridge decks are exactly the same except for the use of MMFX steel in the first deck.

Table 1: Bridge Deck Test Matrix

Bridge Deck	Steel Type	Bottom Reinforcement		Top Reinforcement	
		Transverse	Longitudinal	Transverse	Longitudinal
First	MMFX	#5 @ 6.75” (#16 @ 170) ρ = 0.54%	#5 @ 10” (#16 @ 250) ρ = 0.36%	#5 @ 6.75” (#16 @ 170) ρ = 0.54%	#4 @ 14” (#13 @ 360) ρ = 0.17%
Second	Grade 60	#5 @ 6.75” (#16 @ 170) ρ = 0.54%	# 5 @ 10” (#16 @ 250) ρ = 0.36%	#5 @ 6.75” (#16 @ 170) ρ = 0.54%	#4 @ 14” (#13 @ 360) ρ = 0.17%
Third	MMFX	#5 @ 10” (#16 @ 250) ρ = 0.36%	#5 @ 10” (#16 @ 250) ρ = 0.36%	#5 @ 10” (#16 @ 250) ρ = 0.36%	#4 @ 14” (#13 @ 360) ρ = 0.17%

It should be noted that the reinforcement ratios (ρ) shown in Table 1 were calculated using the total slab thickness. Longitudinal reinforcement ratio is the same for all three decks. Transverse ratio, however, is reduced by 33% in the third deck.

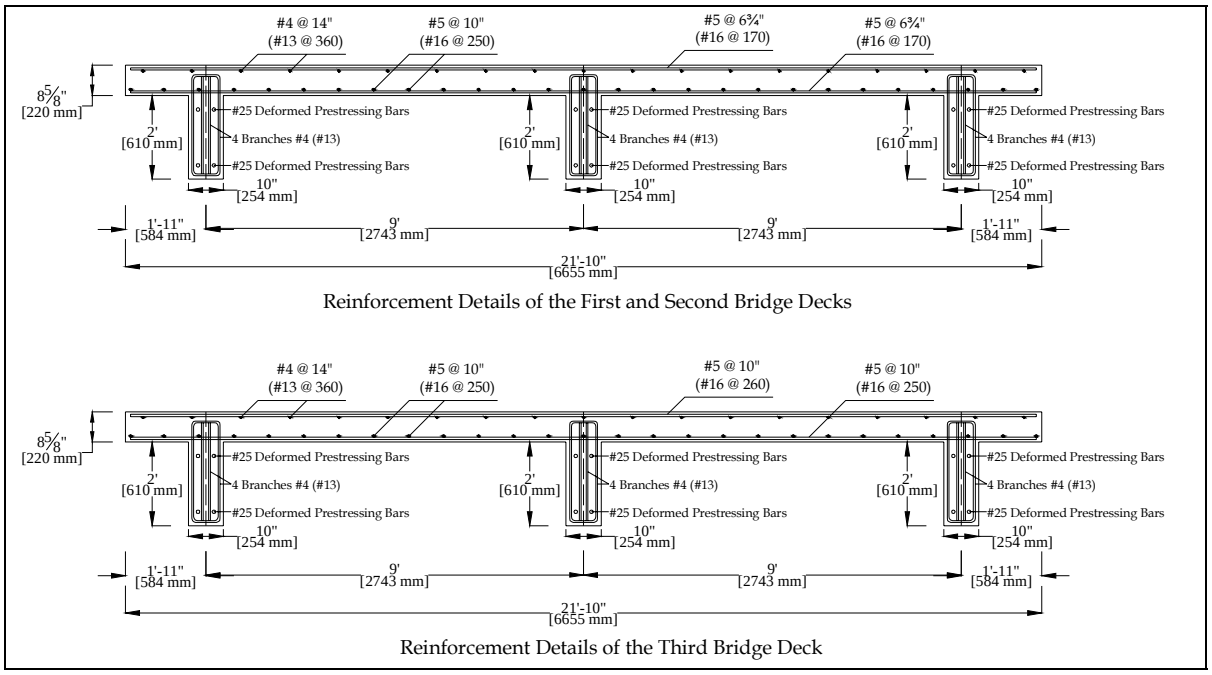

Figure 3-4: Reinforcement Details for All Tested Decks

Construction of the Test Specimens

Each test specimen was cast in the position in which it was tested. The supporting blocks and girders were positioned for each slab, and wooden formwork was constructed around these elements. A concrete deck was cast on the forms, and after 14 days of moist curing, the forms were removed and saved for reuse. After completion of testing, the specimen was cut up and removed, and the next specimen was constructed in the same location using the same procedure. A sketch of the formwork used is shown in Figure 3-5. The plywood casting surface is not shown on the sketch for clarity. The formwork was designed to deflect only minimally under the weight of the fresh concrete so as to ensure as flat a slab as possible. The formwork was also designed to allow for it to be reused for each of the three deck specimens.

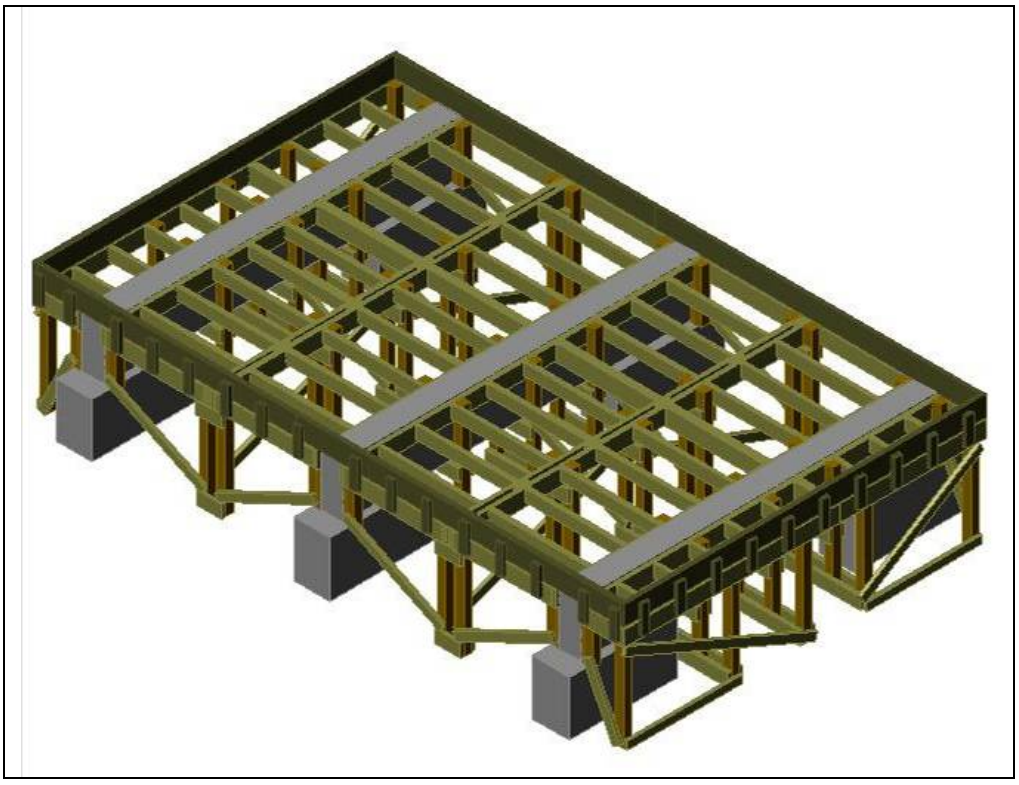

Figure 3-5: Wooden Forms Used for Casting the Decks

Figure 3-6: First Bridge Deck Prior to Casting

Once the wooden forms were in place, they were treated with a form release agent to facilitate stripping. The upper and lower mats of reinforcement were then tied in place using plastic spacers and wire. Concrete clear cover was ¾" top and bottom. Concrete clear cover is defined as the distance from the top or bottom concrete surface to first steel surface (in this case, the surface of the top or bottom transverse bar). Strain gages were applied to the steel bars, and the wires were run out the sides of the form. Concrete was delivered by a local supplier, and was delivered to the forms in a bucket using the overhead crane. Electric vibrators were used to consolidate the concrete prior to screeding the surface flush with the sides of the form. The surface was floated and then treated with a light broom finish. The forms were left in place, and wet burlap and plastic sheeting were kept on the top surface of each deck for 14 days after casting to allow the concrete sufficient opportunity to properly cure.

Test Setup

As is discussed above, each bridge deck was loaded simultaneously in the center of both spans to simulate the effects of truck wheel loading. Two 440 kips capacity (1957 KN) MTS hydraulic actuators were used to apply the loads. The actuators were computer controlled, and were configured to maintain equal load on both spans for the first portion of the test. Up until a load level of 150 kips, the actuators were operated in force control. Load was applied to each span at a rate of 10 kips per minute (44.5 kN per min), with the load being held at 10 kip (44.5 kN) intervals to check for cracking. At the 150 kips (667 kN) load level, the actuators

were switched to displacement control to provide for safe operation during the impending failure. Load was increased at a rate of 0.1 inches per minute (2.5 mm per min) from this point forward. Cracks were observed and photographed after the 150 kip (667 kN) load level, but they were not marked due to the safety concerns of having personnel near the decks at high load levels.

Each of the actuators was suspended over the deck specimen by a steel test frame anchored securely to the strong floor. The concrete support blocks were also anchored to the strong floor. The girders rested directly on a level grout bed which was prepared on each block. Figure 3-7 and Figure 3-8 show a schematic view of the test setup and a photograph of the first bridge deck prior to testing.

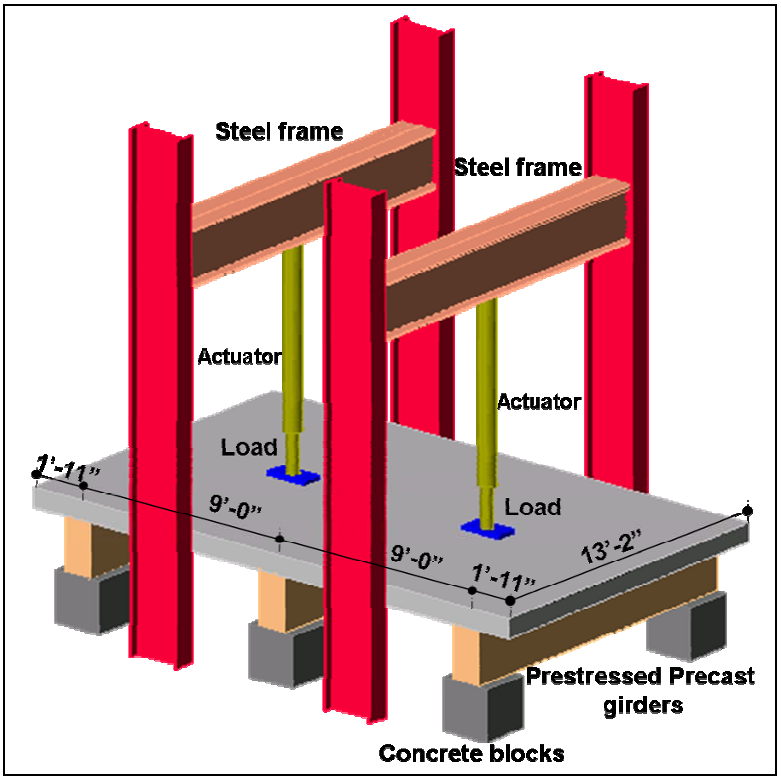

Figure 3-7: Isometric view of the bridge decks test setup

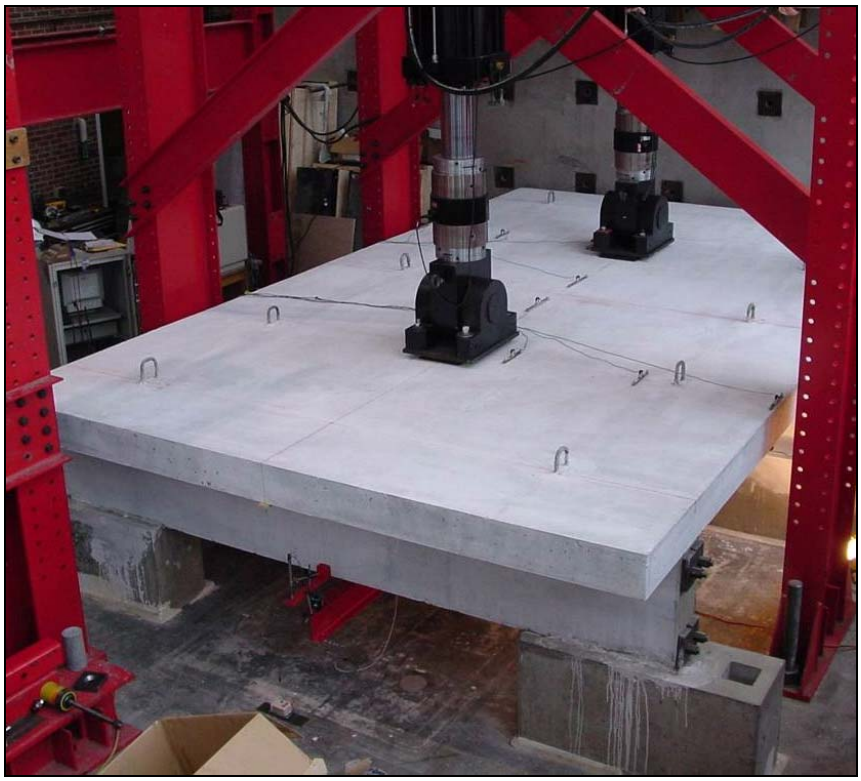

Figure 3-8: First bridge deck prior to testing

Load was transferred from the actuators to the deck through two 10” x 20” x 1” (254x508x25 mm) loading plates in order to comply with the AASHTO LRFD (2004) standard for a truck tire footprint. Each plate was placed on top of a ½” thick (13 mm) neoprene pad to prevent localized crushing of the concrete.

Instrumentation

A total of 72 channels of instrumentation were used to monitor the response of each bridge deck. Data from all channels were electronically recorded by an Optim Megadac data acquisition system. Loads, displacements, rotations, and stains were all measured and recorded.

One 550 kip capacity (1957 KN) load cell was integrated into each actuator, and was used to measure the applied loads. Twenty-four string potentiometers (string pots) were attached to the underside of the bridge deck at the locations shown in Figure 3-9. The string pots were used to measure the bridge deck deflections along profiles in both the longitudinal and transverse directions.

In addition to the string pots, two linear potentiometers were used to measure the vertical rotations of each supporting girder (six linear pots in total). A 24" (610 mm) long bar was attached to the bottom surface of each girder at the midspan. The bar was oriented perpendicular to the length of the girders. A linear potentiometer was used to measure the deflection at each end of this bar, and the difference between those measurements was used to calculate girder rotation. The location of these linear potentiometers is also noted on Figure 3-9.

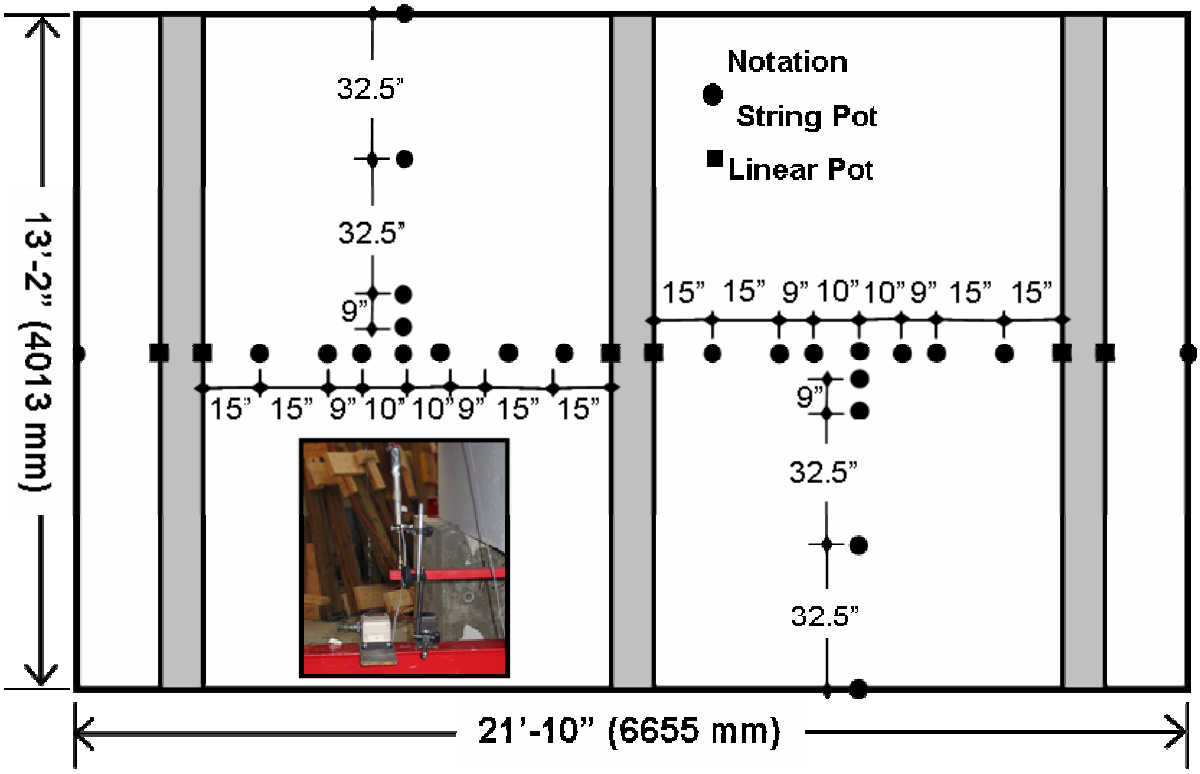

Figure 3-9: Locations of String and Linear Potentiometers

Twenty PI gages (see inset in Figure 3-10) were used to measure concrete strains at various locations on each of the tested decks. The PI gages used monitored the elongation between two gage points fixed to the concrete surface. This measured elongation was divided by an initial gage length of 100, 200, or 300 mm (depending on the specific gage) to calculate the concrete strain. Gages were affixed along the longitudinal and transverse center lines of both spans. Gages adjacent to girders were set with the first gage point located 12" (305 mm) from the girder centerline. Gages were located on the top and bottom surfaces of each deck. Figure 3-10 shows the locations of the PI gages used, and distinguishes between locations that have a gage on the top and bottom surface, or just the top surface. In four locations on each deck, PI gages are attached to the bottom surface only due to restrictions imposed by the actuator configuration. The strains measured from matching locations on the top and bottom surfaces of the decks were used to develop strain profiles for those sections.

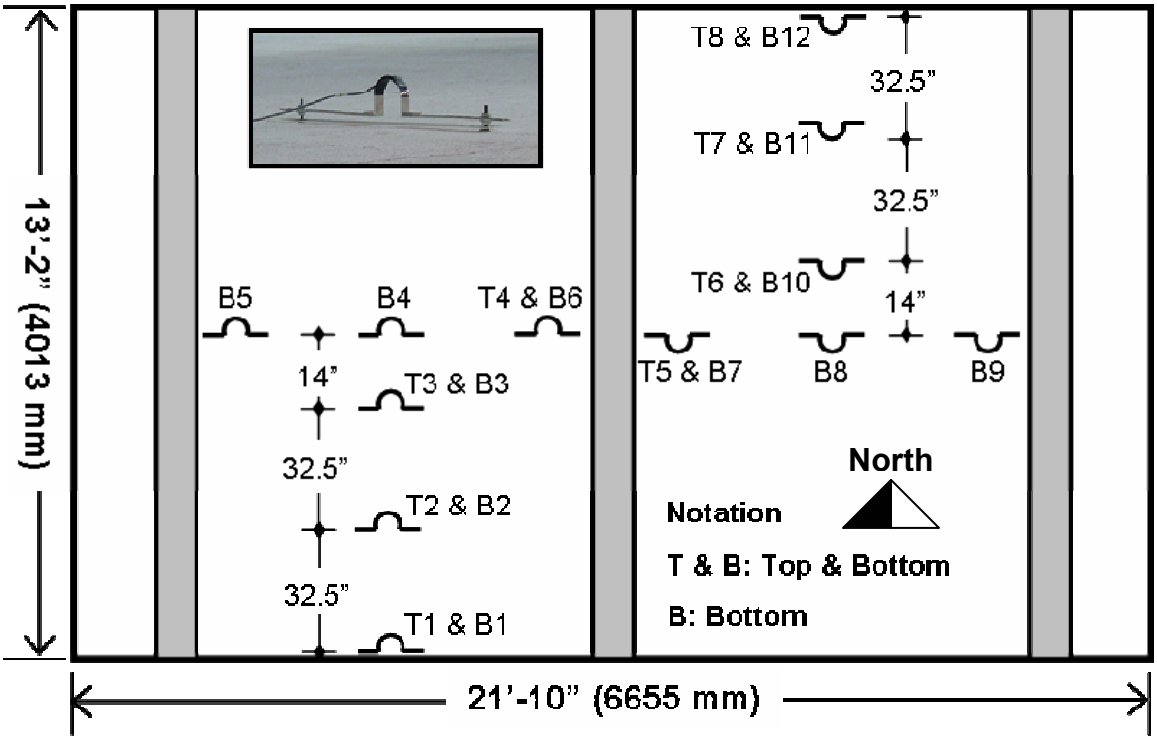

Figure 3-10: Locations of PI Gages

Strains on the steel reinforcement were measured with electrical resistance strain gages of 120 ohm resistance and 6 mm gage length. Twenty of these gages were attached to selected reinforcing bars in each deck. Each strain gage was applied to the bar and then protected with multiple coatings of polyurethane and silicone. The wires were securely attached to the bars immediately adjacent to the gages, and then run to the side of the forms. Bars in the lower mesh having strain gages were oriented with the gages down. Bars in the upper mesh having strain gages were oriented with the gages up. This was done in an attempt to capture the largest strain values possible. Care was taken during casting of the decks not to damage the gages. Figure 3-11 shows a typical strain gage attached to some of the lower level transverse reinforcement before the lower longitudinal reinforcement or the upper mesh were put in place.

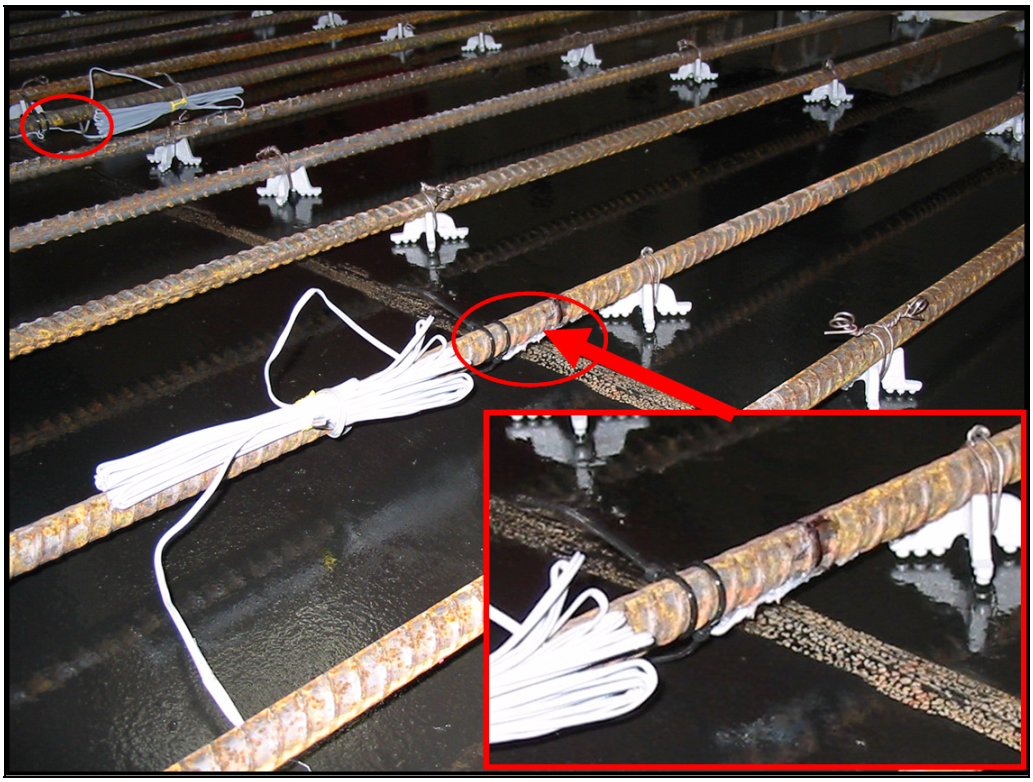

Figure 3-11: Typical Strain Gage on Bottom Transverse Mesh

Figure 3-12 through Figure 3-16 depict the locations of all strain gages used on all three bridge decks. In all of the figures, only the bars having strain gages are shown. All other reinforcing bars are left out for clarity. Strain gages are indicated by the small circles. Both spans of all three bridge decks are symmetrical, so measurements given for either span apply to both spans. The blue dotted lines indicate the transverse centerline of the deck, the midspan of both the left and right spans, and the centerline of the middle girder. The loading plates are shown as black rectangles. Each strain gage is labeled in the format xx-n where n is a sequential number starting with 1. The sequential number is proceeded by a two letter abbreviation indicating the layer of mesh and the direction of the bar each

gage is attached to: LT, UT, or LL indicate “Lower Transverse,” “Upper Transverse,” or “Lower Longitudinal.”

Since the upper and lower longitudinal reinforcement is the same for all decks, the longitudinal strain gage locations are also the same. Note that there are no strain gages on the upper longitudinal reinforcement for any decks. Recall that transverse reinforcement is identical for the first and second decks, but is different for the third deck, however. Thus, the transverse strain gage locations on the third deck are slightly different from those on the first and second deck, and they are shown in separate drawings.

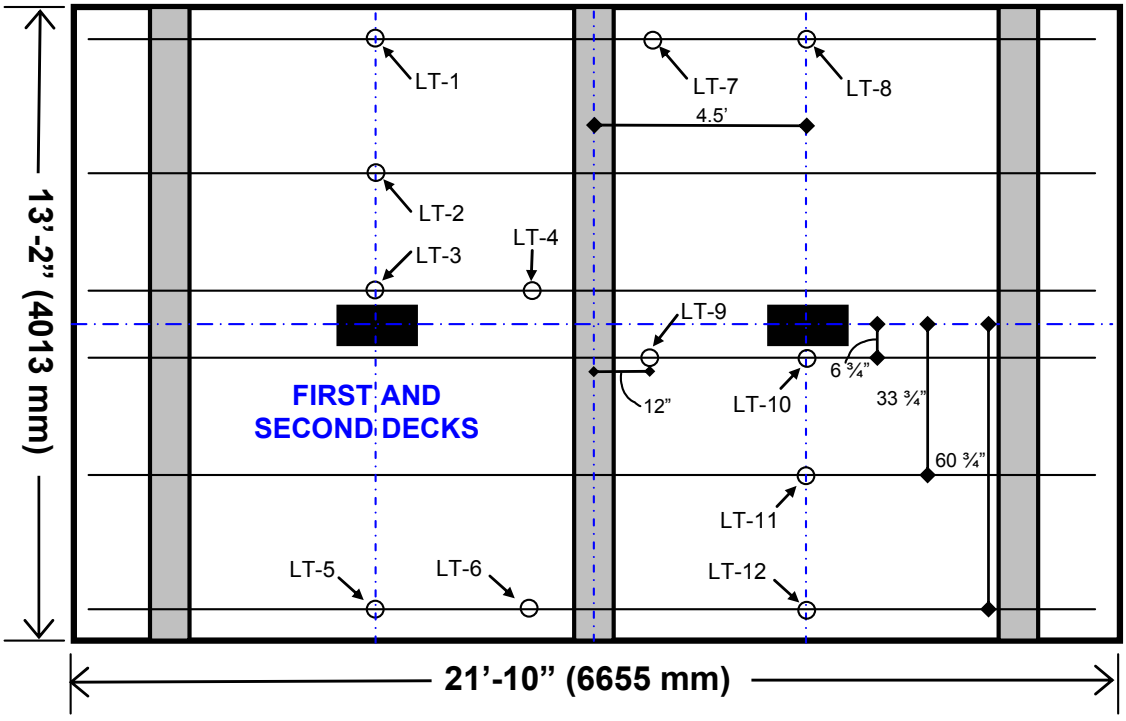

NOTE: Only Lower-Mesh Transverse Bars with Gages Shown

Figure 3-12: Strain Gages on Lower Transverse Bars First + Second Deck

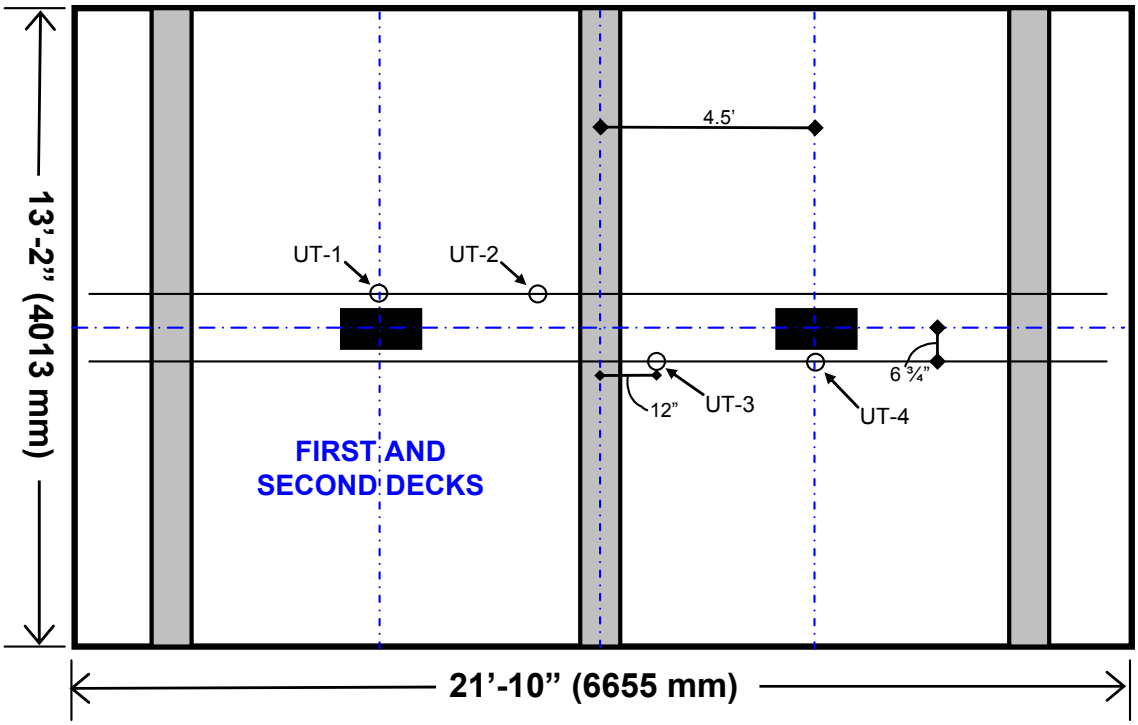

NOTE: Only Upper-Mesh Transverse Bars with Gages Shown

Figure 3-13: Strain Gages on Upper Transverse Bars First + Second Deck

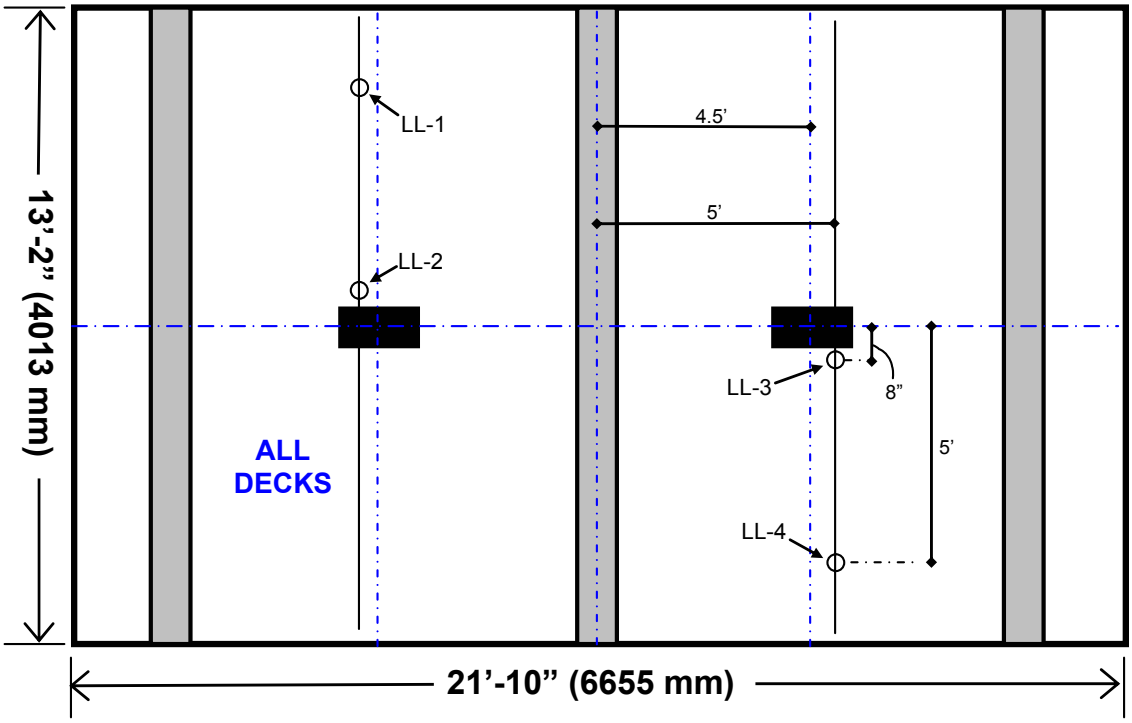

NOTE: Only Lower-Mesh Longitudinal Bars with Gages Shown

Figure 3-14: Strain Gages on Lower Longitudinal Bars All Decks

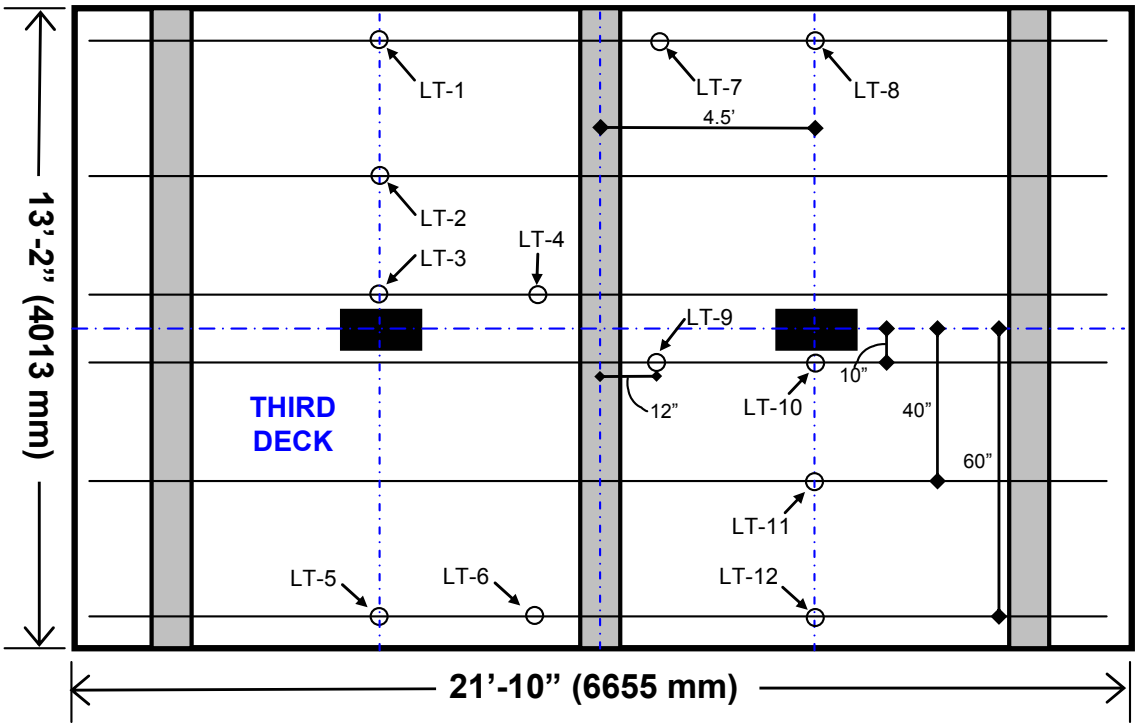

NOTE: Only Lower-Mesh Transverse Bars with Gages Shown

Figure 3-15: Strain Gages on Lower Transverse Bars Third Deck

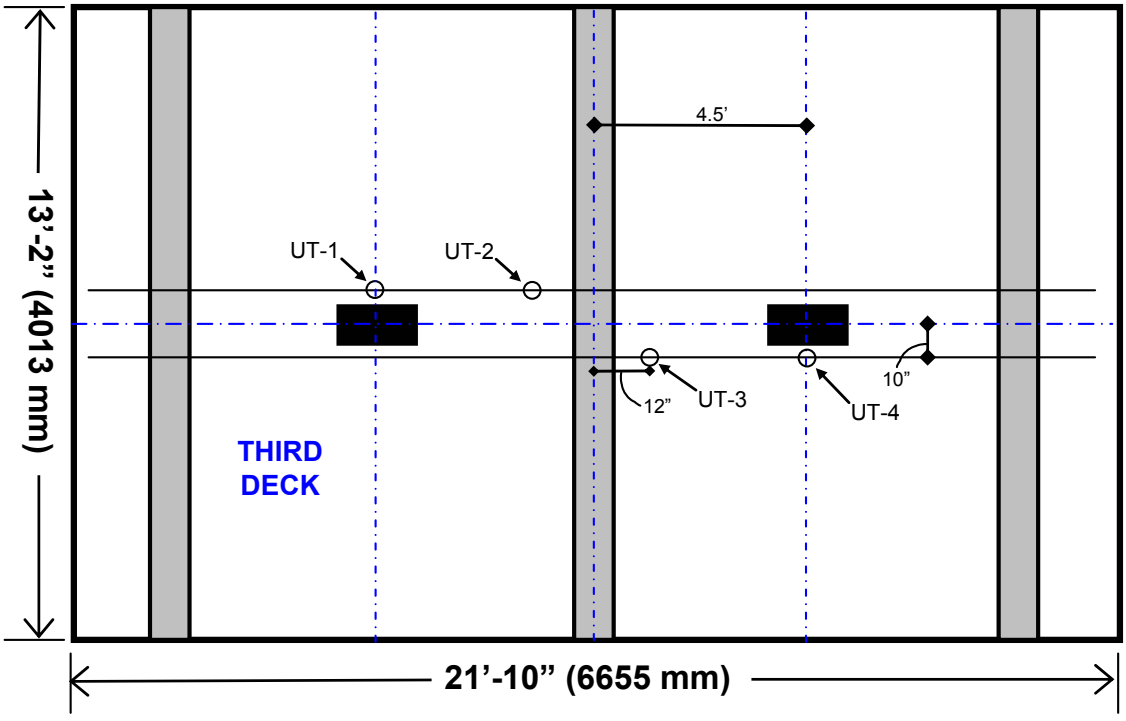

NOTE: Only Upper-Mesh Transverse Bars with Gages Shown

Figure 3-16: Strain Gages on Upper Transverse Bars Third Deck

Loading Protocol

The three bridge decks were all tested under quasi-static loading conditions up to failure. Loads were applied slowly in an effort to eliminate all dynamic response. In addition, loads were applied in cycles up to failure with complete unloading taking place between cycles. This was done in an effort to seat the test setup and specimens before reaching higher loads. In addition, the cyclic loading allowed for monitoring of the relative recovery of the decks at each cycle.

The loading procedure is outlined below. The procedure is identical for all decks with the exception of the last cycle. The first deck was loaded with an extra cycle because it was able to sustained slightly higher loads.

Loading Procedure for the First Bridge Deck:

- Load to 50 kips, Hold Load to Mark Cracks, Unload
- Reload to 100 kips, Hold Load to Mark Cracks, Unload
- Reload to 150 kips, Hold Load to Mark Cracks, Unload
- Reload to 200 kips, Hold Load to Make Observations, Unload
- Reload to Failure

Loading Procedure for the Second and Third Bridge Decks:

- Load to 50 kips, Hold Load to Mark Cracks, Unload
- Reload to 100 kips, Hold Load to Mark Cracks, Unload
- Reload to 150 kips, Hold Load to Mark Cracks, Unload
- Reload to Failure

4. Results, Analysis, and Discussion

4.1. Introduction

This section discusses in detail the experimental results, and the observed behavior of the three bridge decks investigated in this study. English units (kips, feet, and inches) are used as the primary units, and SI units (KN, meter, and millimeter) are typically shown in parentheses. The results for the tests are presented in the order they were conducted. Discussion is provided as the results are presented.

4.2. Material Properties

Steel

Tension specimens of MMFX and Grade 60 steels were taken from the supply of material used to construct the three bridge decks, and were tested according to ASTM-A370 specifications. The measured engineering stress-strain characteristics of all of the MMFX and Grade 60 steel samples are summarized in Figure 4-1.

In general, the MMFX reinforcing bars exhibited a linear stress-strain relationship up to a stress level of approximately 100 ksi (689 MPa). This linear behavior was followed by an increasingly nonlinear behavior up to an ultimate strength of 173 ksi (1193 MPa). The MMFX bars did not exhibit a well-defined yield point. According to the ASTM-A370 offset method (0.2% offset), the yield strength of the MMFX bars was determined to be 120 ksi (827 MPa). The initial modulus of elasticity was determined to be 29,500 ksi (203 GPa) prior to the reduction in modulus at the onset

of nonlinear behavior. The yield strength of the Grade 60 steel was determined to be 68 ksi (469 MPa), and the elastic modulus was determined to be 28,500 ksi (197 GPa).

For comparison purposes, the stress-strain relationships obtained for conventional Grade 60 steel and MMFX steel are plotted in Figure 4-1 alongside an equation that has been proposed to model the behavior of MMFX steel. It has been reported that the stress-strain relationship for the MMFX steel can be approximately modeled by the exponential equation (Zia, 2004):

$$f_{MMFX} = 165\left(1 - e^{-185\varepsilon}\right) \qquad \text{Equation (7)}$$

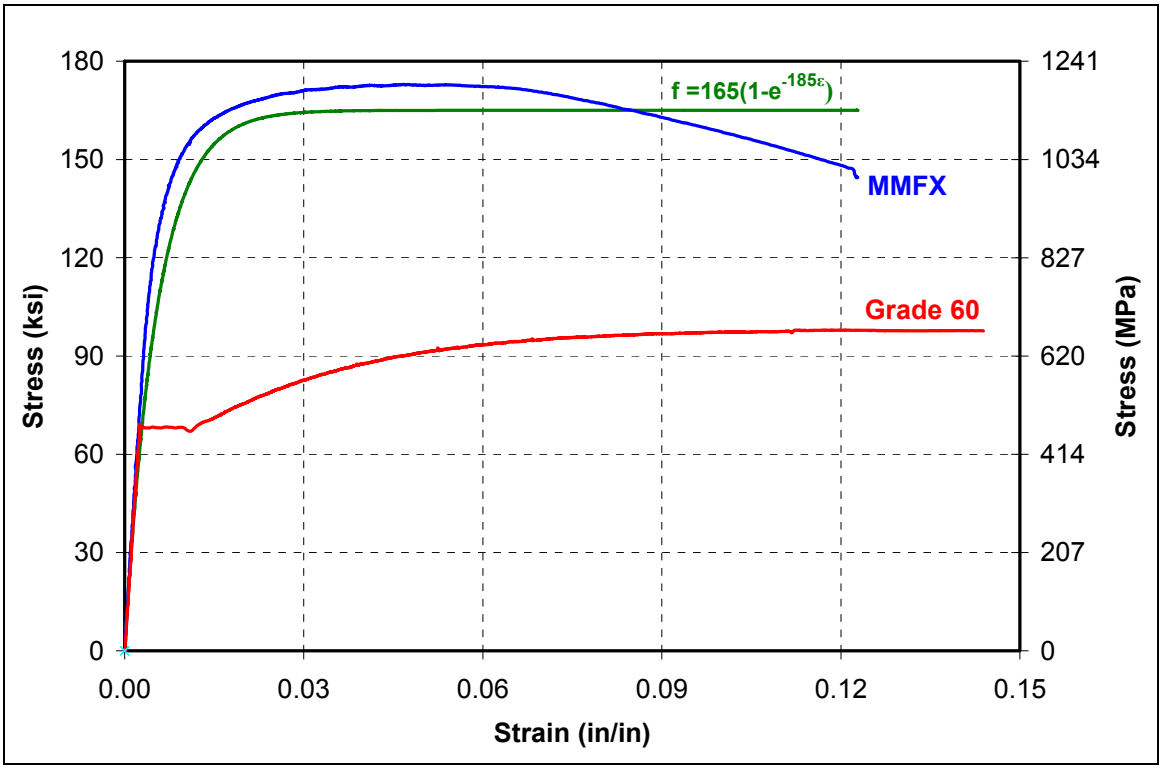

Figure 4-1: Stress-strain Characteristics of Grade 60 and MMFX Steel

.

The measured engineering stress-strain characteristics of the #4 (No. 13) and #5 (No. 16) MMFX bars are shown in detail in Figure 4-2 and Figure 4-3, respectively.

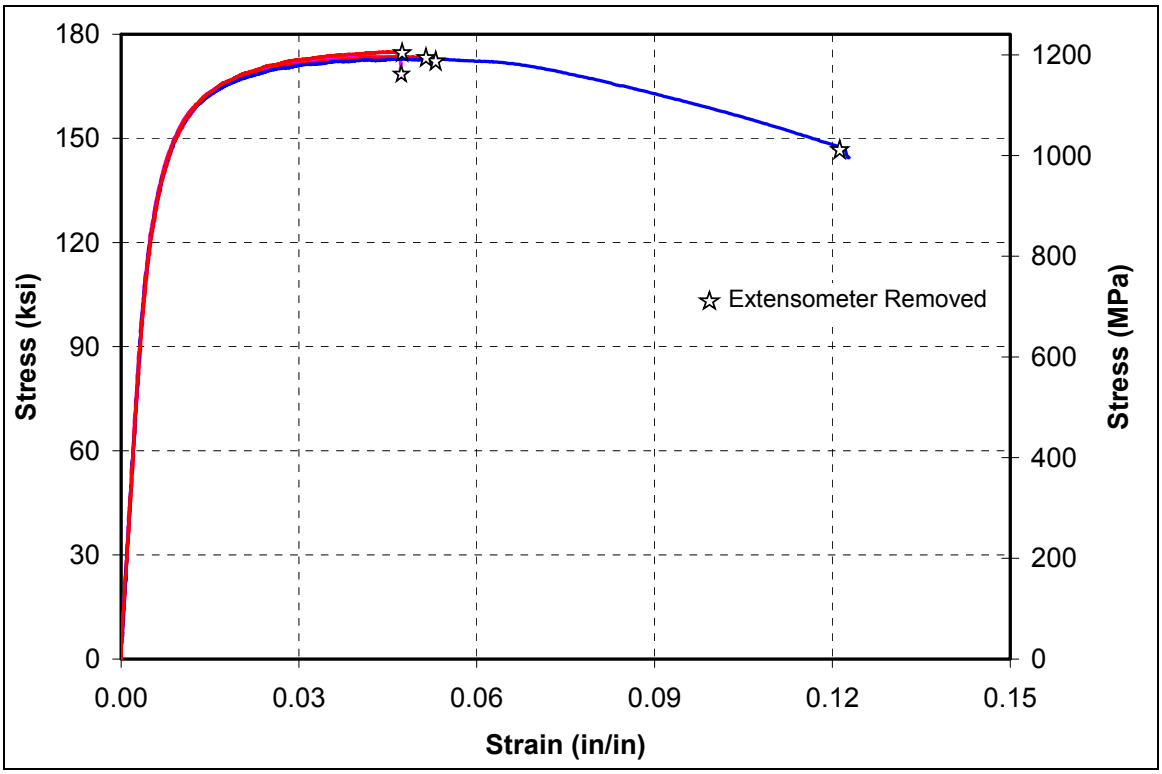

Figure 4-2: Engineering Stress-strain Relationship for #4 MMFX Steel Bars

After the maximum load was reached in all tests, the diameter of the specimen started to decrease, and the reduction of cross-sectional area was clearly visible in one particular location. The behavior, known as "necking," is shown in Figure 4-4. It was observed that rupture occurred along a cone-shaped surface which forms an angle of 45^{o} with the longitudinal axis of the specimen as shown in Figure 4-5.

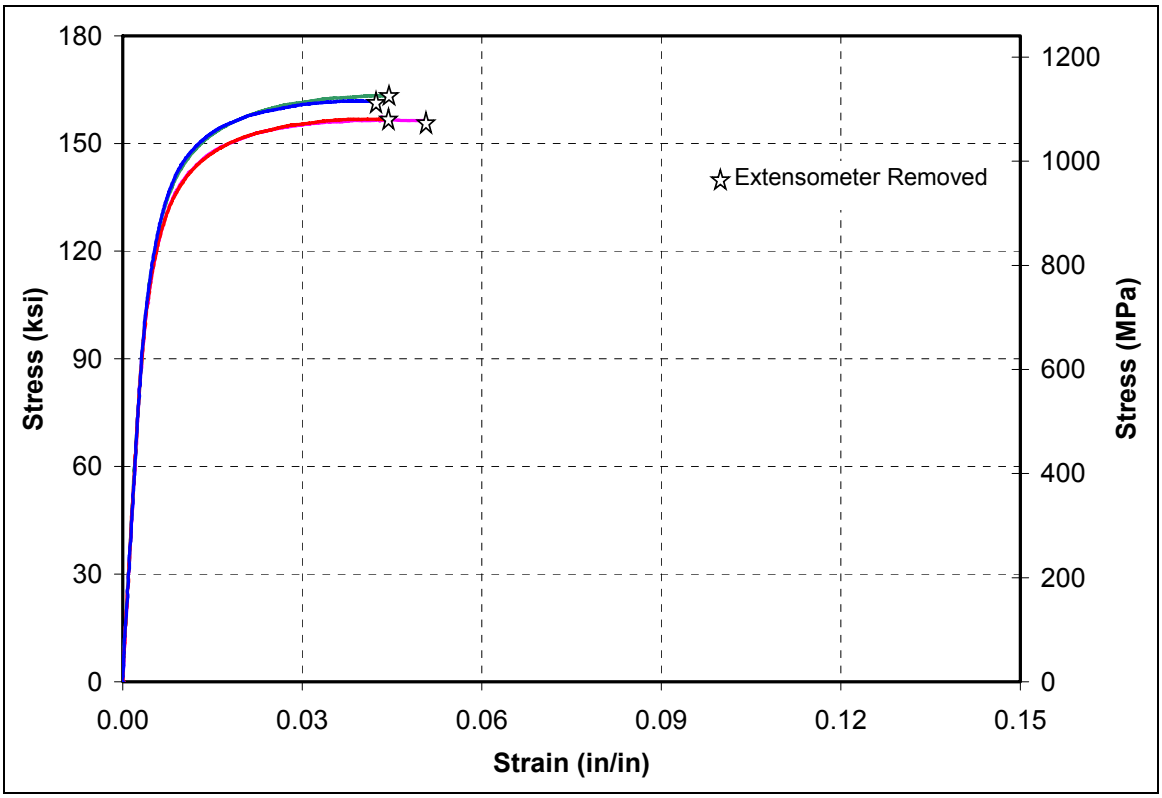

Figure 4-3: Engineering Stress-strain Relationship for #5 MMFX Steel Bars

After rupture of each specimen, the pieces were re-aligned, the final gage length was measured, and the ultimate elongation was recorded. The #4 and #5 bars had an average ultimate elongation of 7.2% and 6.3% in their 8 in gage lengths, respectively. It should be mentioned that necking occurred outside the MTS extensometer (2-in gage length) for all the specimens, except for one #4 (No. 13) MMFX bar. The results from this test were used to obtain the descending branch of the stress-strain curve as shown in Figure 4-2.

Figure 4-4: Necking Inside the MTS Extensometer Gage Length

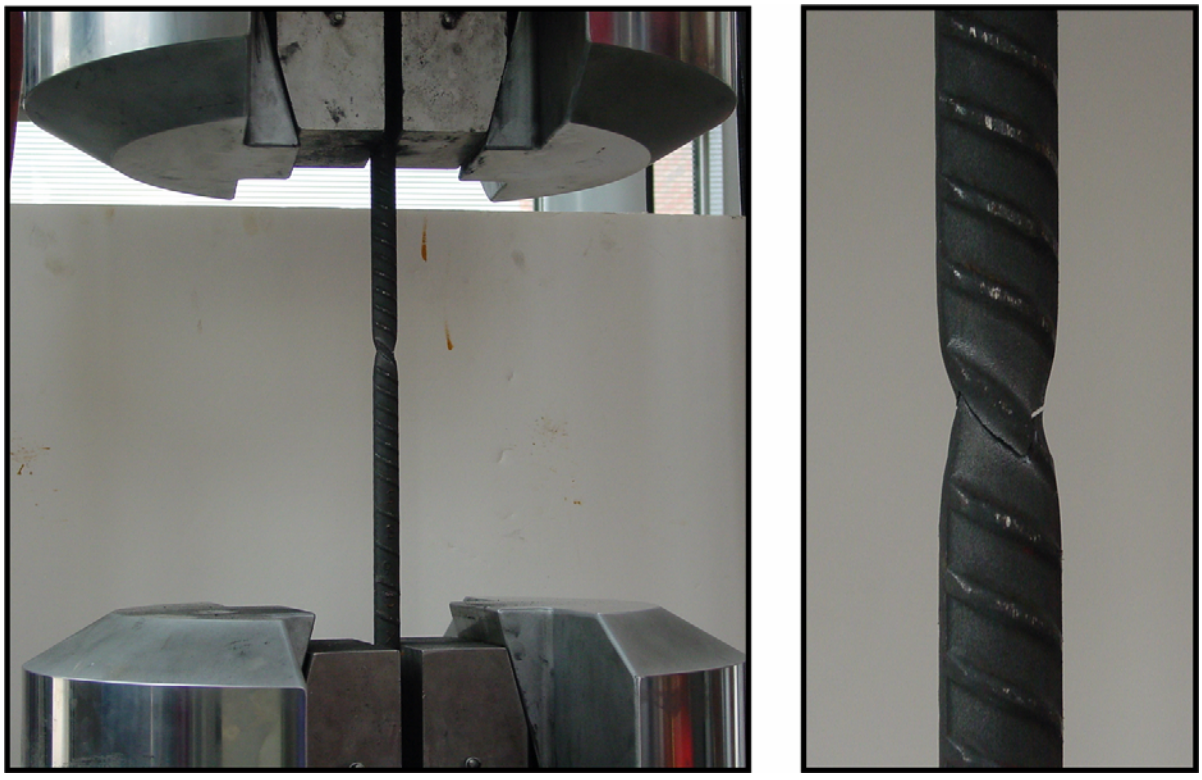

Figure 4-5: Rupture of #5 MMFX Bar After Necking

Concrete

The average concrete compressive strengths on the day of testing for the three bridge decks were 7000 psi, 4500 psi, and 5278 psi (48.2, 31.0, and 36.4 MPa) for the first, second, and third decks, respectively. The concrete compressive strengths were determined using 4x8 in. (102x204 mm) concrete cylinders cast for each deck and cured under the same conditions as the deck. Concrete was provided by a local ready-mixed supplier, and was specified as an NCDOT Standard Class AA mixture with compressive strength of 4500 psi at 28 days. This same specification was used for the actual bridge.

4.3. Failure Modes

General

In general, the behavior of all three bridge decks can be classified as a two-way flexural mode, followed by the development of significant flexural-shear behavior in several spans. Ultimate failure in all three bridge decks was due to punching shear in one or both spans. In the case of the second and third bridge decks, only one of the two loaded spans reached punching capacity. In both of these tests, the right span reached punching capacity prior to the left span. Since the deck was continuous over the middle girder, continued loading on the left span after punching failure in the right only produced excessive flexural-shear deformations. The left spans were unable to reach punching capacity since effective lateral restraint had been lost due to the prior punching failure in the right spans. A summary of failure loads, deflections, and failure modes is given in Table 2.

Table 2: Summary of Test Results

	Span	Maximum Load (kips)	Maximum Deflection (inches)	Failure Mode
First Deck	Left	229	1.84	Punching
	Right	216	1.65	Punching
Second Deck	Left	185	2.18	Flexural-Shear
	Right	204	0.71	Punching
Third Deck	Left	181	1.91	Flexural-Shear
	Right	203	0.97	Punching

First Deck

At the first peak load of the first bridge deck, a gradual drop in the load occurred due to the formation of flexural-shear cracks along the top surface of the bridge deck on both sides of the middle girder, a few inches from the girder face. Further loading led to the widening of those cracks and to a slight increase in the load until punching failure occurred. Punching failure of both spans occurred simultaneously at a load level of 229 kips (1019 N) for the left span and 216 kips (961 N) for the right span. Figure 4-6 and Figure 4-7 show the first bridge deck at the conclusion of the test, where the punching areas underneath the two loading plates can be clearly seen along with the shear cone protruding from the bottom of the left span. This shear cone can be seen in greater detail in Figure 4-8, which shows a section through the shear cone after the bridge deck was cut for removal. This shear cone is perhaps the most recognizable characteristic of a punching shear failure.

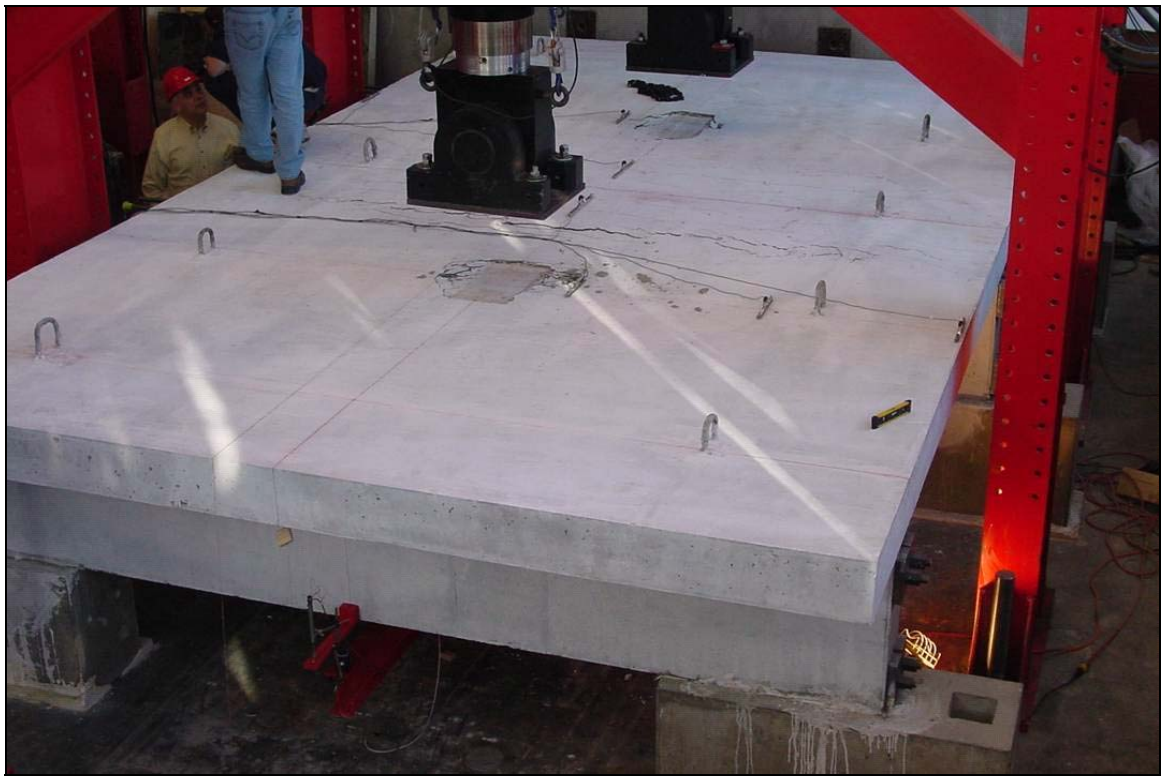

Figure 4-6: First Bridge Deck at the Conclusion of the Test

Figure 4-7: Punching Cone for the Left Span of the First Bridge Deck

Figure 4-8: A Cut Section of the First Bridge Deck Shows Punching Cone

Second Deck

The failure mode of the second bridge deck was similar to that of the first, but punching shear failure did not occur in both spans. At the peak load of the left span, a gradual drop in the load occurred due to the formation of a flexural-shear crack on the top surface of the bridge deck to the left of the middle girder only (in the left span only). This unbalanced drop in load rendered the left span incapable of carrying significantly more load after a loss of lateral restraint due to punching shear failure of the right span. After the punching shear failure in one span, the test was ultimately terminated due to excessive deflections in the left span. The gradual decrease of the load carrying capacity of the left span indicates that flexural-shear failure was the

dominant mode of failure in the left span. The maximum measured load for the left span was 185 kips (823 KN) with a deflection of 2.2 in. (56 mm) prior to termination.

Failure of the right span was due to punching shear at a load level of 204 kips (907 KN). Figure 4-9 shows the second bridge deck after failure, where the punching area under the actuator in the right span, and the flexural-shear crack formed in the left span are both clearly visible.

Figure 4-9: Second Bridge Deck at the Conclusion of the Test

Third Deck

Failure in the third deck was nearly identical to that in the second deck. The right span of the third deck failed in punching shear prior to the left span reaching the punching capacity. A flexural-shear crack formed in the left span only causing a

gradual drop in stiffness of this span, and rendering it incapable of carrying significantly more load. Flexural-shear failure was the mode of failure of the left span, and the test was ultimately terminated due to excessive deflections in the left span. The maximum recorded load for the left span was 181 kips (805 KN) with a deflection of nearly 2 inches.

The right span of the third deck failed in punching shear at a load level of 203 kips. Figure 4-10 shows the third bridge deck at failure, where the punching area under the actuator in the right span, and the flexural-shear crack formed in the left span are clearly visible.

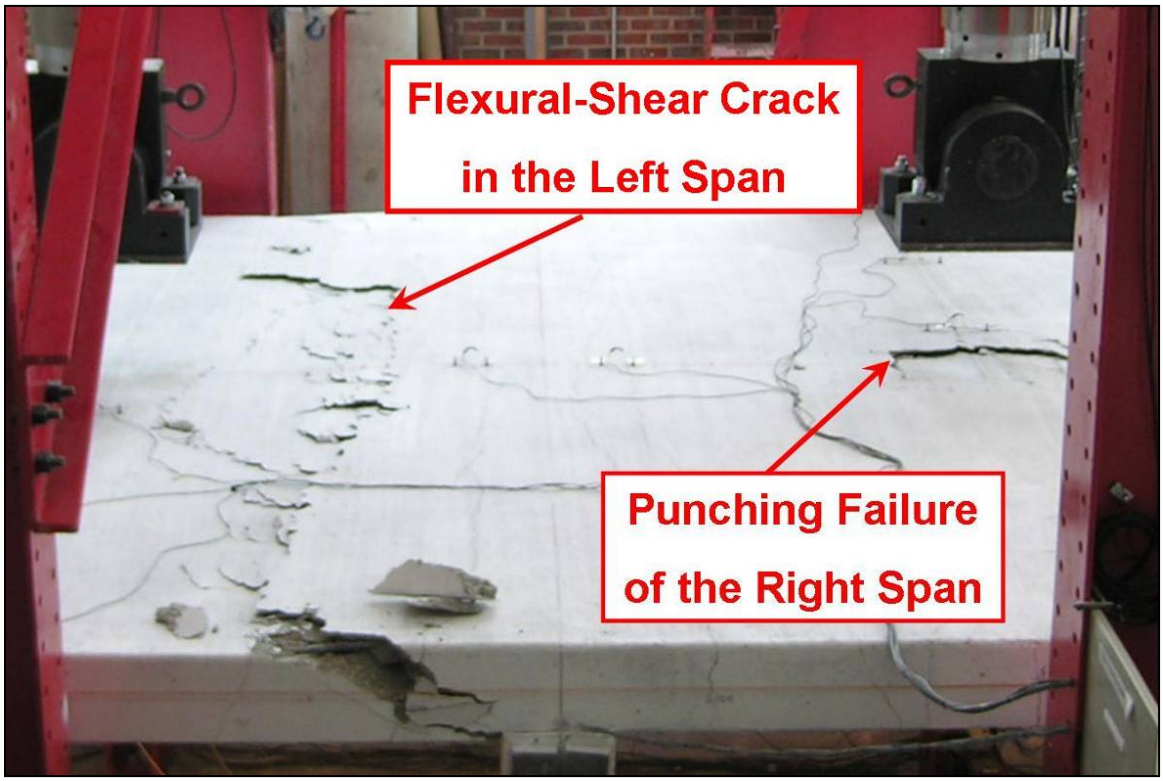

Figure 4-10: Third Bridge Deck at the Conclusion of the Test

4.4. Crack Patterns

The general crack patterns observed for each of the three bridge decks were similar. Cracks developed in the same general fashion at similar load levels for all three tests. Crack patterns were monitored by holding the loading at various increments throughout the test so that cracks could be marked and photographed.

In all three decks, no cracks were observed at a load level corresponding to 50 kips (222 KN) on each span. However, visible top cracks appeared running parallel to the middle girder, a few inches from each face, at a load level of roughly 60 kips (267 KN) for each deck. Figure 4-11 shows these top cracks at a load level of 100 kips (445 KN) for the third bridge deck. The figure is typical of all three decks at that load level. It can be assumed that these negative flexural cracks formed before any positive cracks due to the higher values of negative moments at the center girder in comparison to the positive moments at the center of the spans.

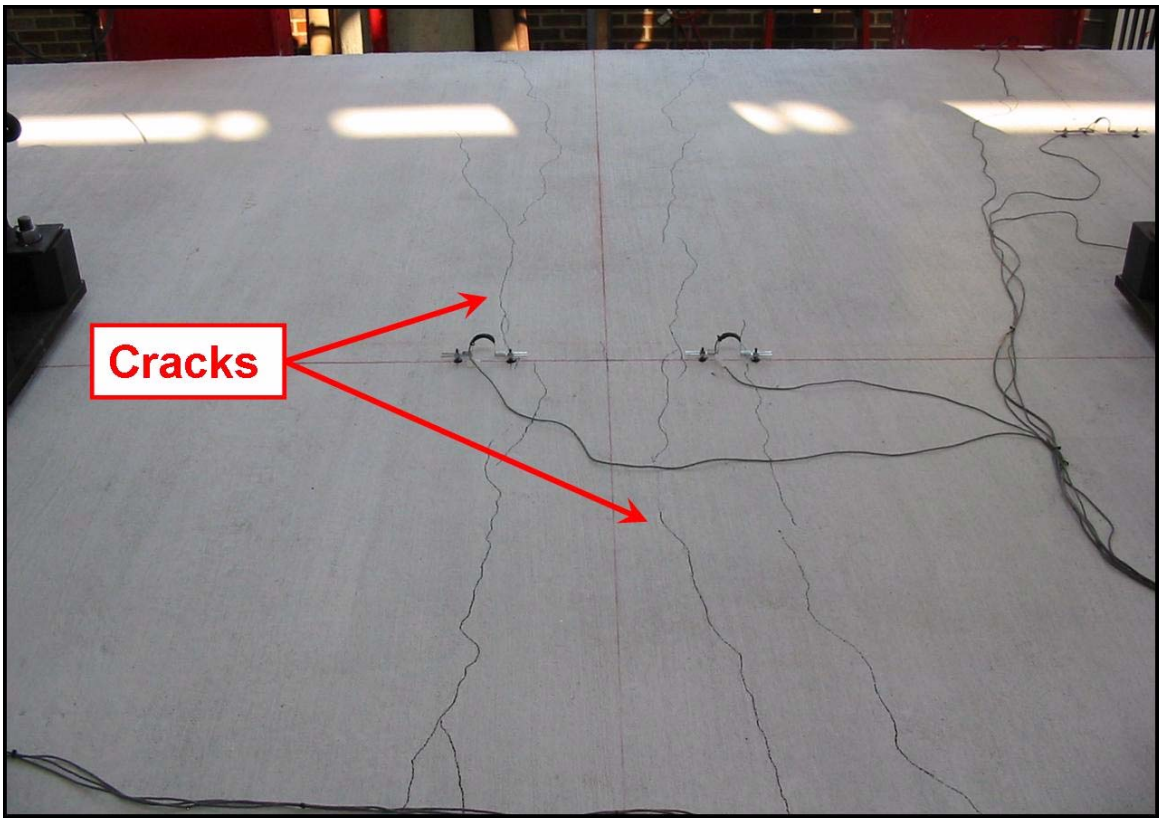

Figure 4-11: Negative Flexural Cracks at 100 kips in Third Deck

Positive moment flexural cracks were clearly developed at load levels of 100 and 150 kips (445 and 667 KN) in all three tests. The cracks at these load levels are shown for the first bridge deck in Figure 4-12 and Figure 4-13. Again, these figures are typical of all three tested decks. The pattern of cracks radiating outward equally in all directions from a point directly under the load confirms that two-way distribution of the load is taking place.

Figure 4-12: Positive Flexural Cracks at 100 kips in First Deck

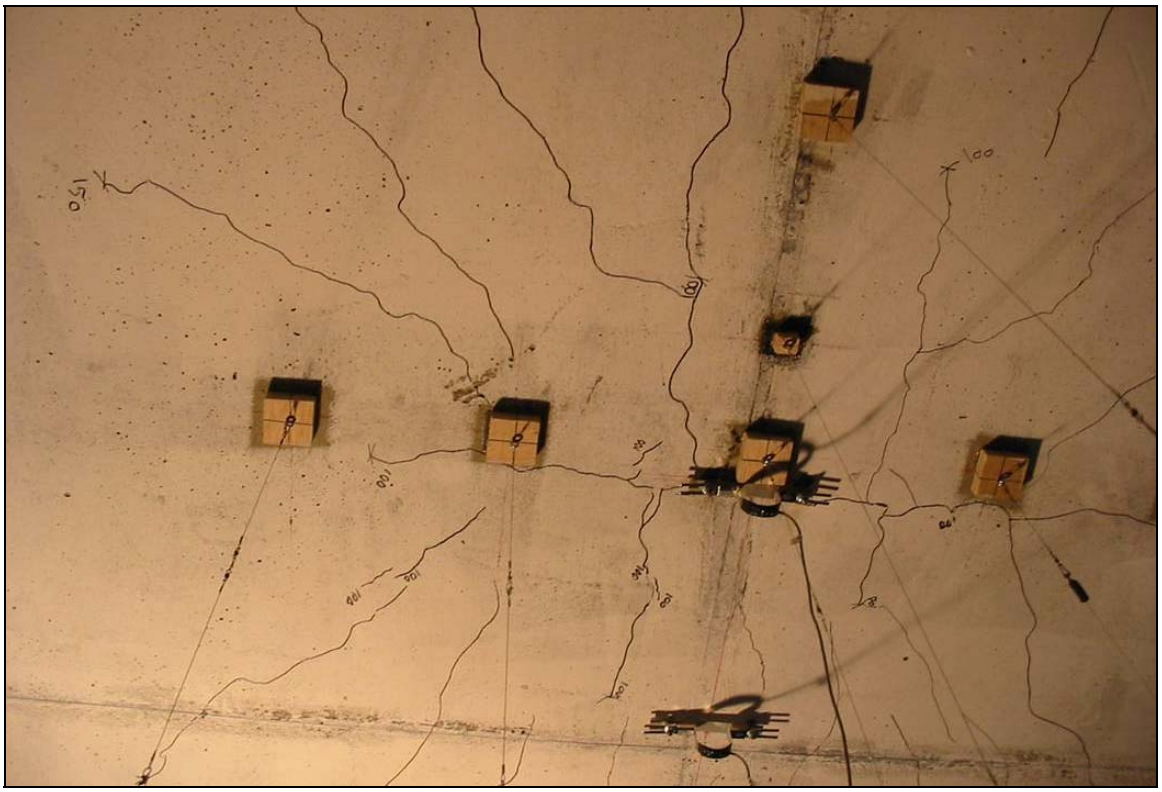

Figure 4-13: Positive Flexural Cracks at 150 kips in First Deck

As loading continued, the negative flexural cracks on the top surface of the slab near the middle girder spread and widened until they developed into flexural-shear cracks. The distinguishing characteristic between the flexural cracks and the flexural-shear cracks was that the concrete on both sides of the flexural cracks was at the same vertical elevation. For the flexural-shear crack however, the concrete on the side of the flexural-shear crack closest to the load was at a noticeably lower elevation than was the concrete on the side of the flexural-shear crack opposite the load. Formation of these flexural-shear cracks led to a gradual drop in load as the stiffness of the spans deteriorated. In the first bridge deck, these flexural-shear cracks formed simultaneously on both sides of the middle girder, as shown in Figure 4-14. This symmetry allowed for a subsequent simultaneous increase of the load on both spans which caused the nearly-simultaneous punching shear failure in both spans.

In the tests of the second and third bridge decks, however, significant flexural-shear cracks developed only on the left side of the middle girder. This allowed the load to remain virtually constant in the left span while continuing to increase in the right span, subsequently causing a punching shear failure in the right span only, as shown in Figure 4-9 and Figure 4-10 above.

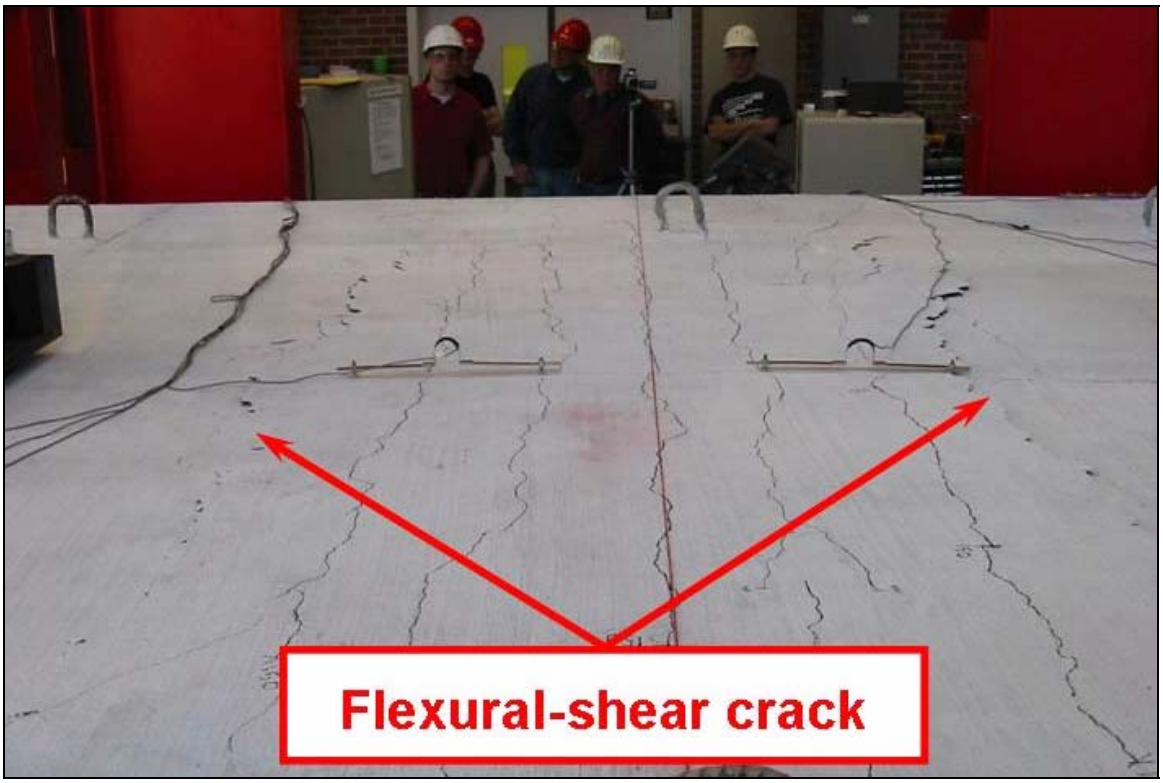

Figure 4-14: Flexural-Shear Cracks in the First Bridge Deck

4.5. Load-Deflection Behavior of Test Specimens

The load-deflection envelopes up to failure for the three bridge decks are given in Figure 4-16 and Figure 4-17 for the left and right spans, respectively. Data in these deflection envelopes are plotted from measurements taken from the bottom of each deck, in the center of each respective deck span, directly underneath the applied load. Loads were monitored using load cells mounted on the hydraulic actuators. In the deflection envelopes, data are plotted for the failure cycle only, and thus, residual deflections may exist at zero load from previous cycles. Figure 4-15 shows the entire load-deflection response for a typical span throughout all loading cycles. Note how subsequent cycles initiate from the residual values of previous cycles, and

then meet those previous cycles at their peak loads. This cyclical behavior was typical of all spans tested, and can bee seen in Figure 4-15 showing the complete load-deflection profile for the right span of the first deck.

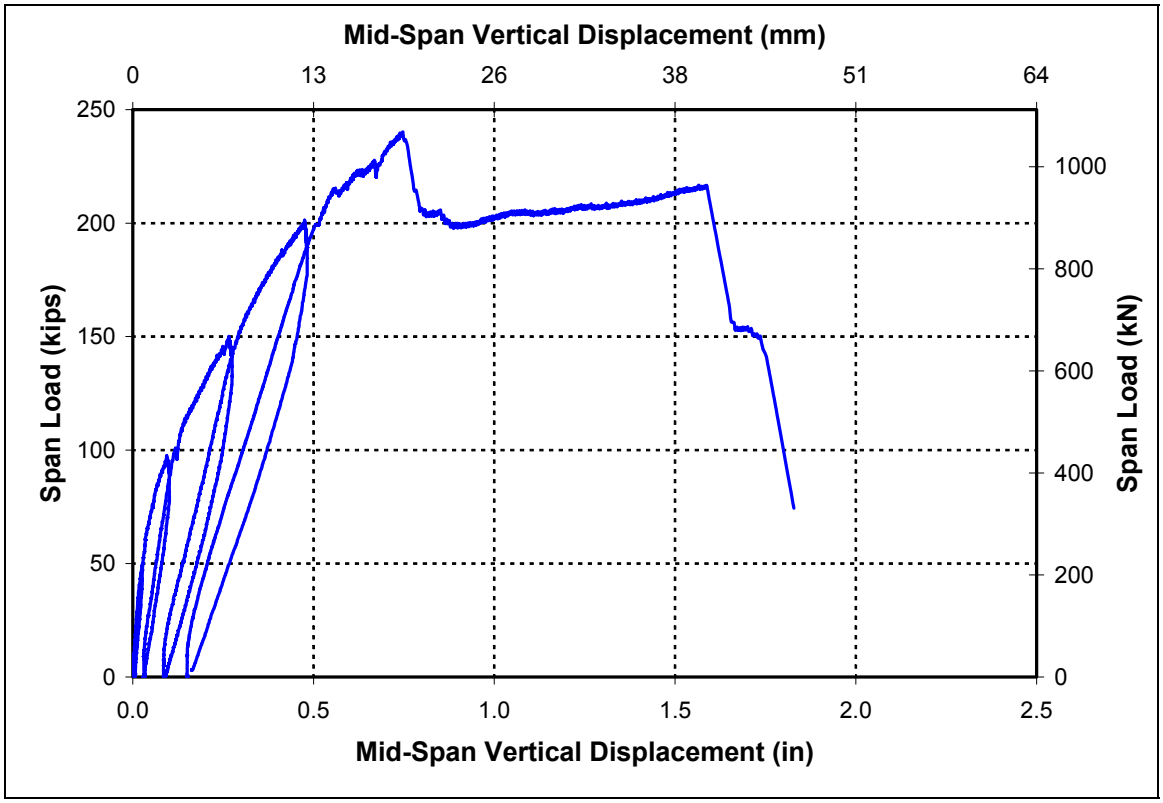

Figure 4-15: Load-Deflection Curve for the Right Span of First Deck

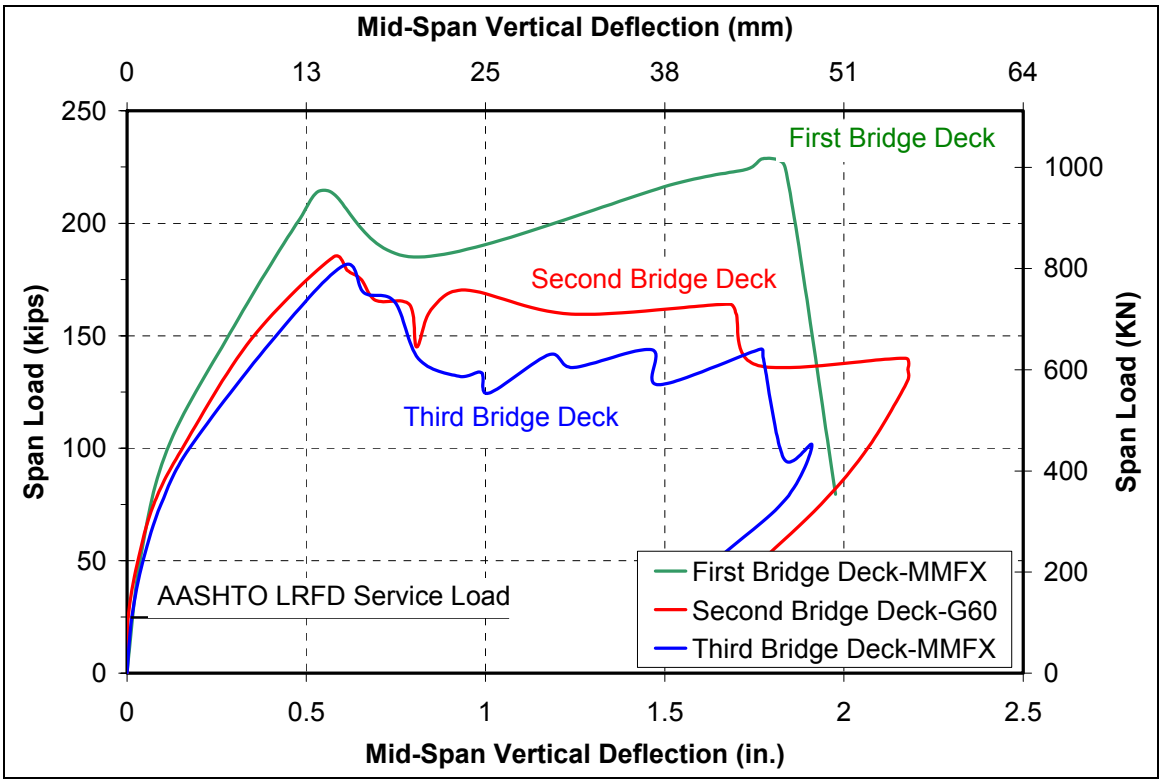

Figure 4-16: Load-Deflection Envelopes for the Left Spans Tested Decks

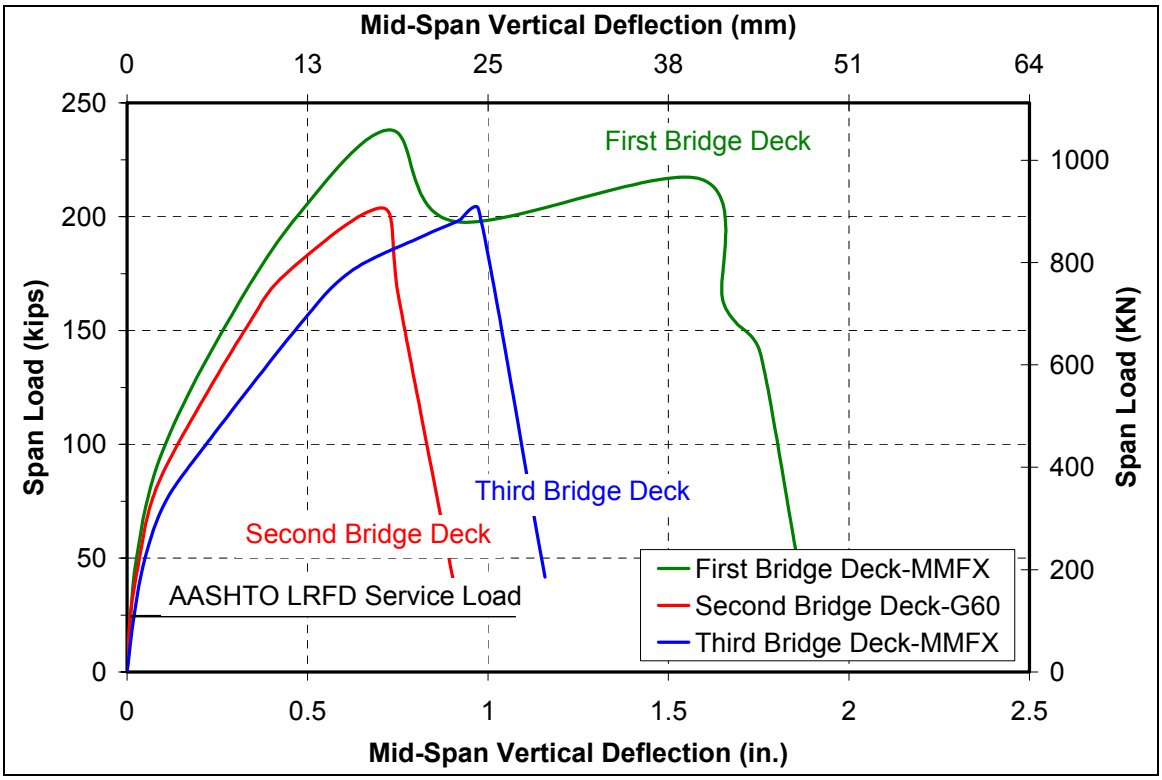

Figure 4-17: Load-Deflection Envelopes for the Right Spans Tested Decks

It is readily apparent from Figure 4-16 and Figure 4-17 that the first bridge deck exhibited smaller deflections than did the other two bridge decks. Recall that the first deck was reinforced with MMFX steel at the same reinforcement ratio as the actual bridge. The higher reinforcement ratio (when compared to the third deck) and the higher strength of the MMFX steel reinforcement (when compared to the second deck) combined to enhance the stiffness of the first deck with respect to the other two. It is important to mention the possibility that the higher stiffness could partially be due to the higher strength concrete used to construct the first deck. Note, however, that the deflections measured for the first deck are lower than those of the other two decks even after significant cracking. Contribution of the concrete strength to the post-cracking stiffness would have been minimal. These reduced deflections are most likely due to the fact that MMFX steel maintains a high elastic modulus well past a tensile stress of 60 ksi.

The above figures also show that despite the lower reinforcement ratio used for the third bridge deck (33 percent less than the first two decks), it was capable of sustaining the same loads at similar deflections as the second bridge deck reinforced with Grade 60 steel. This behavior is attributed to the utilization of the higher tensile strength of MMFX steel. The slight increase in the deflections measured for the third deck over the second deck is possibly due to the slight reduction of the modulus of elasticity of MMFX steel at higher stress levels (well over 60 ksi). These slightly increased deflections are not particularly significant, however. Recall that the AASHTO LRFD design tandem consists of a pair of 25 kips (111 KN) axles. At a load level of 25 kips (111 KN), which is less than the cracking load, the

service load deflection was identical for the three bridge decks. Even at a load level of 50 kips (still less than visible cracking), the measured vertical deflections at midspan of all three decks are still nearly identical at roughly 0.05 inches (less than the span divided by 2100). Thus, load-deflection behavior at service load was more than satisfactory for all three decks, since the most stringent AASHTO deflection criteria applied to concrete decks is span divided by 1200 (AASHTO, 2005).

In examining the load-deflection envelopes, the differences between spans which failed prior to significant flexural-shear cracking and those that failed after are readily apparent. In Figure 4-17, the load-deflection envelopes of the right spans of decks two and three peak and then drop off suddenly. These two spans failed in punching shear prior to the development of significant flexural-shear cracking. Note, however, that even though the drop in load was sudden for these two spans, deflections nearing 0.75 inches for the second deck, and 1 inch for the third deck were recorded prior to failure. This indicates that both spans exhibited at least some degree of nonlinear, ductile behavior. The right span of the third deck with reduced amount of MMFX steel actually provided more ductility prior to failure than did the right span of the conventional Grade-60 steel reinforced deck.

The load-deflection profiles of spans which exhibited significant flexural-shear cracking are more elongated than are the profiles from the punching only spans. The load-deflection behavior of the left span of the first bridge deck, shown in Figure 4-16, is an excellent example of flexural-shear action prior to punching failure. The load carrying capacity of the deck reached a peak before a gradual drop, and then a gradual increase in load was recorded. The changes in load post-peak are

accompanied by drastic increases in deflections, as the flexural-shear cracks develop and widen. Ultimately, the span failed in punching shear, as is shown by the last sudden drop in load carrying capacity. The right span of the first bridge deck has a load-deflection envelope nearly identical to that of the left.

The third type of load-deflection envelope seen in the above figures is that corresponding to the left spans of the second and third bridge decks. These two spans developed significant flexural-shear cracks, but did not fail in punching shear. The corresponding right span in each case did fail in punching shear, but did not develop significant flexural-shear cracks (as is discussed above). This behavior created an imbalance in stiffness across the middle girder. This imbalance prevented the left spans from reaching their punching capacities. The load-deflection envelopes show the gradual decrease in load following a peak, accompanied by the drastic increases in vertical deflection seen with flexural-shear behavior. Notice, however, that there is no sudden, dramatic drop in load for either of these spans. These spans even recovered slightly as load was released after terminating the test due to excessive deflections.

4.6. Deflection Profiles of Test Specimens

Deflection profiles along the transverse direction (perpendicular to the girders) of the three bridge decks are given in Figure 4-18 through Figure 4-23. The profiles shown for zero applied load represent the residual deflections from previous loading cycles. Deflection profiles are plotted for the failure cycle only. Note that the figures are all of a North-South view, with a section of the deck sketched above each graph

to assist the reader in visualizing the position at which each measurement was taken. Downward deflections are plotted as negative, and upward deflections are plotted as positive. The slab was assumed to have zero deflection immediately prior to applying load with the actuators. Note that deflections of the loaded spans are all downward while deflections of the unloaded cantilevers are all upward.

The deflection profiles indicate that the maximum deflection occurred at the mid-spans underneath the applied loads. Also, it is clear that the spans which failed in punching shear prior to developing a pronounced flexural-shear crack (right spans of decks two and three) exhibited significantly lower deflections than the spans which failed after the development of a flexural-shear crack.

The maximum deflections recorded for all spans in which a flexural-shear crack developed was nearly 2 inches. Deflections at service loads, however, were significantly less. At a load level of 50 kips, deflections were minimal. Maximum recorded values at this level of loading did not even reach 0.25 inches. This deflection is less than span length divided by 430. Note that the load level of 50 kips far exceeds the design service load on the bridge. Recall that the AASHTO design truck has an axle loading of 32 kips – a load which is spread out over two wheels. Even if the design tandem were considered, the 50 kips axle loading is spread over four discrete points in the tandem situation. The 50 kip load level discussed here would represent a fictitious situation in which an entire design tandem were concentrated on a single loading area. Thus, the 50 kip load level, which was reached early in the testing procedure, represents a situation which far exceeds any condition the bridge is likely to experience in service.

In the two spans that failed in punching shear prior to developing flexural-shear cracking (the right spans of decks two and three), the measured deflections just prior to failure were less than half of the nearly two inches seen in the other spans. In fact, the right span of the second deck deflected less than 0.75 inches just prior to punching failure at a load exceeding 200 kips. At the load level of 50 kips, deflections in these spans were similar to those of the spans ultimately exhibiting flexural-shear cracking behavior. This similarity is predictable since none of the three bridge decks showed any visible cracking at the 50 kip load level.

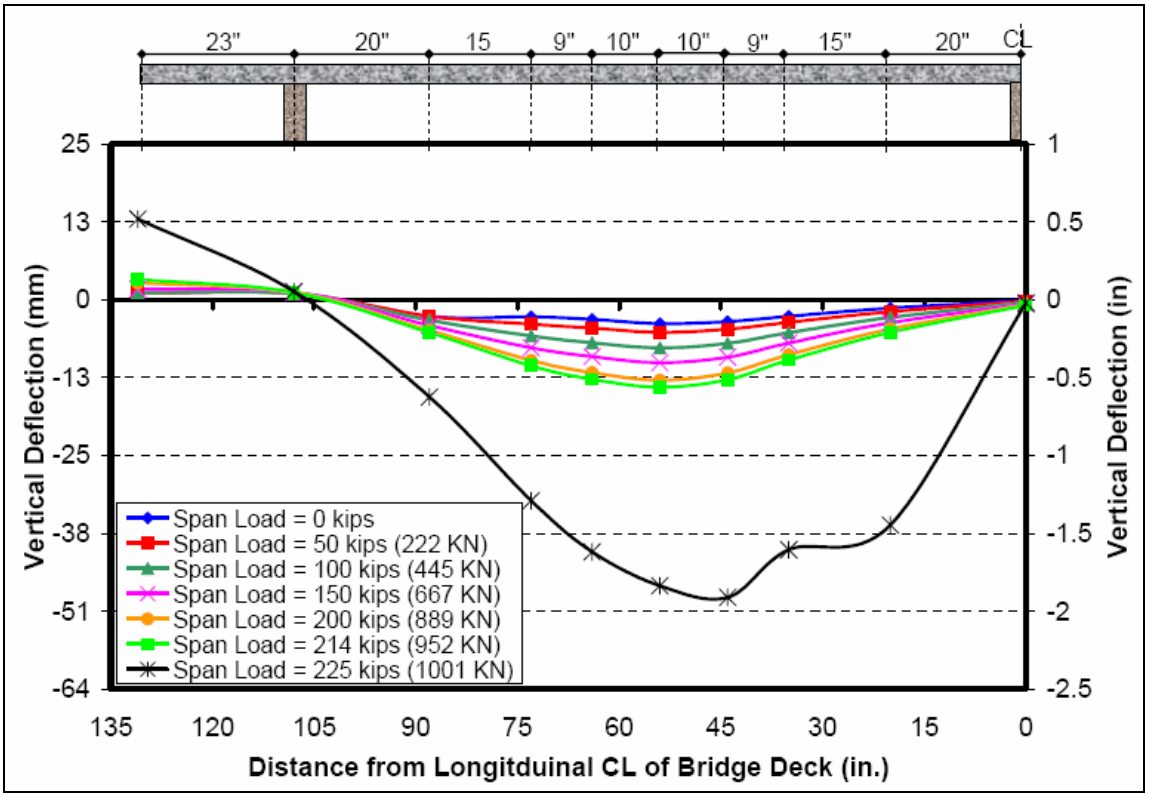

Figure 4-18: Transverse Deflection Profile for Left Span of First Deck

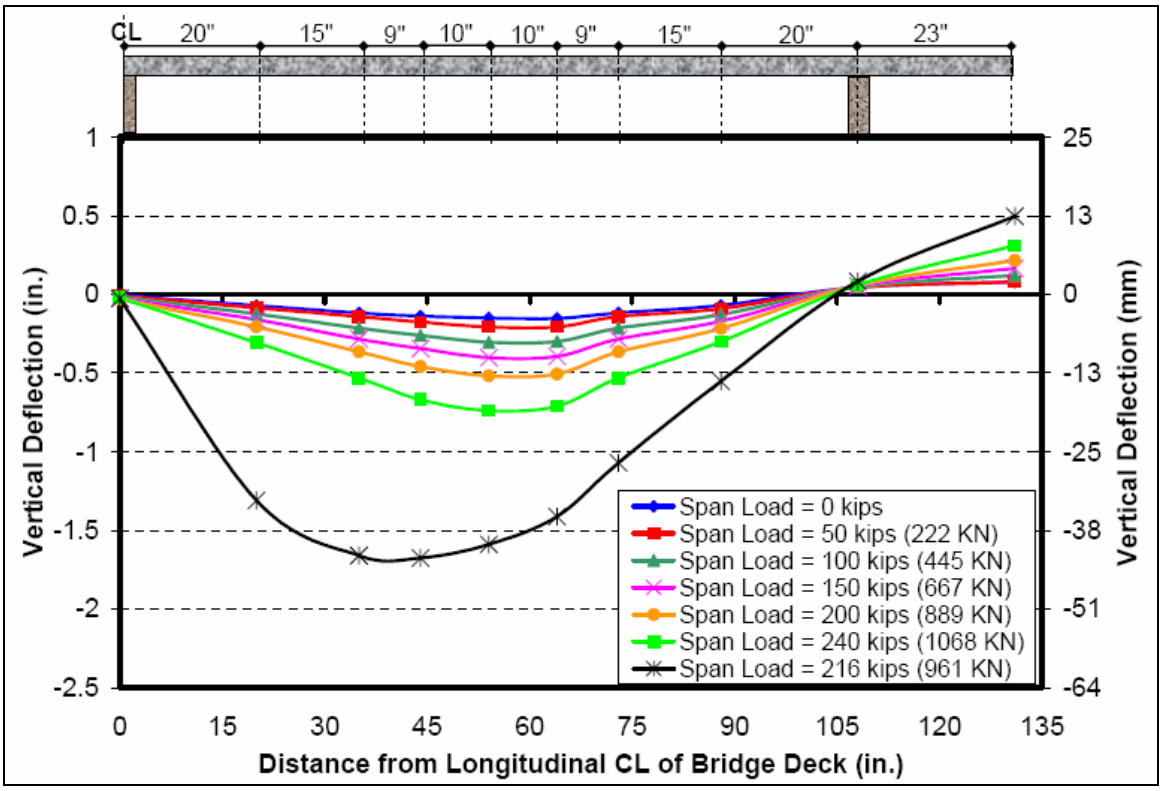

Figure 4-19: Transverse Deflection Profile for Right Span of First Deck

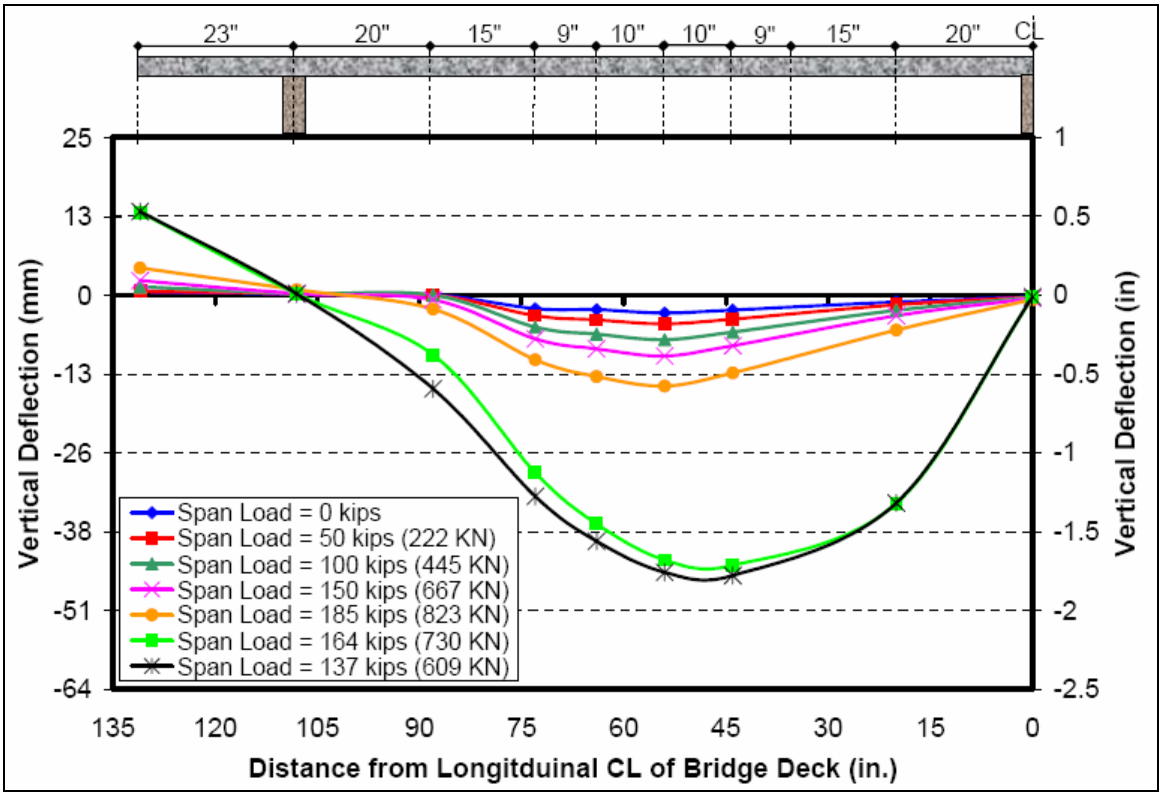

Figure 4-20: Transverse Deflection Profile for Left Span of Second Deck

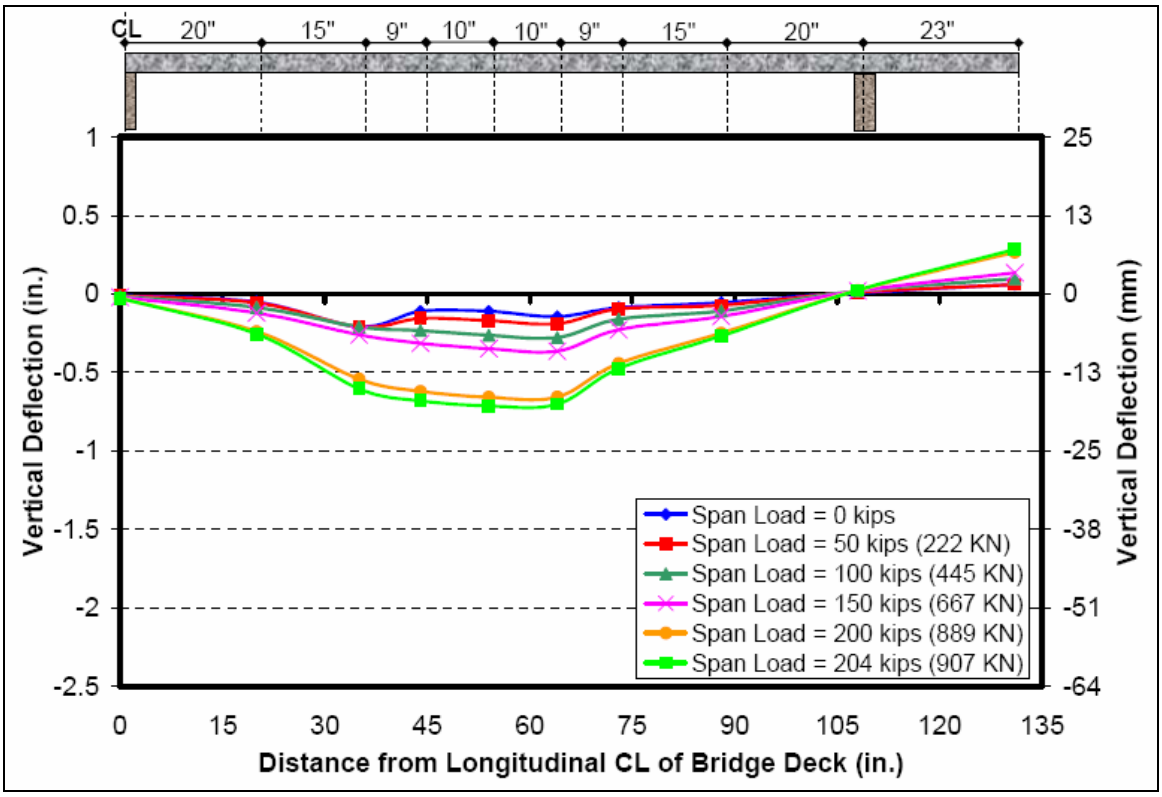

Figure 4-21: Transverse Deflection Profile for Right Span of Second Deck

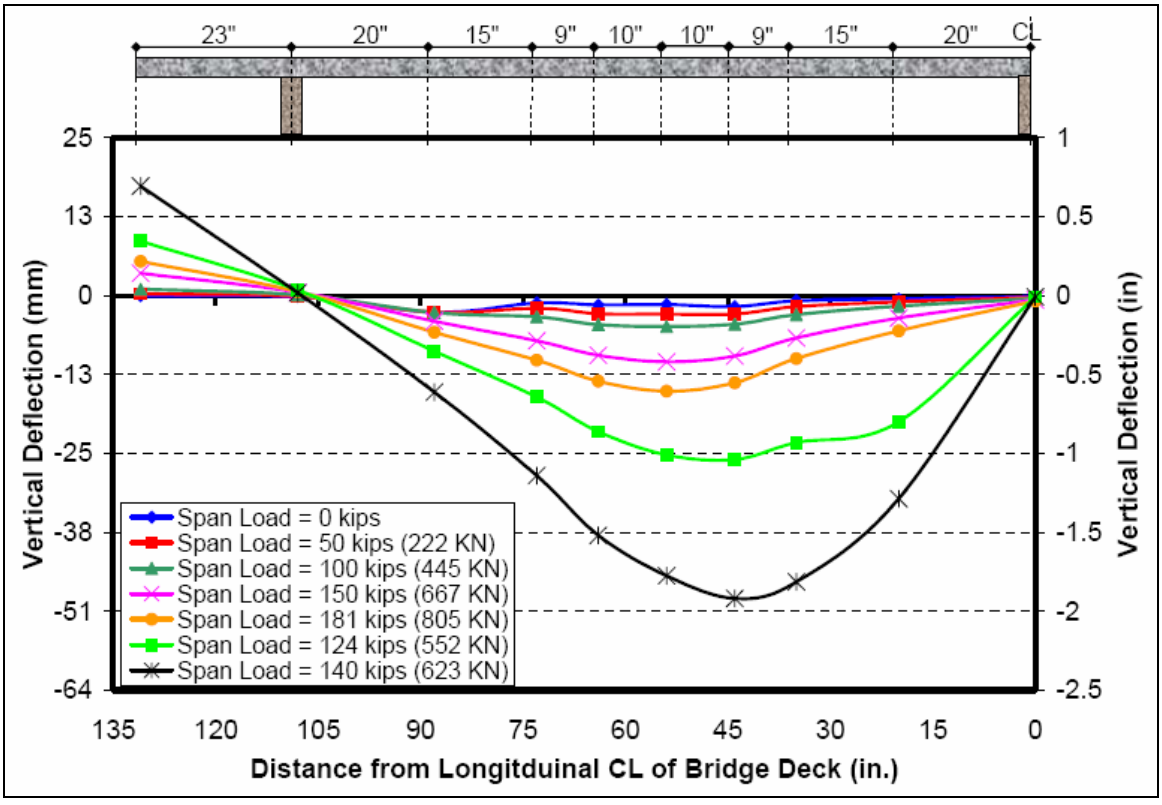

Figure 4-22: Transverse Deflection Profile for Left Span of Third Deck

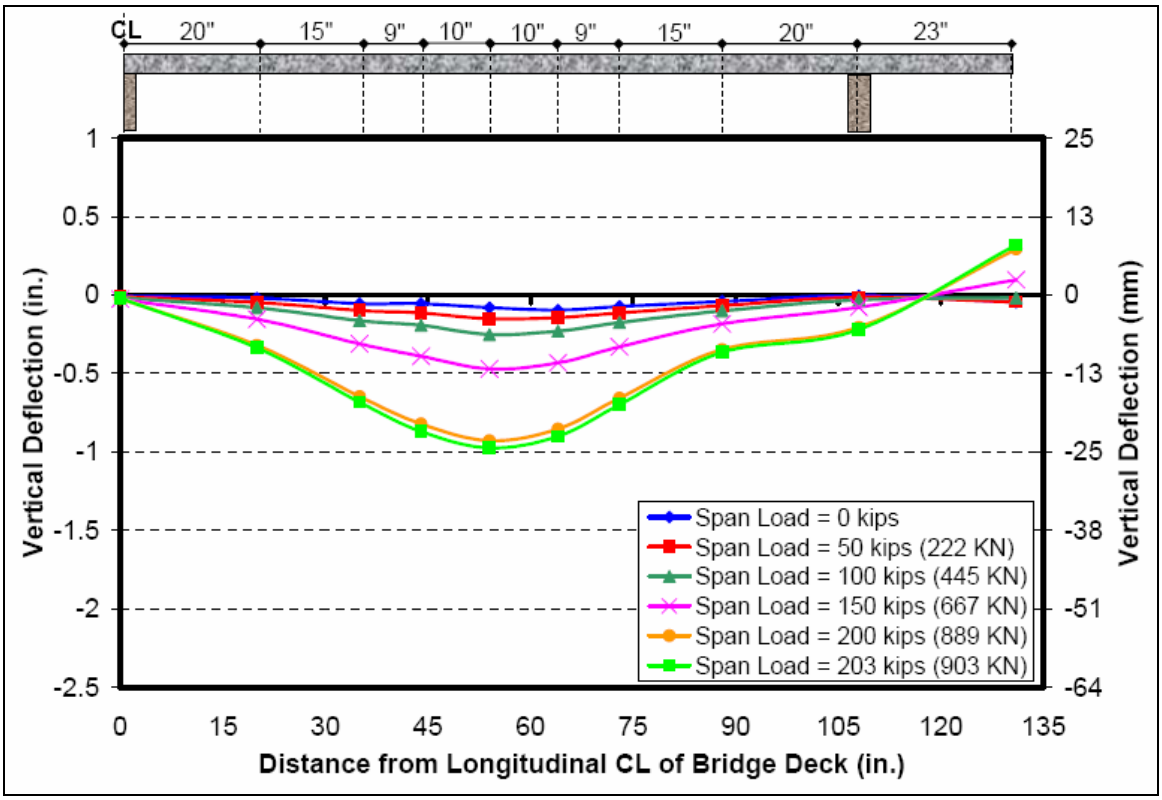

Figure 4-23: Transverse Deflection Profile for Right Span of Third Deck

Deflection profiles plotted along the longitudinal direction (parallel to the girders) of the three bridge decks are shown in Figure 4-24 through Figure 4-29. These profiles are plotted using the same conventions that were used in above figures corresponding to transverse profiles. Again, a section of the tested deck is sketched above each deflection profile to assist in visualizing where the measurements were taken.

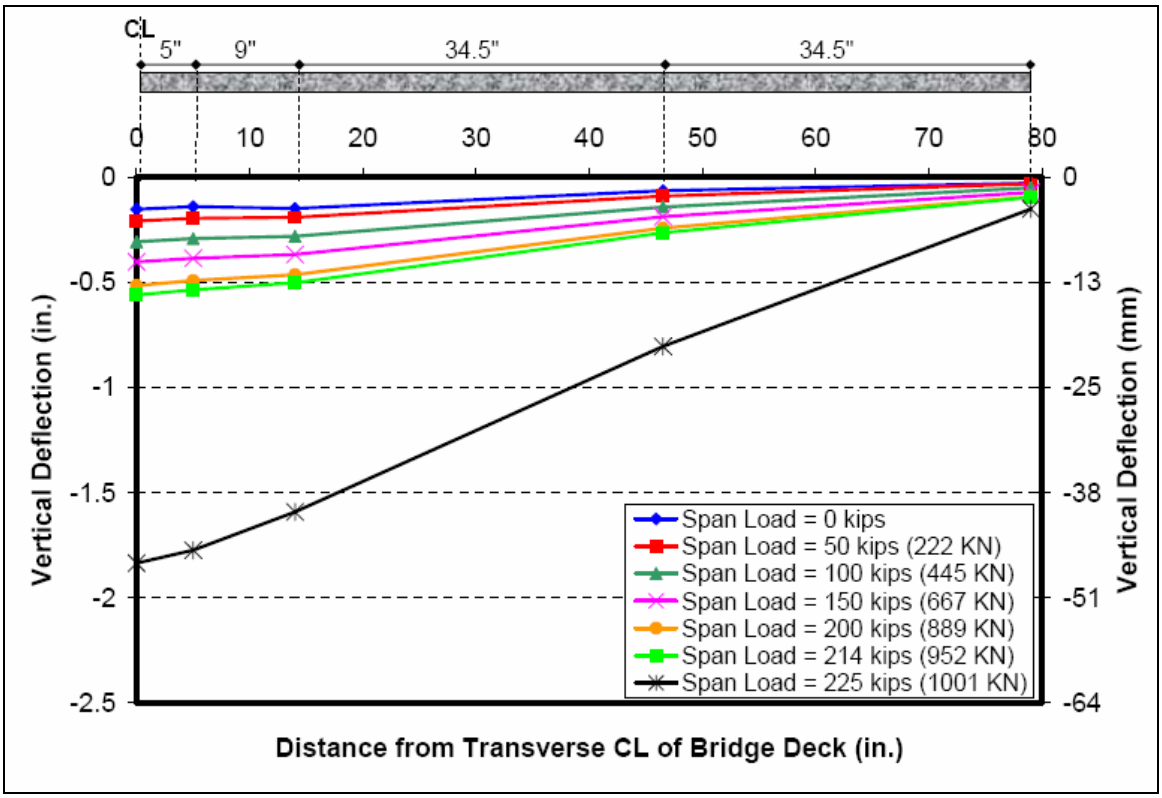

Figure 4-24: Longitudinal Deflection Profile for Left Span of First Deck

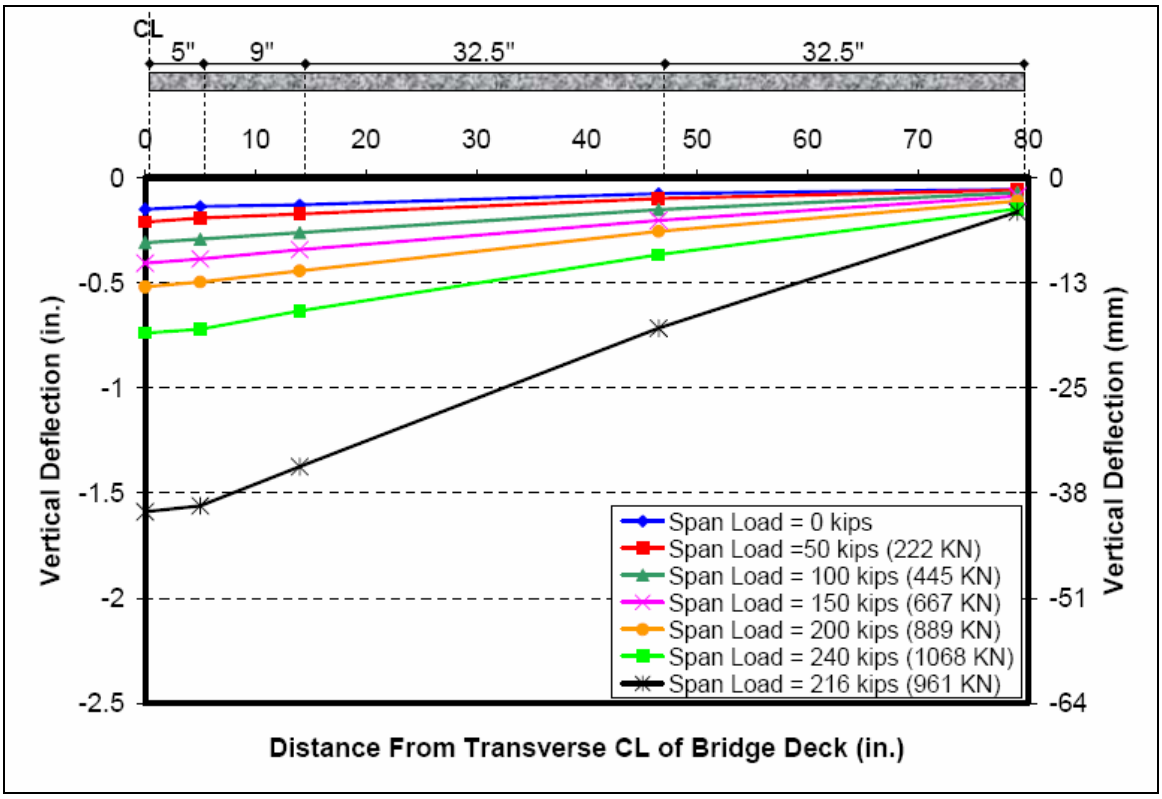

Figure 4-25: Longitudinal Deflection Profile for Right Span of First Deck

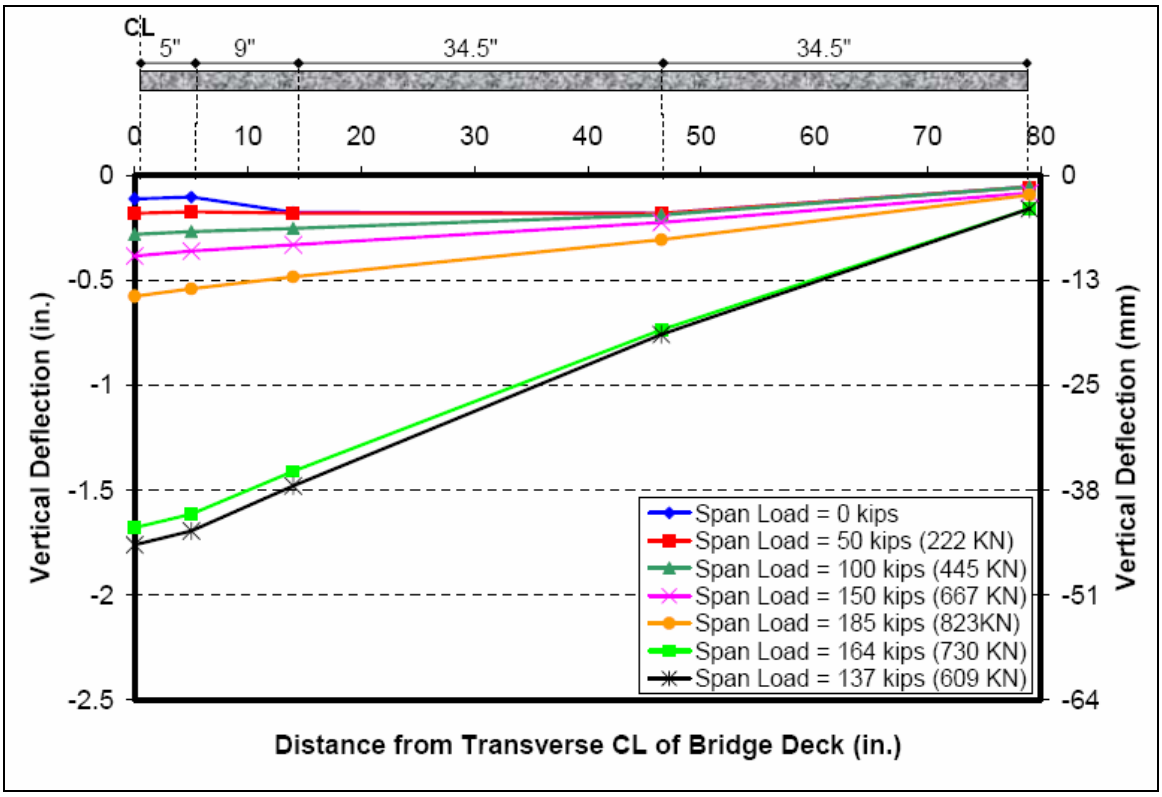

Figure 4-26: Longitudinal Deflection Profile for Left Span of Second Deck

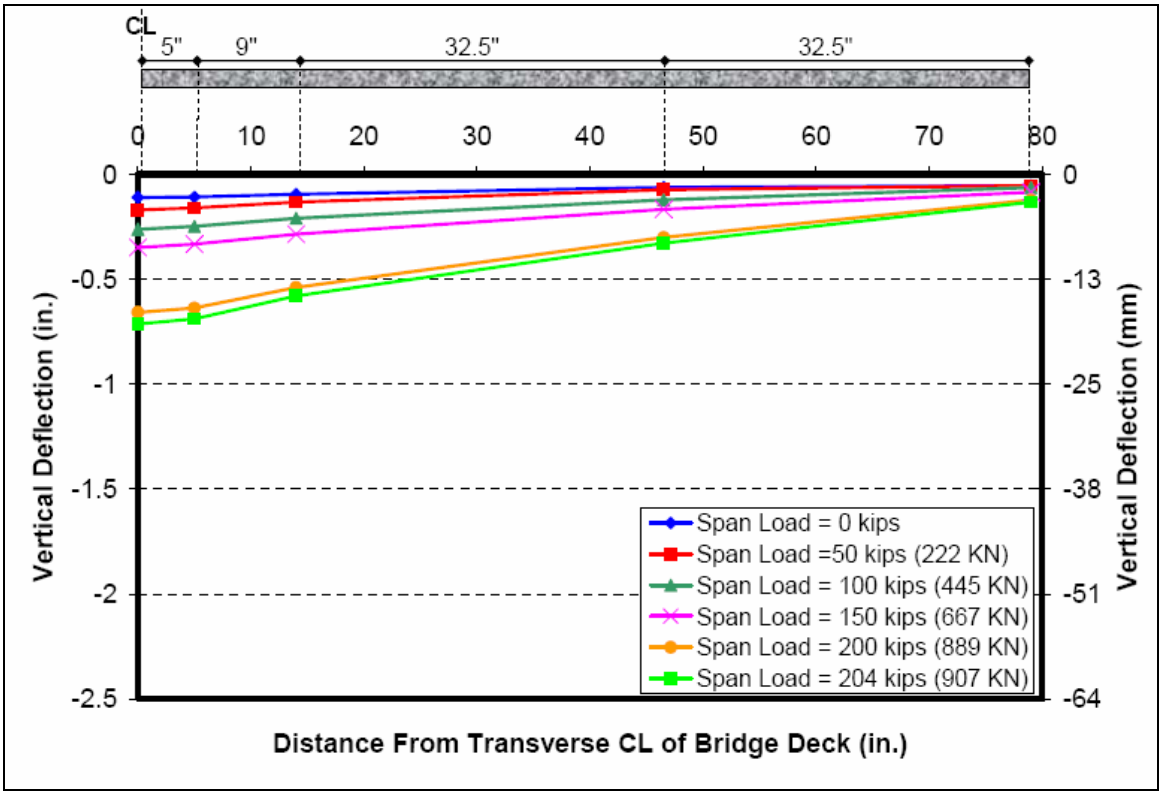

Figure 4-27: Longitudinal Deflection Profile for Right Span of Second Deck

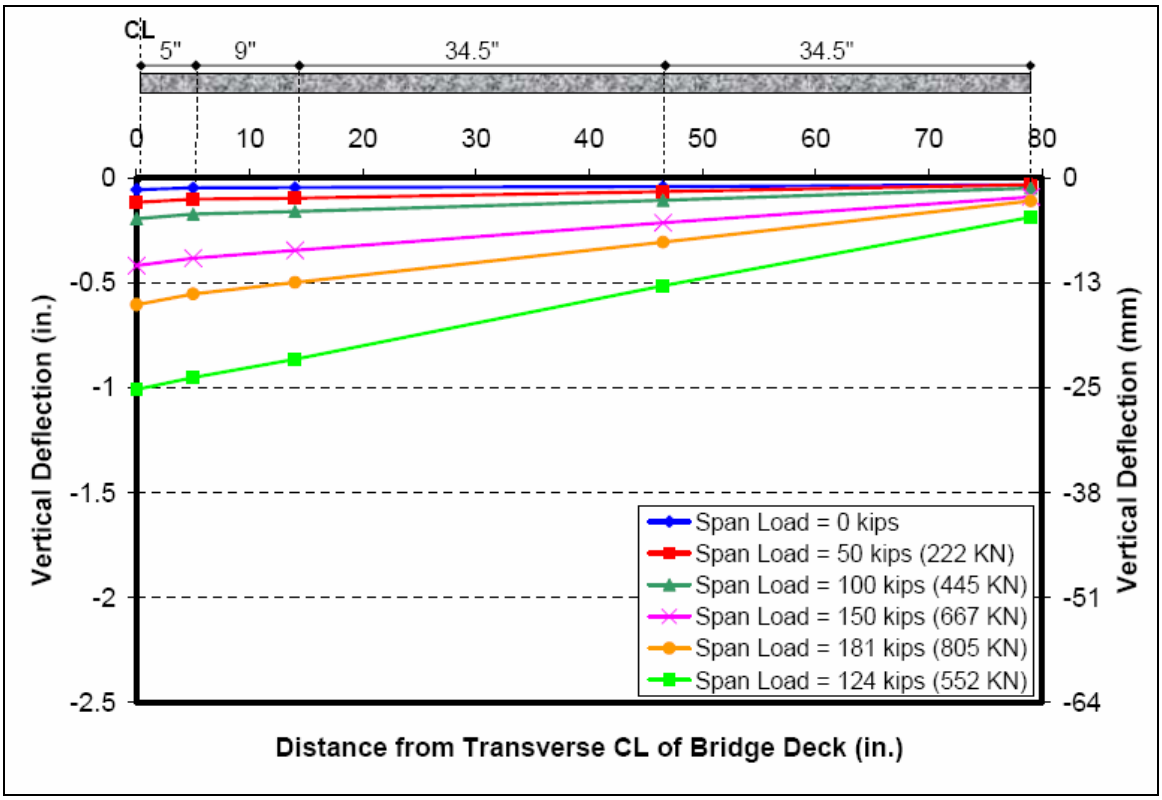

Figure 4-28: Longitudinal Deflection Profile for Left Span of Third Deck

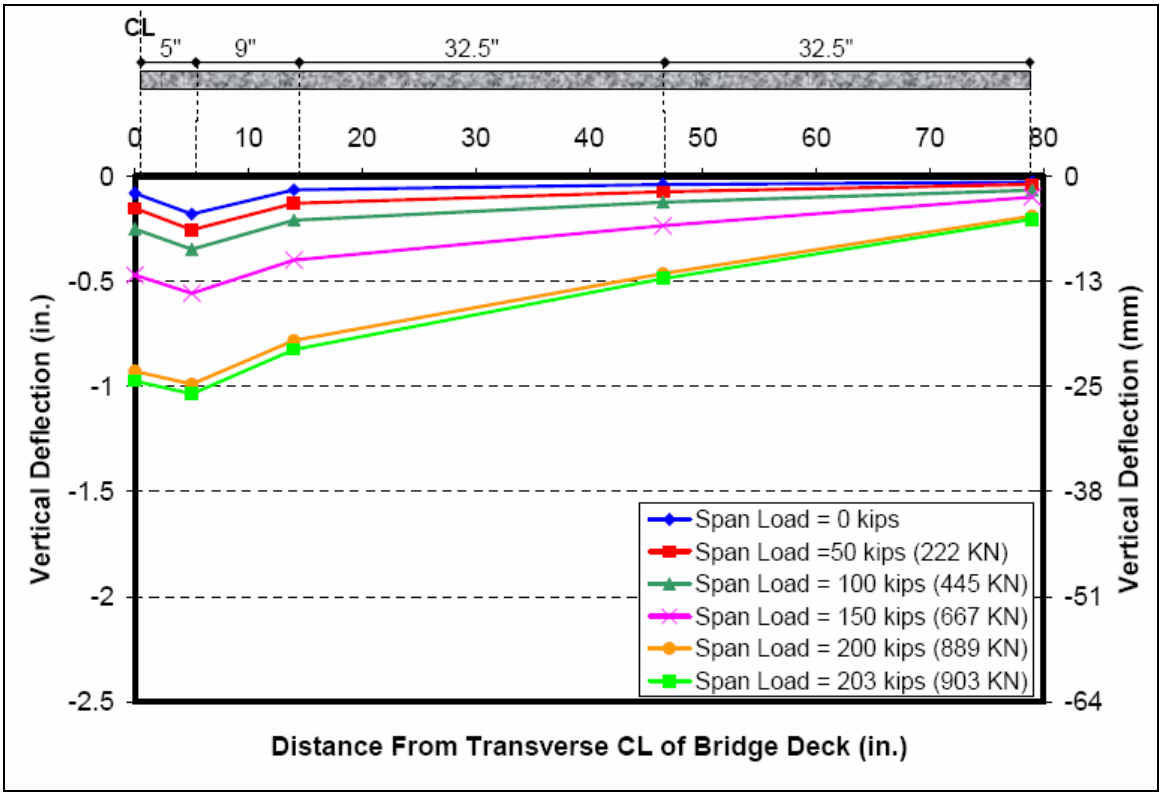

Figure 4-29: Longitudinal Deflection Profile for Right Span of Third Deck

The most significant feature of the longitudinal deflection profiles is that the deflections measured at the edges of each deck were very small in all cases. This minimal edge deflection confirms that the length of the tested decks was appropriately selected. The small deflections indicate that two-way slab action is taking place, and that the behavior of the test models is representative of the actual bridge.

4.7. Concrete Strain Profiles

Strain profiles over the depth of the concrete slabs were determined using the strains measured by pairs of PI gages at the extreme top and bottom fibers of each bridge deck. It was assumed that plane sections remained plane over the thickness of the deck. Strain profiles are plotted for the final loading cycle only, so residual strains from previous cycles may exist at zero load. A positive strain value indicates tension, and a negative value indicates compression. The strain profiles obtained from two PI gages (T6 and B10) located on the right spans of the three decks are shown in Figure 4-31 through Figure 4-33. Figure 4-30 shows the location of PI gage T6 with respect to the punching area of the first bridge deck. PI gage B10 is located directly below T6 on the underside of the deck, and is not visible in the photograph.

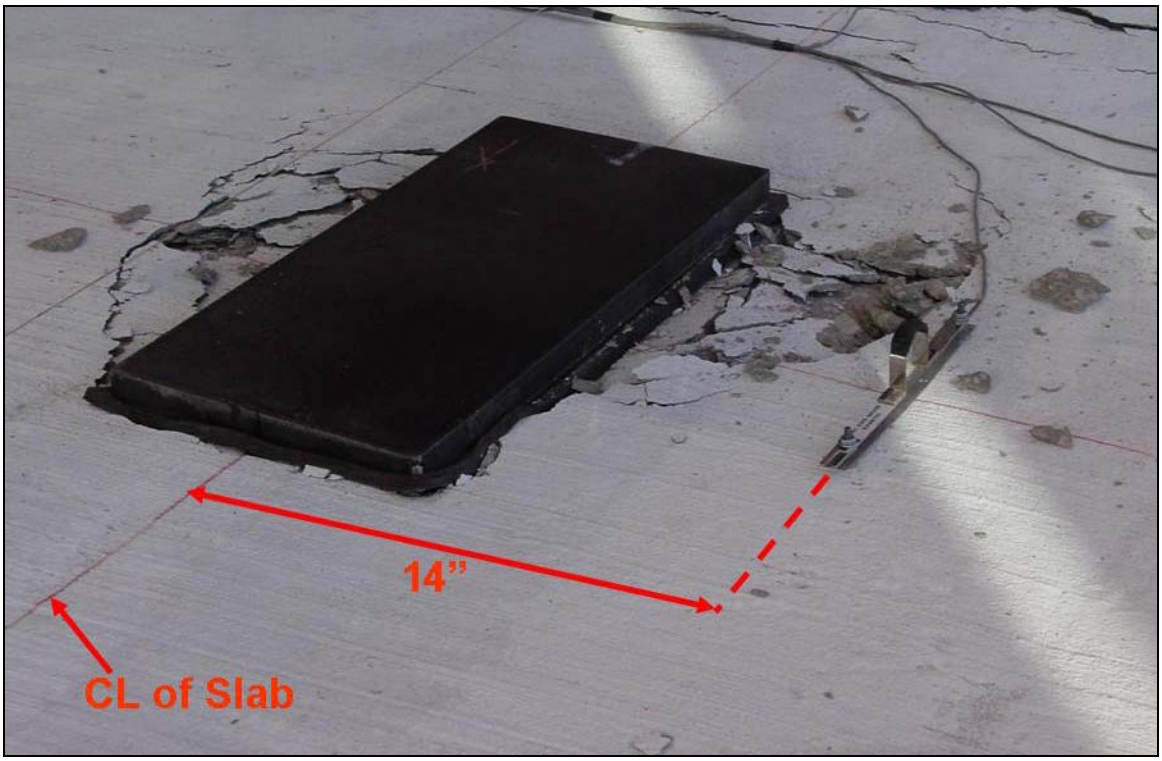

Figure 4-30: Location of PI Gage T6

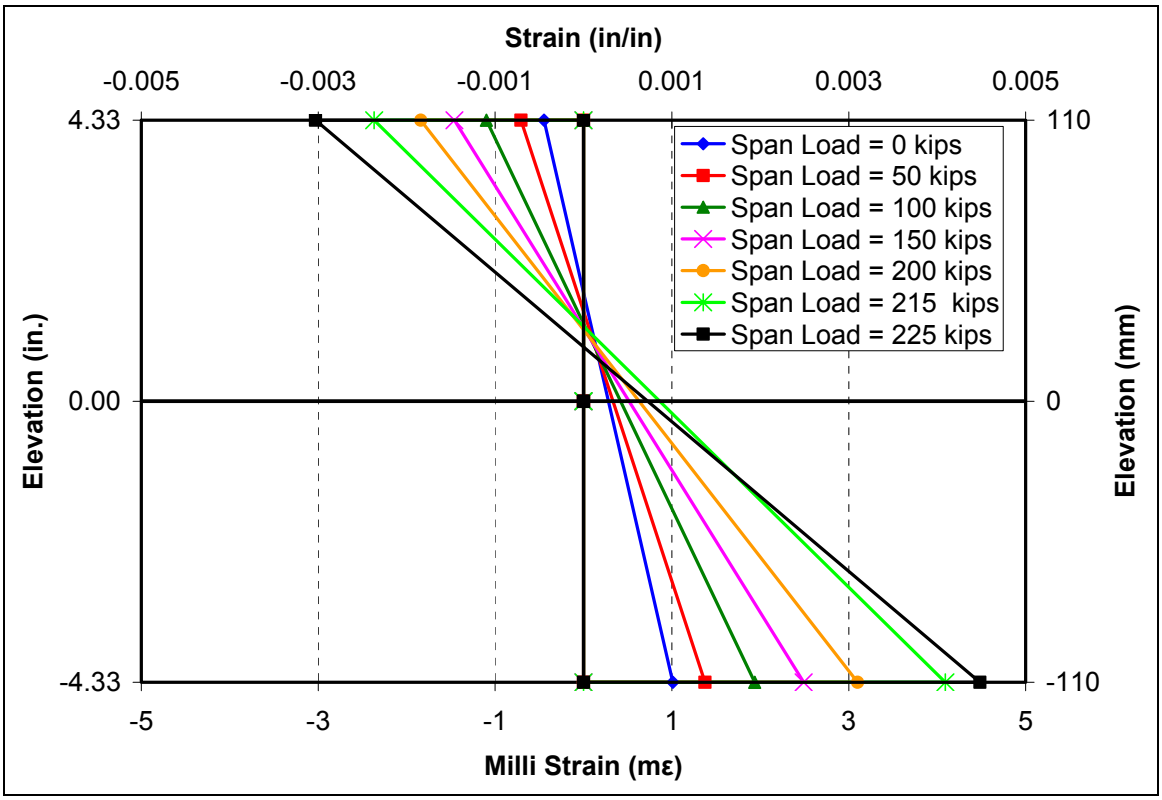

Figure 4-31: Strain Profiles from PI gages T6 and B10 First Deck

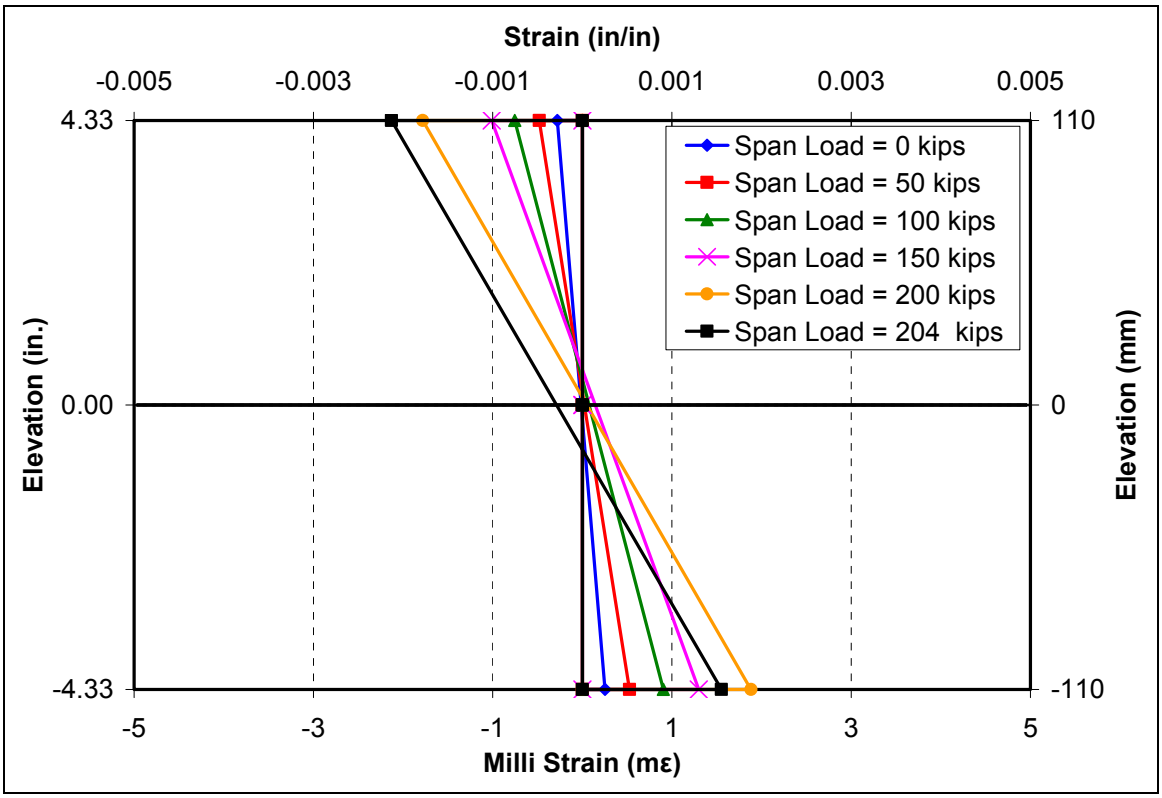

Figure 4-32: Strain Profiles from PI Gages T6 and B10 Second Deck

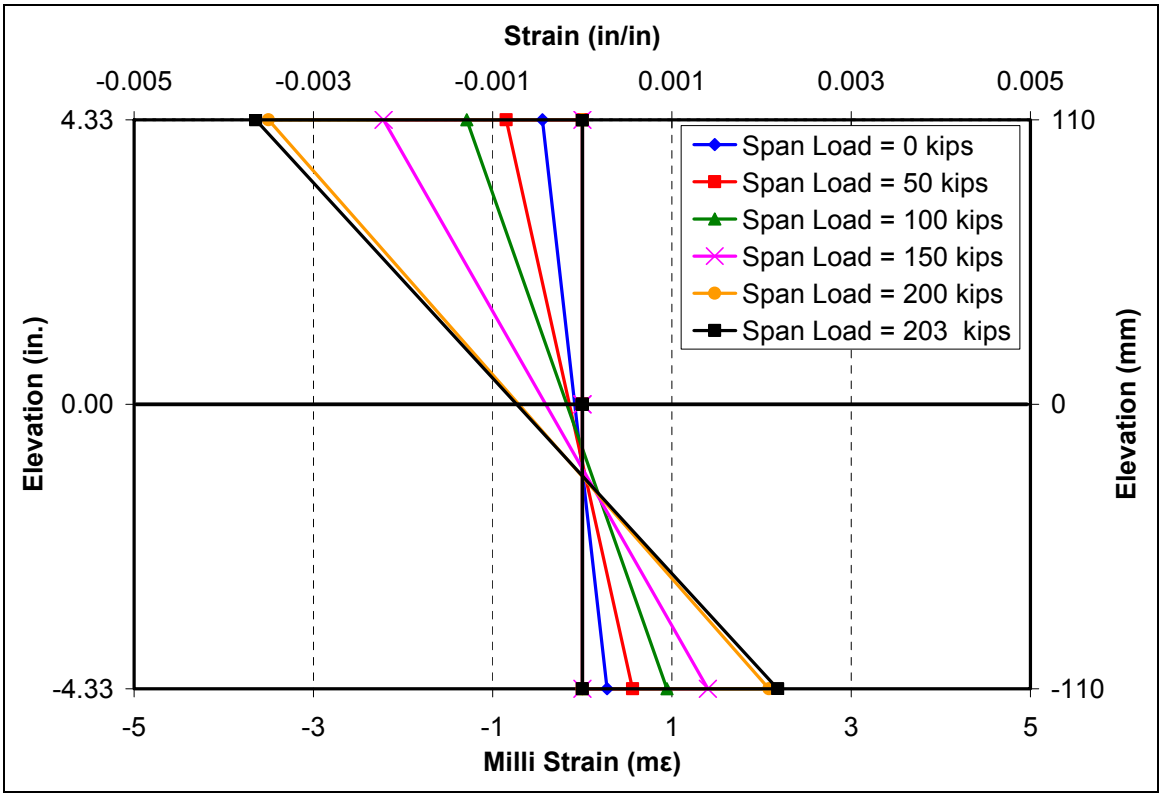

Figure 4-33: Strain Profiles from PI Gages T6 and B10 Third Deck

Strain profiles obtained from the PI gages T8 and B12 are shown in Figure 4-34, Figure 4-35, and Figure 4-36 for the three bridge decks, respectively. These gages are located at the outer edge of the right span, centered between the girders. Refer to Figure 3-10 for detailed gage locations. Gage T8 is located on the top of the deck and B12 is located directly beneath T8 on the bottom of the deck. The strain profiles for the three decks show that the strain values in these locations were very small, especially in compression. This finding is another indication that two-way slab action is taking place, and that the selected length of the bridge deck is representative of the actual bridge behavior. Strain profiles from the rest of the gages are provided in Appendix A.

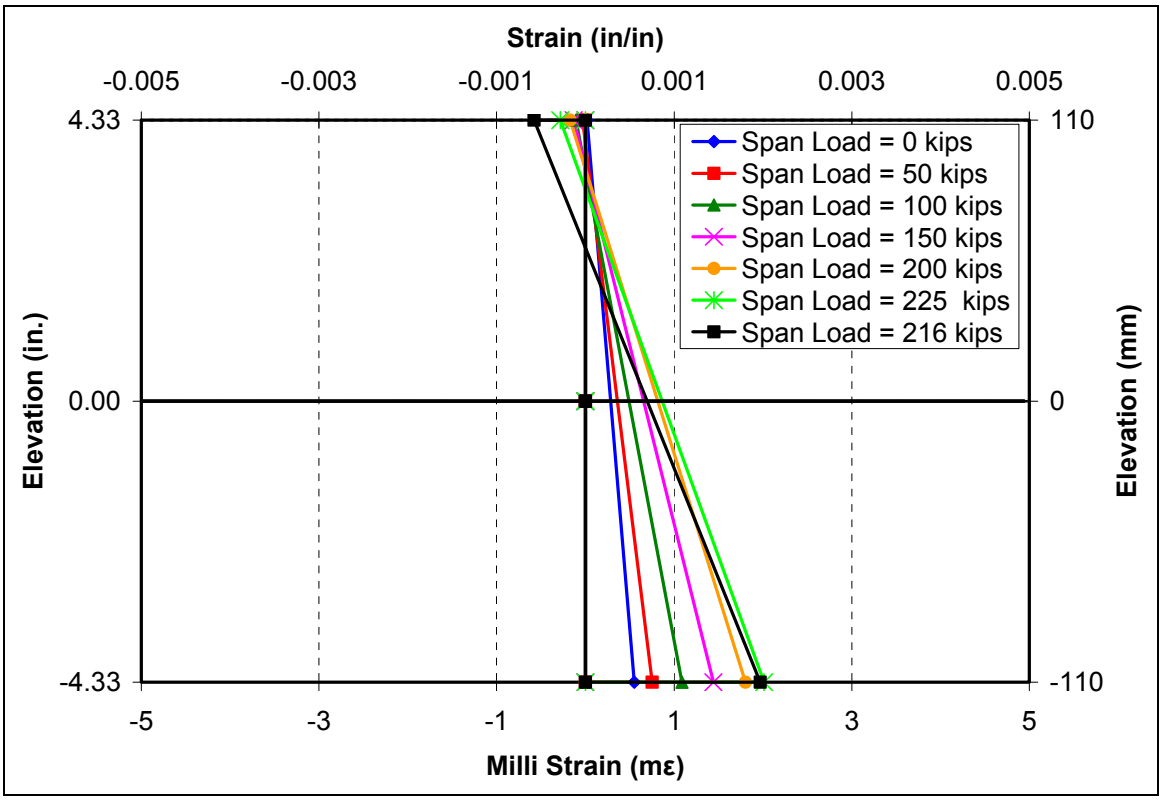

Figure 4-34: Strain Profiles from PI Gages T8 and B12 for First Deck

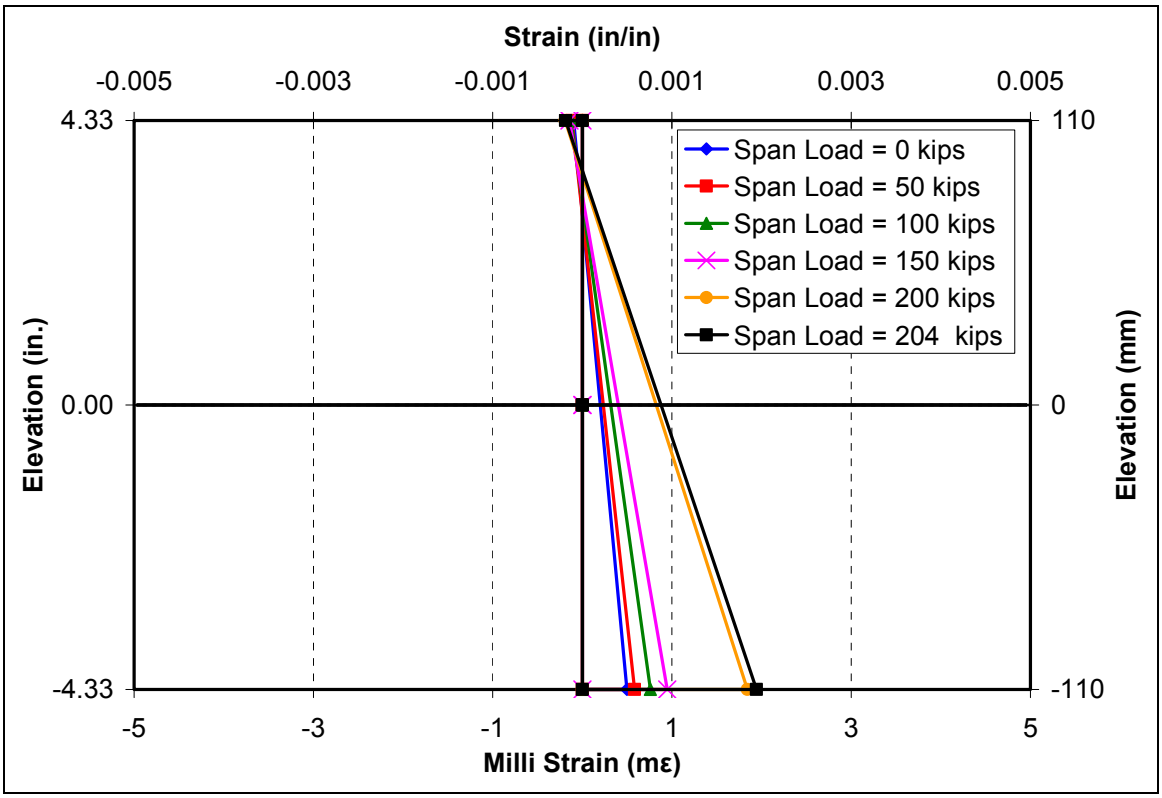

Figure 4-35: Strain Profiles from PI Gages T8 and B12 for Second Deck

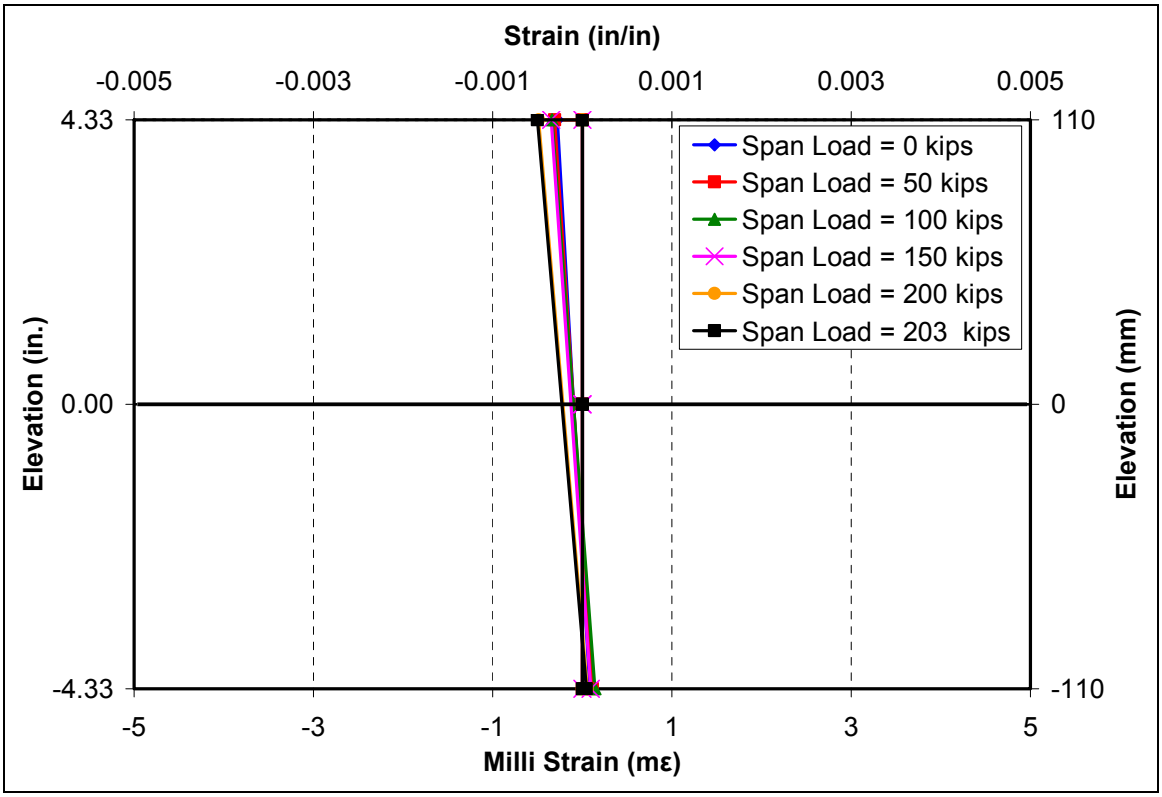

Figure 4-36: Strain Profiles from PI Gages T8 and B12 for Third Deck

4.8. Steel Strain

Selected data from the electrical strain gages attached to the reinforcing steel are presented in this section. All measured strain gage data are provided in Appendix B. Strain profiles are plotted for the final loading cycle only. Again, residual strains may exist from previous cycles at zero load. Tensile strains are plotted as positive, and compressive strains are plotted as negative. If a data series is shown in the legend on a plot, but does not appear in that plot, it is because that gage was damaged prior to testing. Recall that according to the ASTM-A370 offset method (0.2% offset), the yield strain of MMFX steel was determined to be 0.006 (6000 με), and the measured yield strength of Grade 60 steel was 68 ksi (469 MPa) at a strain of 0.0023 (2300 με).

Figure 4-38 shows data plotted from three strain gages running along the longitudinal centerline of the left span of the second deck. It can be clearly seen that the transverse bar near the center of the deck was under significant strain towards the end of the test, while the bar towards the outer edge was strained much less. This finding is another excellent indication that the longitudinal dimension selected for the decks was sufficient to allow for two-way slab action, and was representative of actual behavior. The results are typical of the other spans and the other decks. Figure 4-37 shows the general locations of these gages. Refer to Section 3 for detailed information on the exact locations of the various gages.

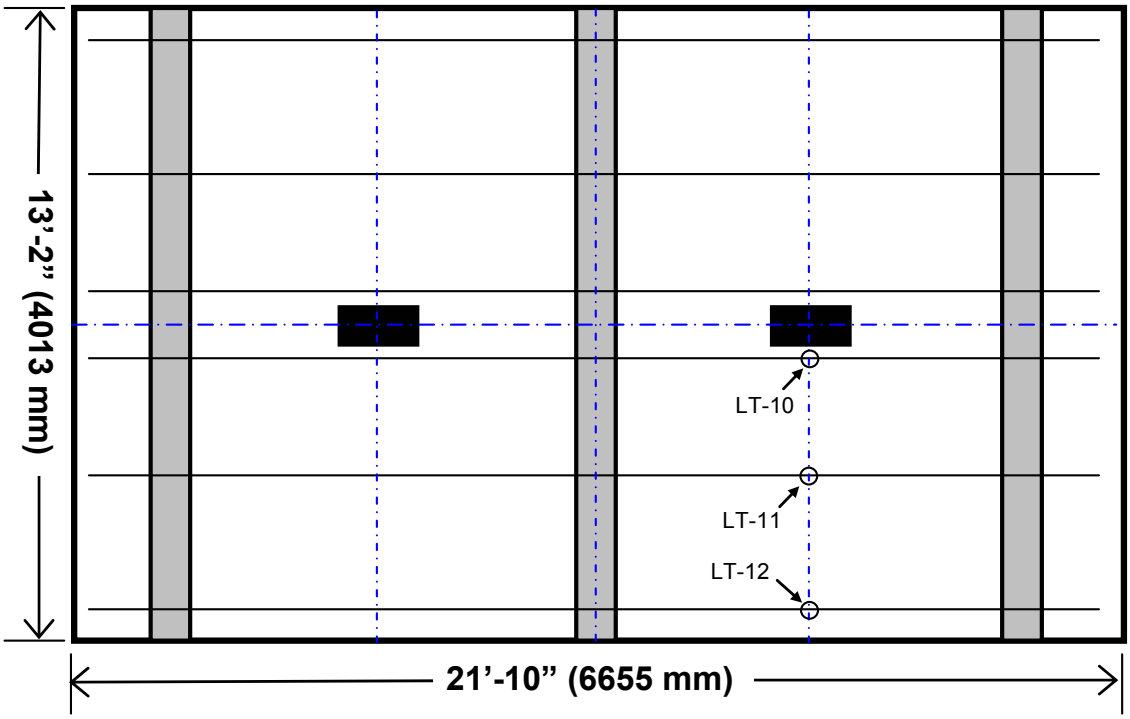

NOTE: Only Lower-Mesh Transverse Bars with Gages Shown

Figure 4-37: Location of Strain Gages LT-10, LT-11, and LT-12

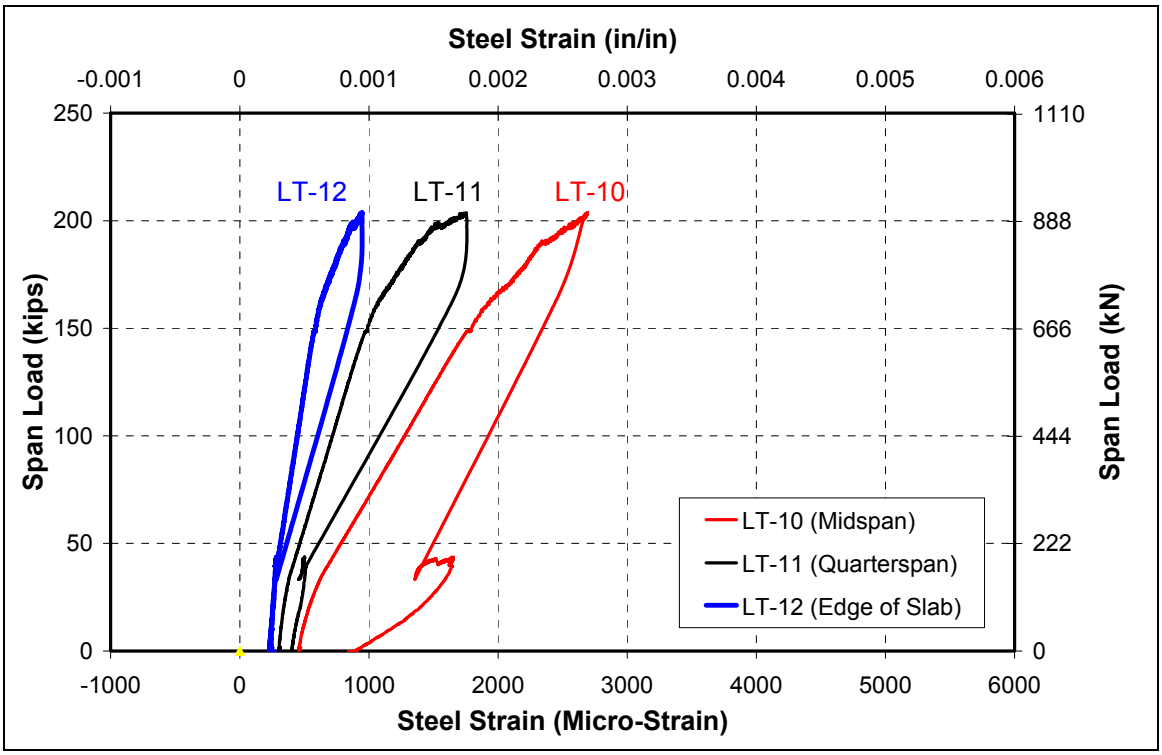

Figure 4-38: Right Span Lower Transverse Steel Strain of Second Deck

Figure 4-41 through Figure 4-42 plot data from the lower transverse reinforcing mesh in the left span of the first, second, and third decks respectively. Both of the gages in each plot are located on the same transverse bar, one near the load point, and one near the face of the center girder. Figure 4-39 shows the general locations of the gages in the plots.

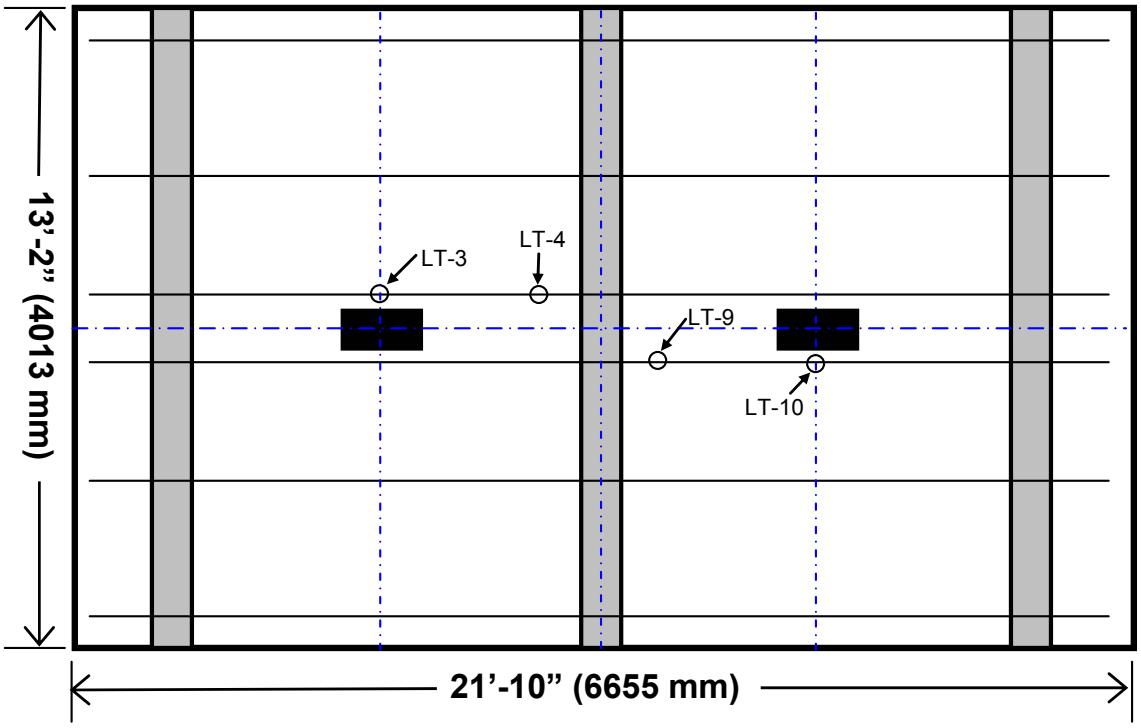

NOTE: Only Lower-Mesh Transverse Bars with Gages Shown

Figure 4-39: Locations of Strain Gages LT-3, LT-4, LT-9, and LT-10

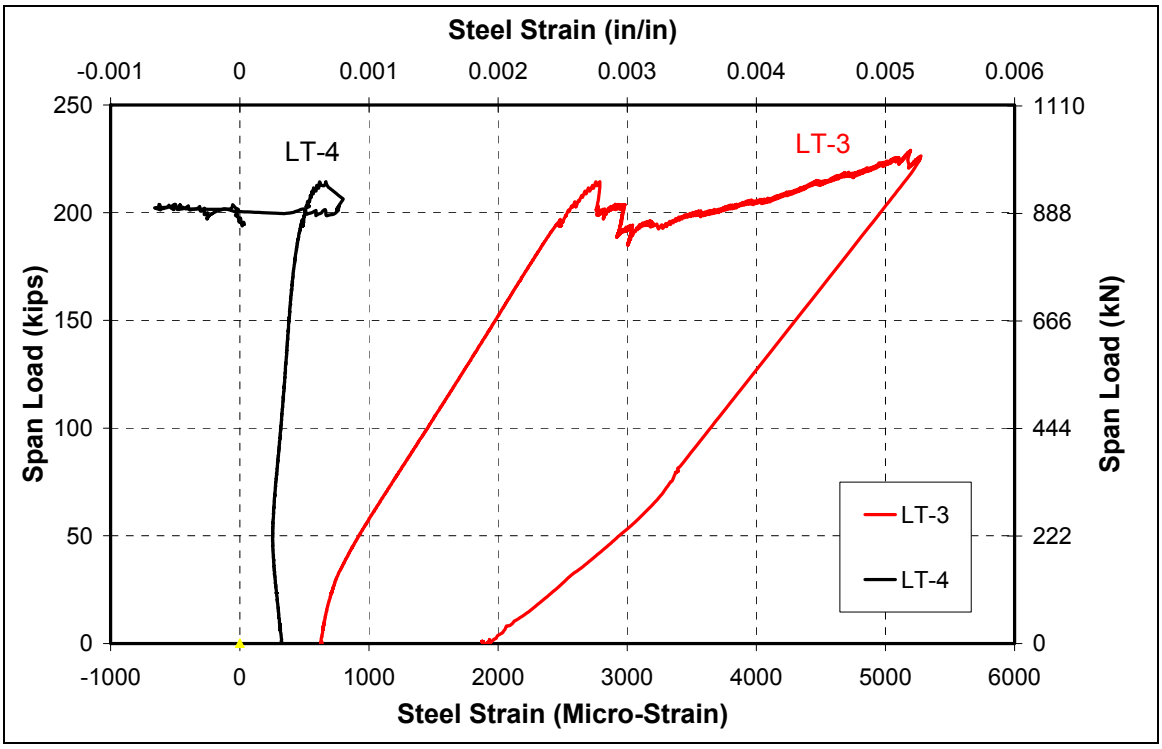

Figure 4-40: Left Span Lower Transverse Steel Strain of First Deck

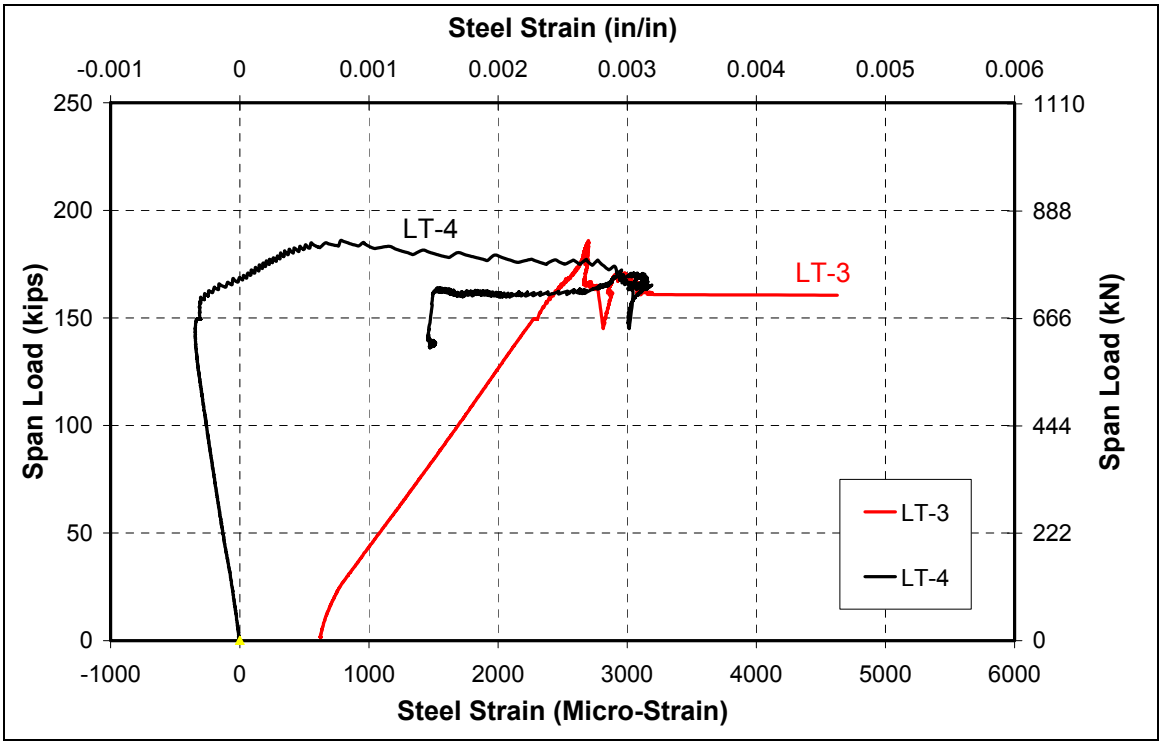

Figure 4-41: Left Span Lower Transverse Steel Strain of Second Deck

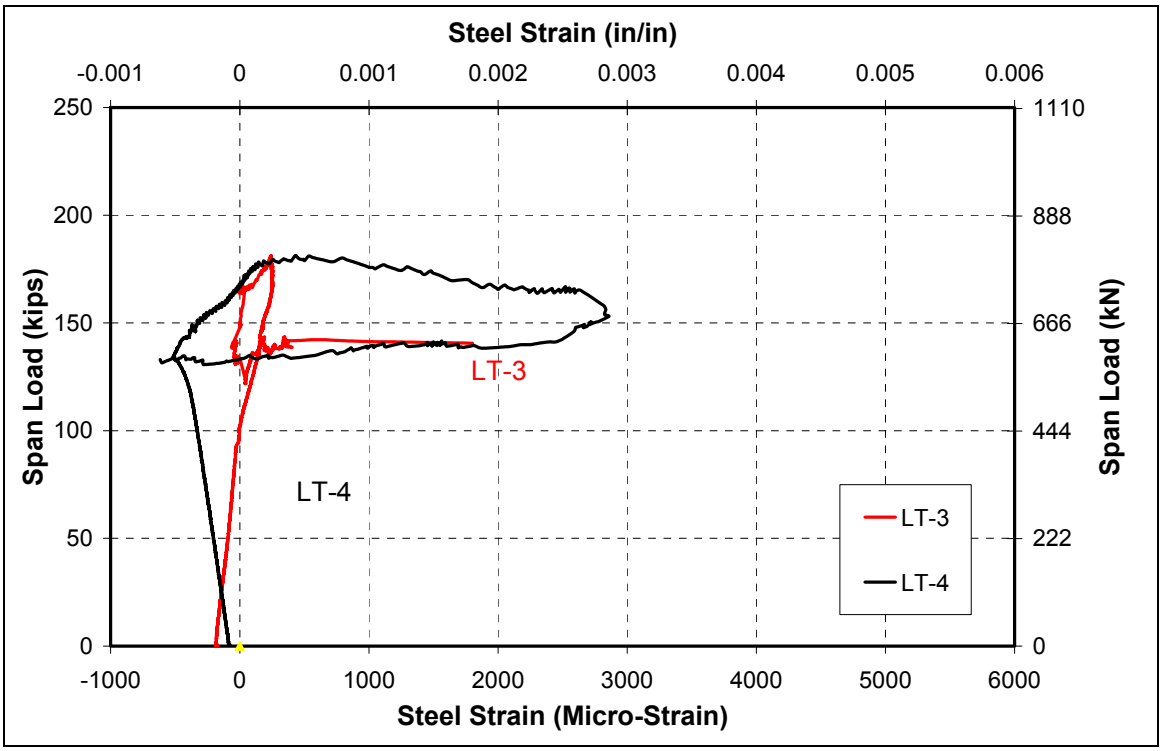

Figure 4-42: Left Span Lower Transverse Steel Strain of Third Deck

It can clearly be seen in the figures that the transverse bars in the bottom reinforcing mesh, near the load point, remained in tension throughout the entire loading range. This behavior would be expected for any typical flexural loading condition. However, the data are quit different for strains near the face of the center girder from the same lower transverse bars. In all spans which developed significant flexural-shear cracking, strains from the lower mesh near the center girder developed in compression (as would be expected in flexural behavior for the negative moment region), but then switched to tension as the flexural-shear cracking developed. Gages from the top mesh transverse bars in the same locations remained in tension throughout the entire test (see Appendix B for these data). This finding indicates that after significant flexural-shear cracking, the deck spans were

suspended from the center girder by both layers of reinforcing steel in a sort of net action.

To confirm the presence of so called net action for the spans with significant flexural-shear cracking only, consider the data from the same gages in the right span of the third deck. These data are presented in Figure 4-43. Recall that the right span of the third deck failed in punching shear, prior to the development of significant flexural-shear cracking. Data plotted for the lower transverse strain gage near the face of the center girder (LT-9) show that the bar in this location remained in compression for the duration of testing, up until punching failure. The strain gage on the upper mesh, directly above LT-9, remained in tension for the duration of testing (see Appendix B for data from gage UT-3). For such a negative moment region, this is classical flexural behavior for a doubly-reinforced section.

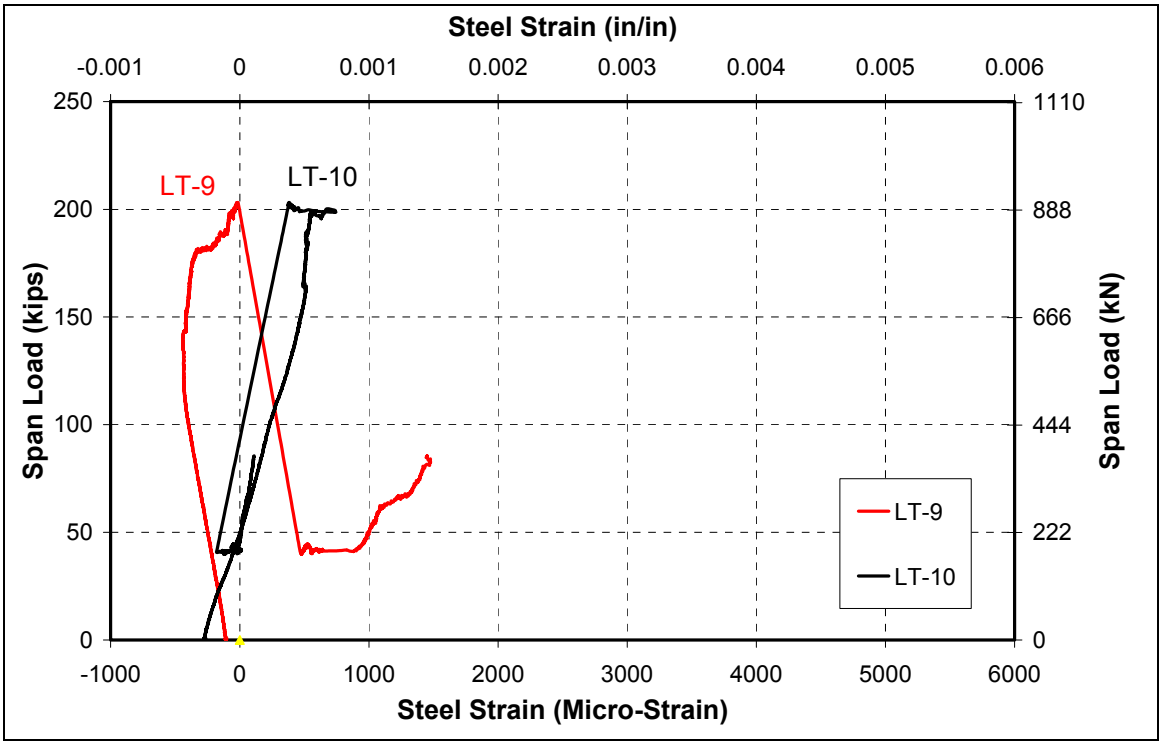

Figure 4-43: Right Span Lower Transverse Strains of Third Deck

None of the decks were instrumented with strain gages near the faces of the outer girders, so it is impossible to say whether this net action behavior was symmetric across the span. It is presumed that the transverse bars in the lower mesh, near the outer girders, remained in compression throughout the entire test since flexural-shear cracking did not develop in this region.

Again, for detailed strain data from all gages, see Appendix B.

4.9. Girder Rotation

Rotation of the three supporting girders was monitored throughout the test of each bridge deck. The rotations of each of these girders are shown in Figure 4-44 through Figure 4-46 for each of the decks, respectively. Data are plotted in radians with zero radians being defined as vertical, and positive rotation being defined as rotation towards the right side of a given bridge deck. Again, data is plotted for the final loading cycle only, and thus, some plots show rotations at zero load, representing residual rotation from previous cycles. Note that after failure, the rotation of some girders trends back towards vertical, representing the recovery of a bridge deck after loading was terminated due to failure.

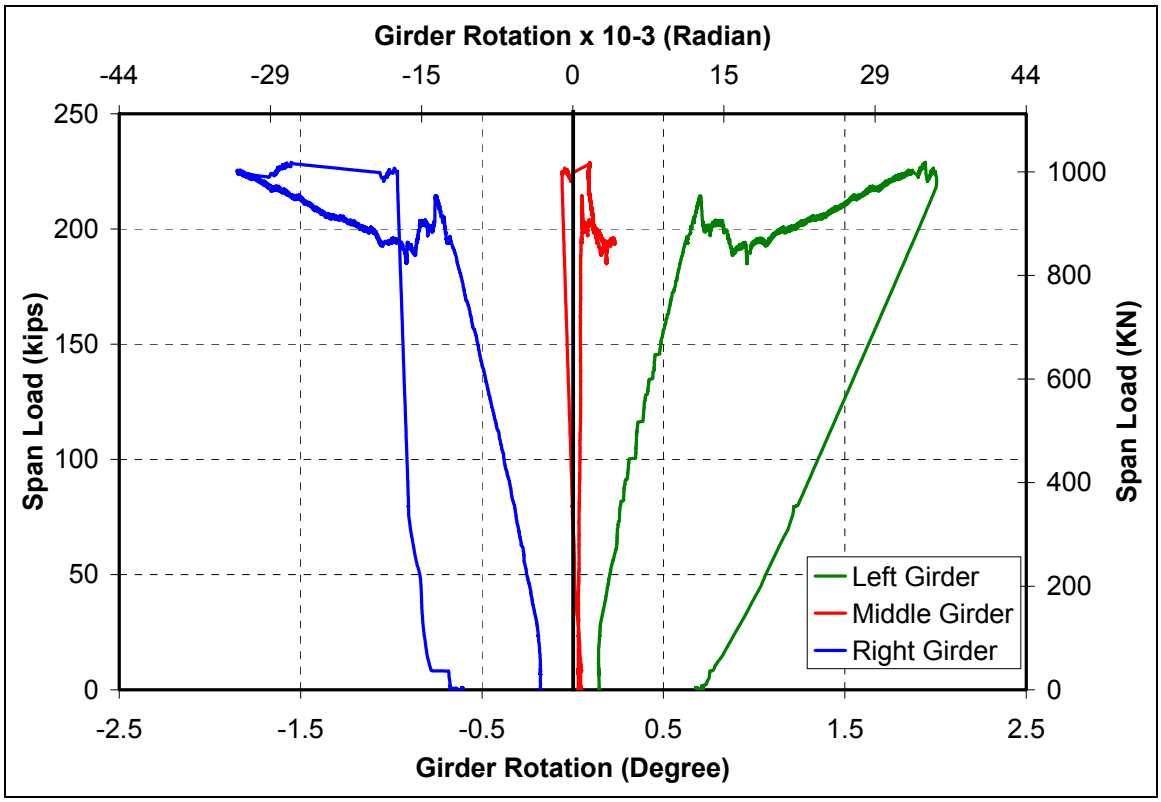

Figure 4-44: Girder Rotation for the First Deck

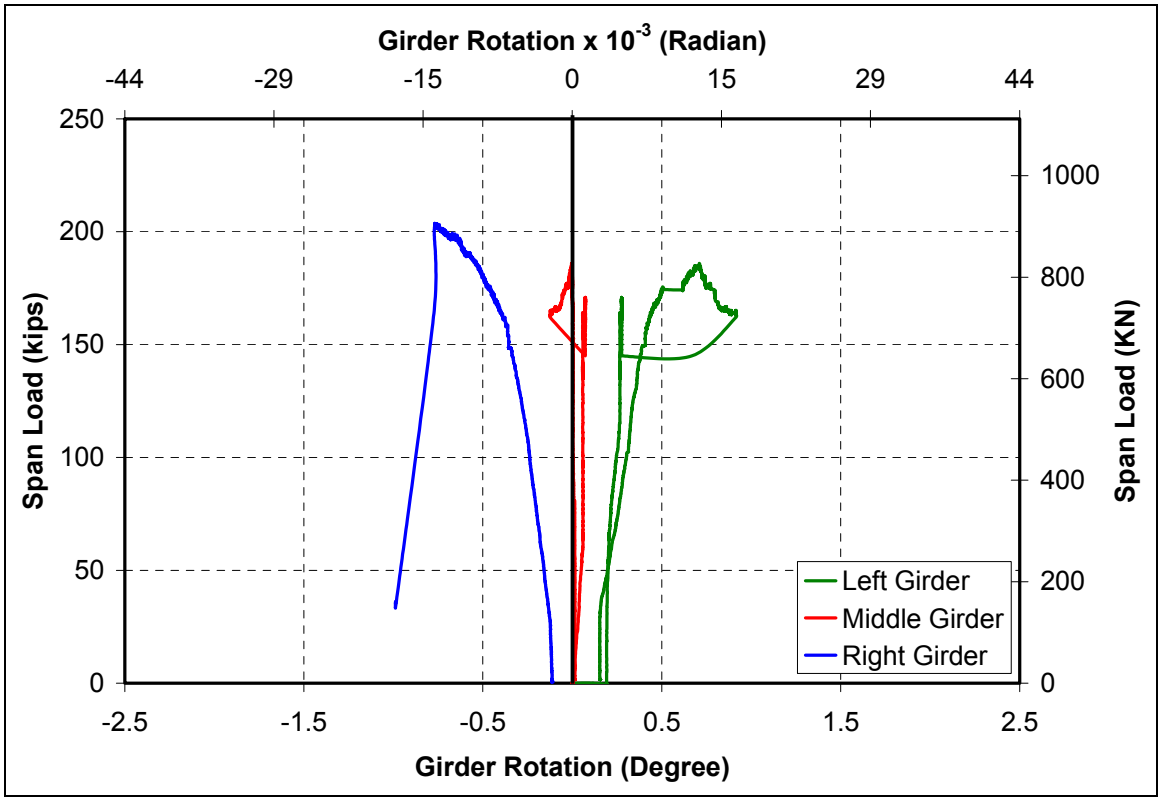

Figure 4-45: Girder Rotation for the Second Deck

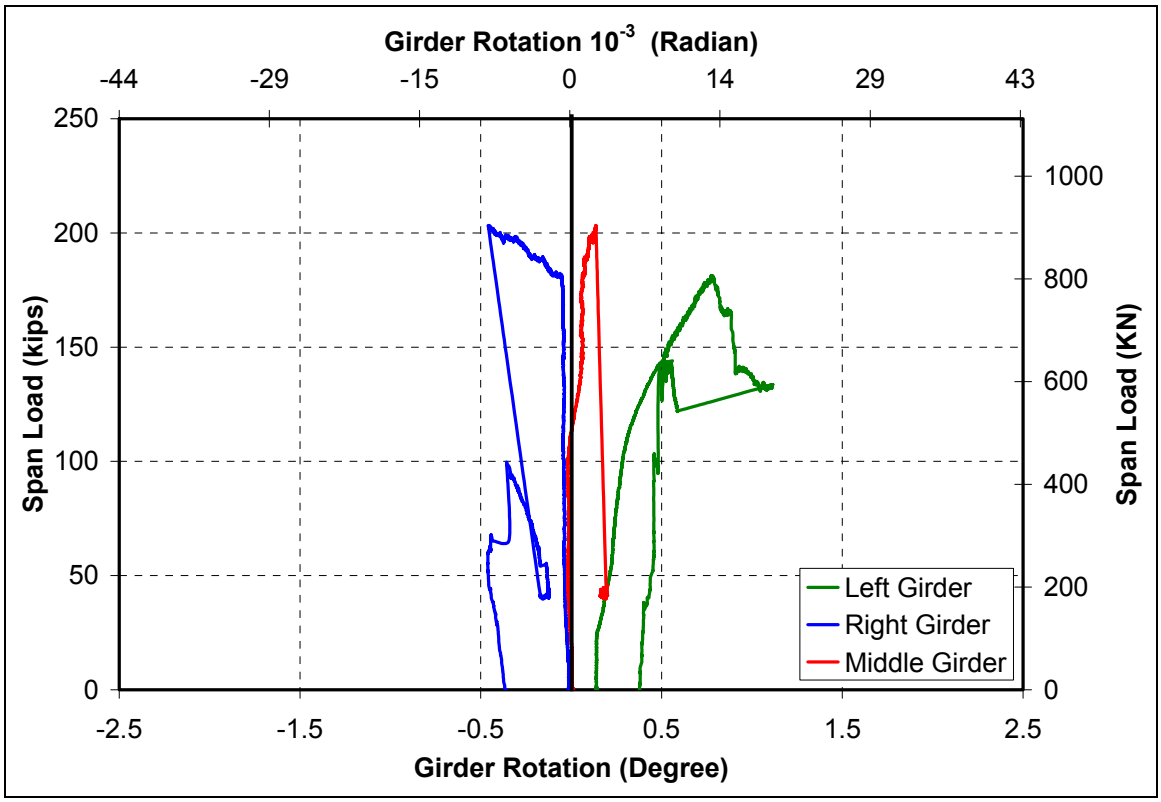

Figure 4-46: Girder Rotation for the Third Deck

In all of the tests, the two outside girders exhibited larger rotations than did the middle girder, as would be expected due to the unbalanced moment effect. Since the spans were loaded simultaneously with virtually identical loads, the moment in the slab immediately to the left of the middle girder would balance with the moment in the slab immediately to the right of the middle girder. For each outside girder, a loaded span on one side was offset by an unloaded cantilever on the other. As load was applied to the spans, the outer girders rotated inward towards the load so that equilibrium would be maintained. Under ideal conditions, the middle girder would have remained perfectly vertical throughout the entire test. While there was some rotation of the middle girder in each of the three tests, it was not dramatic, indicating

that satisfactory load distribution was maintained between the left and right spans up to failure for all three tests.

In addition, the outside girders of the first bridge deck underwent larger rotations than did the outside girders of the other two decks. This behavior can be explained by the higher failure load of the first deck.

4.10. Failure Mechanism

The failure mechanism of the three bridge decks can be summarized as follows:

1) Behavior starts out in flexure, as evidenced by the longitudinal cracks in the negative moment region.

2) Initial behavior is followed by a two-way flexural action, with load being distributed from the points of application outward towards the edges of the decks. This two-way action is evidenced by the radial crack pattern on the underside of the slabs.

3) Flexural behavior may be augmented by an arching action, as compressive membrane forces are developed in the bottom layer of reinforcement.

4) A flexural-shear crack develops near the face of the center girder in one of the spans.

5) As the flexural-shear crack grows and widens, a plastic-hinge forms, dramatically reducing the stiffness of the span. This reduction in stiffness causes punching shear failure in only one span. In the event that flexural-shear cracks develop simultaneously on both sides of the center girder, the stiffness of both spans will remain balanced, and may allow for punching failure to occur in both spans. Under this condition, punching failure will only be possible if the steel reinforcing the negative moment region has sufficient reserve capacity to capture load past the formation of the flexural-shear cracks, as was the case for the deck reinforced with the larger amount of MMFX steel.

4.11. Predicted Strength

The predicted shear strengths for the three bridge decks as determined by relevant design codes are given in Figure 4-47. These values are compared to the values for punching strength that were determined experimentally. The design codes included are: American Concrete Institute ACI 318-05(2005), American Association of State Highway Transportation Officials AASHTO LRFD (2004), and Ontario Highway Bridge Design Code (1991). The code equations used are given in the literature review.

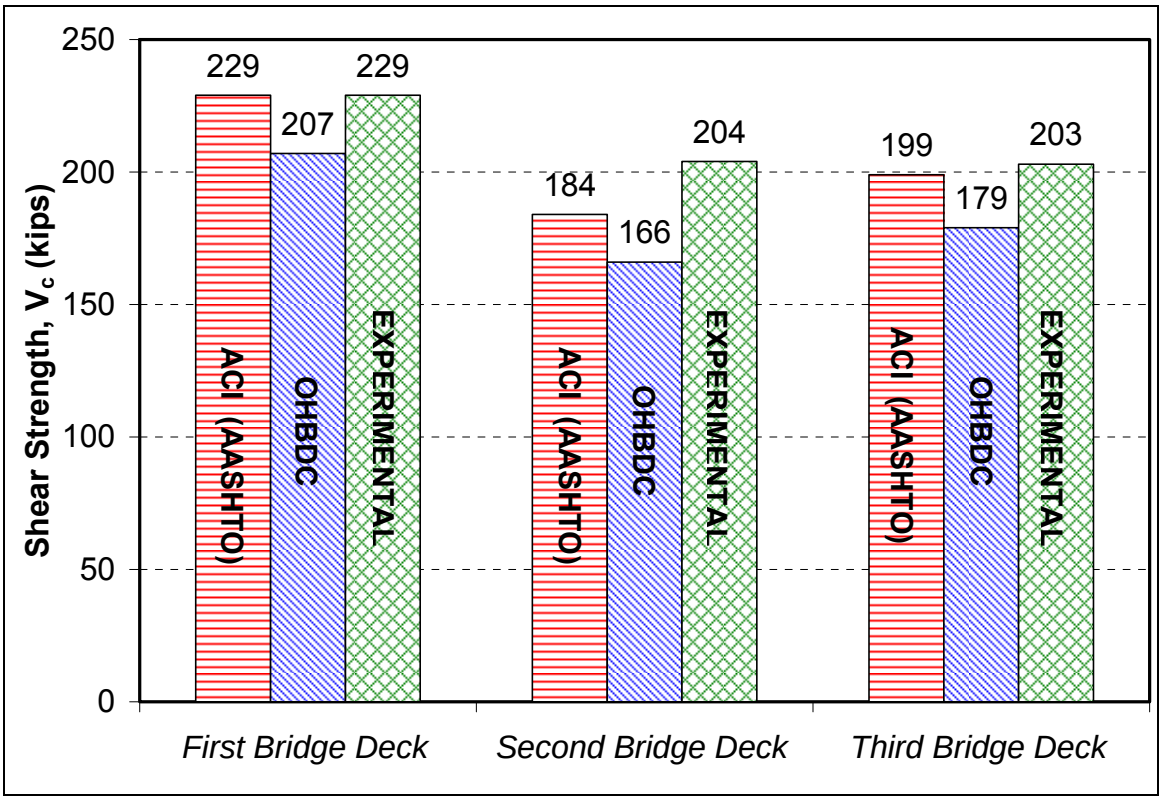

Figure 4-47: Predicted and Experimental Shear Strengths

Figure 4-47 shows that the punching capacities predicted by all of the code equations compared closely with the values obtained experimentally. Note that the AASHTO and ACI equations are shown together on a single bar. These codes predict virtually the same value for punching shear capacity since they use different formulations of the same equations. The Ontario Bridge Code equation seems to under-predict punching capacity in all cases. This is expected, as the OHBDC equation is somewhat more conservative than the ACI and AASHTO equations, as is discussed in Section 2.

It is important to note that the type of steel does not factor into the predictions of punching shear strength. The models used by all the codes take only concrete properties and geometry into account. Thus, the differences in punching strength

predictions between the three bridge decks are due entirely to differences in concrete strengths. Recall that the concrete strength from the first bridge deck was determined to be 7000 psi while the second and third decks were determined to be 4500 psi, and 5300 psi, respectively.

What is important to note from the above graph, is that all three bridge decks reached their predicted punching capacities and ultimately failed in punching shear. The significance of this observation is that other failure modes, such as flexural-shear failure, or even flexural failure did not ultimately control – even in the bridge deck reinforced with significantly less MMFX steel. Since the decks maintained sufficient flexural rigidity throughout the tested range (enough to reach punching shear capacity in each case), the ability of the third deck with reduced reinforcement to utilize the higher strengths offered by MMFX steel was demonstrated. The higher strength MMFX reinforcement in lesser amounts prevented a premature flexural failure equally well as did a larger quantity of lower-strength Grade 60 reinforcement.

4.12. Field Application: Construction of Johnston County Bridge

As is mentioned previously, the test specimens in this experimental program are based on an actual bridge constructed by the NCDOT in Johnston County, NC. The Johnston County Bridge is located over I-95 on the SR 1178 interchange at Four Oaks, NC. The location is shown on the maps in Figure 4-48 and Figure 4-49. The bridge layout is shown in Figure 4-50, and Figure 4-51 gives a general drawing for the bridge. The bridge measures 250’-10” (76.5 m) in total length, and consists of a cast-in-place concrete deck slab supported in composite action by steel girders as

shown in Figure 4-52. Cross-bracing was used on a 21 ft (6.4 m) spacing to provide lateral stability to the steel girders. MMFX steel reinforcing bars were the only type of reinforcement used in the concrete deck.

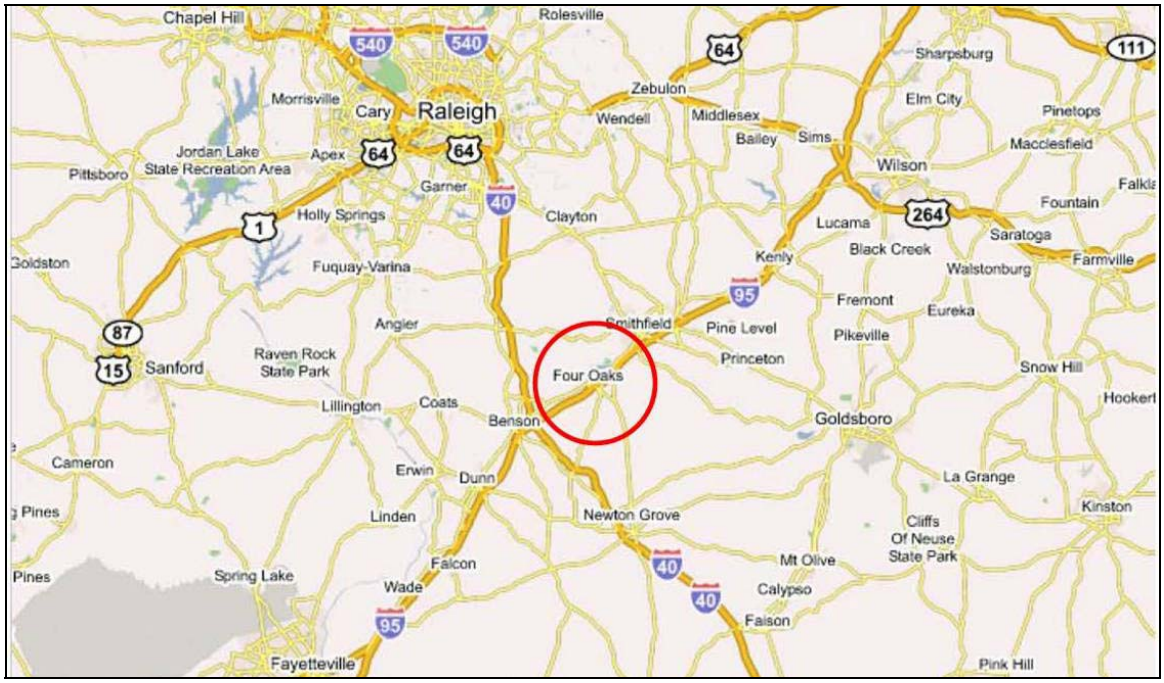

Figure 4-48: Vicinity Map of the Johnston County Bridge Location

Figure 4-49: Close-up of the Johnston County Bridge Location

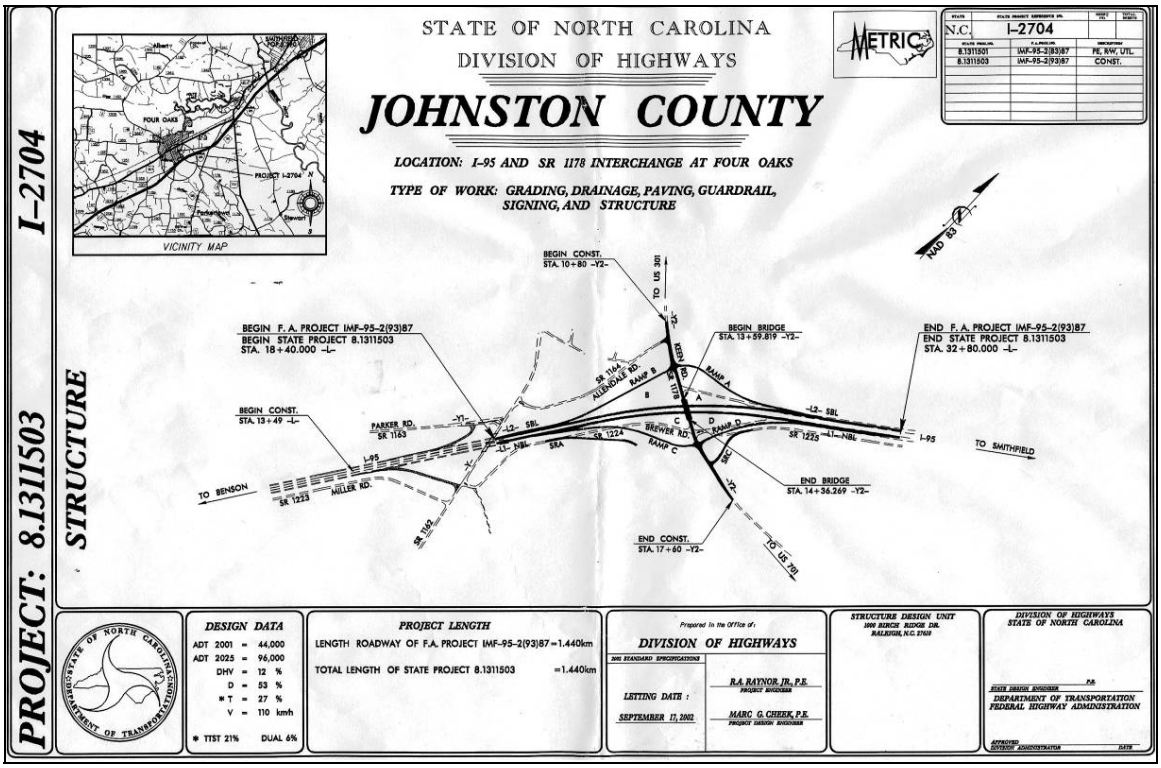

Figure 4-50: General Layout for the Johnston County Bridge

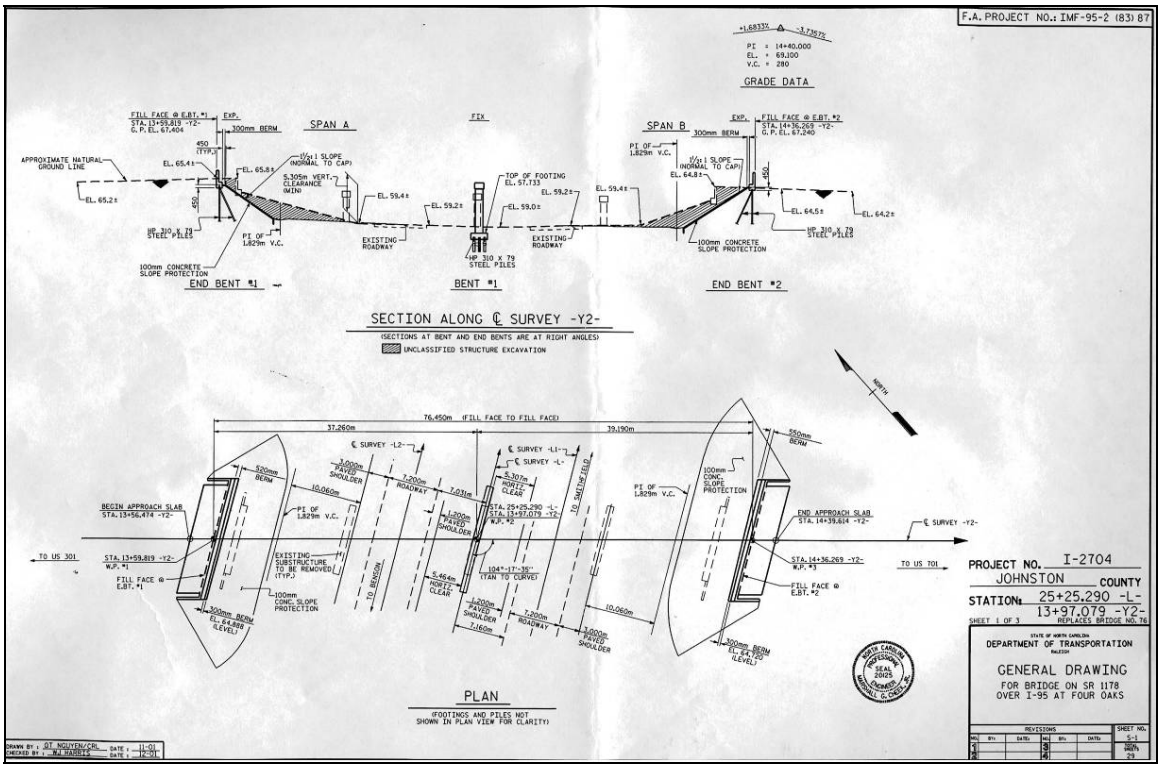

Figure 4-51: General Drawing for the Johnston County Bridge

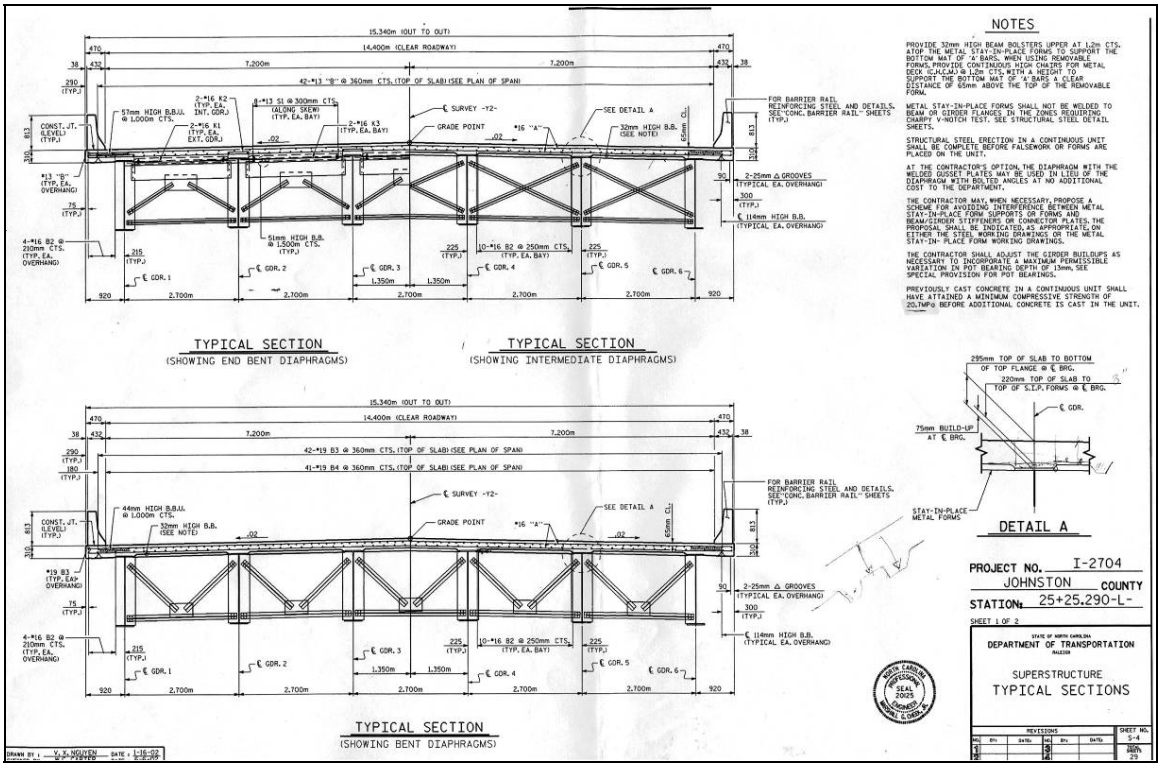

Figure 4-52: Typical Superstructure Sections for the Johnston County Bridge

The bridge site was visited several times by the Constructed Facilities Laboratory (CFL) research team to monitor progress during construction. The bridge deck slab, reinforced with MMFX steel, was cast in August of 2004. The following is a brief description of the construction sequence of the bridge according to the dates of site visits. No data were recorded in the field. Photographs from the site visits are given in Appendix C.

April 20th:

> Construction of the abutments and the forms for the double bent piers were completed. See Figure 9-1 and Figure 9-2.

May 18th:

> Casting of concrete for the double bent bridge piers was completed. See Figure 9-3.

June 17th:

> Erection of the steel girders was complete, and the cross-bracing was in place. See Figure 9-4 and Figure 9-5.

July 1st:

> Installation of the stay-in-place deck forms was complete. All MMFX steel had been delivered to the site. See Figure 9-6 and Figure 9-7. Figure 9-7 shows the engraved markings on the MMFX steel at the site.

July 23rd:

> Placement of all the MMFX steel bars was completed. See Figure 9-8.

July 27th:

NCDOT and NCSU research teams visited to inspect the steel prior to casting of the concrete deck. See Figure 9-9.

August 5th:

Casting concrete of the bridge deck started very early in the morning, and was completed well before noon. See Figure 9-10 and Figure 9-11.

August, 2004

The bridge is complete.

5. Summary and Conclusions

5.1. Summary

The potential for a new type of steel to be used in concrete bridge decks was evaluated with a full-scale testing program. The manufacturer claims that the new steel, commercially known as MMFX steel, offers greatly enhanced corrosion-resistance and significantly higher strength when compared to conventional Grade 60 steel. The aim of the research was to evaluate the new steel with respect to cast-in-place, reinforced concrete bridge decks. If the claims of corrosion resistance are verified by an ongoing study, the use of MMFX steel has the potential to greatly enhance the service lives of newly constructed concrete decks. In addition, results from this experimental program indicate the potential to take advantage of the higher strength offered by MMFX steel bars, thereby reducing the material requirements of a particular design.

Three full-size reinforced concrete bridge deck sections were tested to failure in order to evaluate the effectiveness using MMFX steel in concrete bridges. The bridge decks were all continuous two-span structures supported in composite action by three post-tensioned concrete girders. The decks were designed to replicate an actual bridge constructed in Johnston County, NC by the NCDOT.

The three decks were loaded with two concentrated point loads applied simultaneously to both spans. These loads were intended to simulate the effects of truck wheel loading. At least one of the two spans in each of the three bridge deck specimens ultimately failed due to punching shear.

Significant observations from the testing program are summarized below:

1) The ultimate load-carrying capacities recorded for all three bridge decks tested in this investigation were at least eight to ten times the service load specified by the AASHTO Design Specifications (2004).

2) As was expected, punching shear was the primary mode of failure for all three of the bridge decks that were tested. Flexural-shear failure was observed as a secondary failure mode.

3) Punching shear failure resulted in a sudden decrease of the load-carrying capacity of a given deck, while flexural-shear failure resulted in gradual decrease of the load-carrying capacity.

4) The two bridge decks reinforced with MMFX steel exhibited the same deflections at service load as the deck reinforced with Grade 60 steel.

5) For the two bridge decks having the same reinforcement ratio, the bridge deck reinforced with MMFX steel developed more load-carrying capacity than did the deck reinforced with Grade 60 steel.

6) The bridge deck reinforced with 33-percent less MMFX steel in the transverse direction developed the same ultimate load-carrying capacity as did the deck reinforced with Grade 60 steel. This result is partially attributed to the higher tensile strength offered by MMFX steel.

7) The bridge deck reinforced with 33-percent less MMFX steel in the transverse direction exhibited the same deflections at service load as did the deck reinforced with Grade 60 steel. These two decks also exhibited nearly identical ductility, as evidenced by their closely matching load-deflection plots.

8) The MMFX reinforcing bars exhibited a linear stress-strain relationship up to 100 ksi (689 MPa). This was followed by a nonlinear behavior up to an ultimate strength of roughly 173 ksi (1193 MPa). According to the ASTM-A370 offset method (0.2% offset), the yield strength was determined to be 120 ksi (827 MPa). The initial modulus of elasticity was determined to be 29,500 ksi (203 GPa).

9) The experimental results indicate that the higher strength of MMFX steel can be taken advantage of in design to allow for significantly reduced reinforcement ratios.

10) The model employed by the AASHTO and ACI codes to predict punching shear capacity in reinforced concrete decks seems to be just as accurate when applied to decks reinforced with MMFX steel as it is when applied to decks reinforced with Grade 60 steel. This is to be expected, as the model does not consider the properties of steel reinforcement in determining punching shear capacity.

11) Provided that the claims of higher corrosion-resistance of MMFX steel can be verified by the ongoing components of this research program, the use of MMFX steel can potentially increase the service lives of new concrete bridge decks.

5.2. Conclusions

A number of conclusions can be reached in regards to the results obtained in this experimental testing program.

1) The results show that substituting MMFX steel directly for Grade 60 steel in a design, as was done for the Johnston County Bridge, is an overly-conservative approach.

2) MMFX steel can be used as the main flexural reinforcement for cast-in-place concrete bridge decks at a reinforcement ratio corresponding to 33% less than that required for Grade 60 steel. Therefore, a design of reinforced concrete bridge decks using MMFX steel may utilize an equivalent yield stress of 80 ksi for the MMFX steel bars.

3) Any bridge deck design utilizing MMFX steel should still satisfy all minimum reinforcement ratios required by the AASHTO LRFD Bridge Design Specifications.

4) Deck designs using MMFX steel should still satisfy all servicability requirements found in the AASHTO LRFD Bridge Design Specifications. This includes providing adequate crack control with well-distributed reinforcement.

5) Provided that the claims of corrosion resistance can be verified in the ongoing portions of this research, the use of MMFX steel will increase the service life of concrete bridge decks due to its high corrosion resistance.

6) Since the proportional limit of MMFX steel exists near 100 ksi, the potential exists to further reduce reinforcement ratios by increasing allowable design stresses to 100 ksi or more. Further studies would be necessary to investigate this possibility.

6. References

American Association of State Highway and Transportation Officials, “AASHTO LRFD Bridge Design Specifications (US Customary Units),” Washington, D.C, 2004.

American Concrete Institute (ACI), “Building Code Requirements for Structural Concrete,” ACI 318-05, Farmington Hills, Michigan, 2005.

American Society of Civil Engineers, “Report Card for America’s Infrastructure: 2003 Progress Report,” www.asce.org, 2005.

ASTM A 370-03, “Standard Test Methods and Definitions for Mechanical Testing of Steel Products,” West Conshohocken, PA, American Society for Testing and Materials, 2003.

ASTM C31-03a, “Making and Curing Concrete Test Specimens in the Field,” West Conshohocken, PA, American Society for Testing and Materials, 2003.

ASTM C39-05, “Standard Test Method for Compressive Strength of Cylindrical Concrete Specimens,” West Conshohocken, PA, American Society for Testing and Materials, 2005.

Concrete Innovations Appraisal Service (CIAS), “High Corrosion Resistance MMFX Micorcomposite Reinforcing Steels,” May, 2003, 42 pp.

Dilger, W., Birkle, G., and Mitchell, D., “Effect of Flexural Reinforcement on Punching Shear Resistance,” ACI SP-232, 2005, pp. 57-74.

El-Hacha, Raafat and Rizkalla, Sami, “Fundamental Material Properties of MMFX Steel Rebars,” Technical Report 02-04 Submitted to MMFX Steel Corporation, July, 2002, 61 pp.

Emmons, Peter, Concrete Repair and Maintenance Limited, RS Means Company: Kingston, MA, 1993, 295 pp.

Federal Highway Administration, “Corrosion Costs and Preventative Strategies in the United States,” Publication No. FHWA-RD-01-156, 2001, 773 pp.

Hallagren, M., “Punching Shear Capacity of Reinforced High Strength Concrete Slabs,” Ph.D. Thesis, KTH Stockholm, TRITA-BKN. Bulletin No. 23, 1996, pp. 150.

Hassan, T., Abdelrahman, A., Tadros, G., and Rizkalla, S., “Fibre Reinforced Polymer Bars for Bridge Decks,” Canadian Journal of Civil Engineering, V. 27, 2000, pp. 839-849.

Hon, A., Taplin, G., and Al-Mahaidi, R. S., “Strength of Reinforced Concrete Bridge Decks Under Compressive Membrane Action,” ACI Structural Journal, V. 102, No. 3, May-June 2005.

Hunkler, F., “Corrosion in Reinforced Concrete: Process and Mechanisms,” Corrosion in Reinforced Concrete Structures, Hans Böhni, Woodhead Publishing Limited, 2005, pp. 1-42.

James, R.G., “ANACAP Concrete Analysis Program Theory Manual,” Version 3.0, Anatech Corporation, San Diego, CA, 2004.

Khanna, O. S., Mufti, A. A., and Bakht, B., “Experimental Investigation of the Role of Reinforcement in the Strength of Concrete Deck Slabs,” Canadian Journal of Civil Engineering, V. 27, 2000, pp. 475-480.

Kinnunen, S., and Nylander, H., “Punching of Concrete Slabs without Shear Reinforcement,” Transactions of the Royal Institute of Stockholm, Sweden, 1960.

Kuang, J. S. and Morely, C. T., “Punching Shear Behavior of Restrained Reinforced Concrete Slabs,” ACI Structural Journal, V. 89, No. 1, January-February 1992, pp. 13-19.

Marzouk, H. and Hussein, A., “Punching Shear Analysis of Reinforced High-Strength concrete Slabs,” Canadian Journal of Civil Engineering, V. 18, 1991, pp. 954-963.

Marzouk, H. and Hussein, A., “Experimental Investigation on the Behavior of High-Strength Concrete Slabs,” ACI Structural Journal, V. 88, No. 6, November-December 1991, pp. 701-713.

MMFX Steel Corporation of America, “MMFX Steel Product Bulletin,” February, 2002. Available at www.mmfx.com

Mufti, A. A., Jaeger, L. G., Bakht, B., and Wegner, L. D., “Experimental Investigation of Fibre-Reinforced Concrete Deck Slabs Without Internal Steel Reinforcement,” Canadian Journal of Civil Engineering, V. 20, 1993, pp. 398-406.

Mufti, A. A., and Newhook, J. P., “Punching Shear Strength of Restrained Concrete Bridge Deck slabs,” ACI Structural Journal, V. 95, No. 4, July-August, 1998, pp. 375-381.

OHBDC, “Ontario Highway Bridge Design Code,” Ministry of Transportation of Ontario, Downsview, Ontario, 1991.

Rashid, Y. R., “Ultimate Strength Analysis of Prestressed Concrete Pressure Vessels,” Nuc. Eng & Design, 1960, pp. 334-344.

Richart, F. E., “Reinforced Concrete Wall and Column Footings, Part 1,” Journal of the American Concrete Institute, V. 45, No. 2, October 1948, pp. 97-127.

Richart, F. E., “Reinforced Concrete Wall and Column Footings, Part 2,” Journal of the American Concrete Institute, V. 45, No. 2, October 1948, pp. 237-260.

Seliem, H., Lucier, G., Rizkalla, S., and Zia, P., “Evaluation of MMFX Steel for NCDOT Concrete Bridges,” Technical Report: 2004-27, Constructed Facilities Laboratory, North Carolina State University, Raleigh, NC, December, 2005, 122 pp.

Taylor, R. and Hayes, B., “Some Tests on the Effect of Edge Restraint on Punching Shear in Reinforced Concrete Slabs,” Magazine of Concrete Research, V. 17, 1965, pp. 39-44.

Vanderbilt, M. D., “Shear Strength of Continuous Plates,” Journal of Structural Division, ASCE, V. 98, No. ST5, May 1972, pp. 961-973.

Zia, P., “Structural Design Criteria for High-Strength MMFX Microcomposite Reinforcing Bars,” Farmington Hills, Concrete Innovations Appraisal Service, 2004, 34 pp.

Appendix

7. Appendix A: Additional Concrete Strain Profiles

Additional strain gage data is given in this section. Figure 7-1 is reproduced here showing PI gage locations.

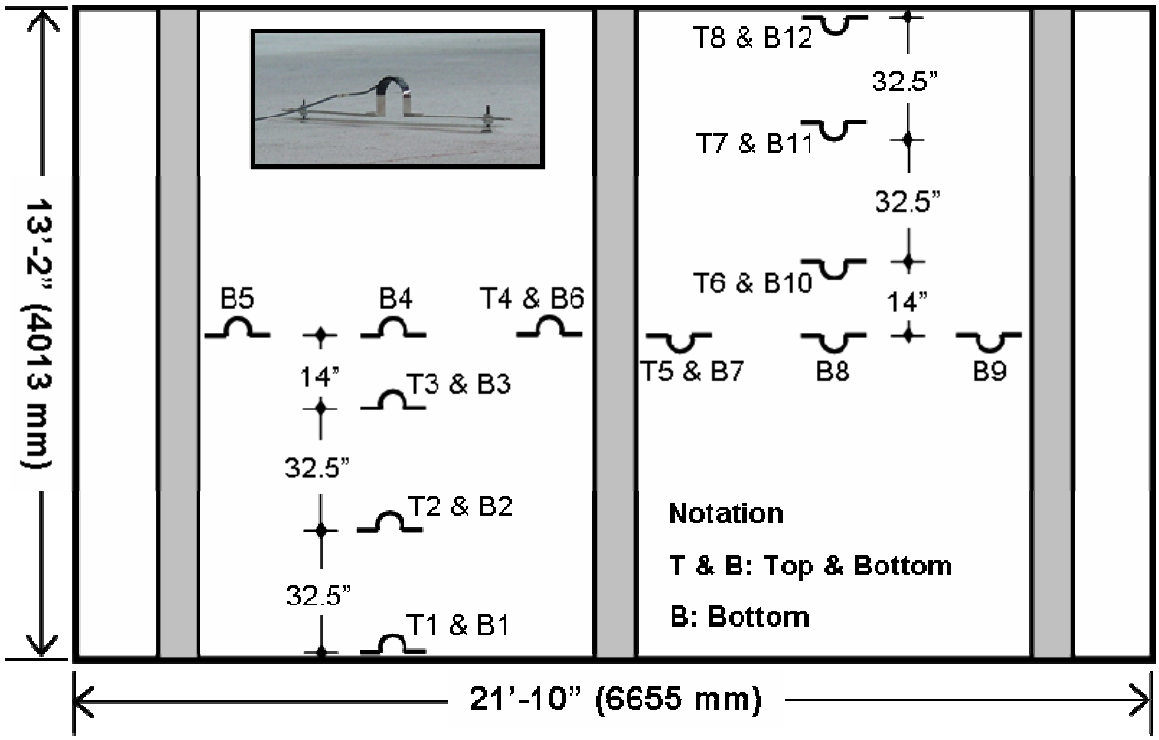

Figure 7-1: Locations of PI Gages

First Bridge Deck

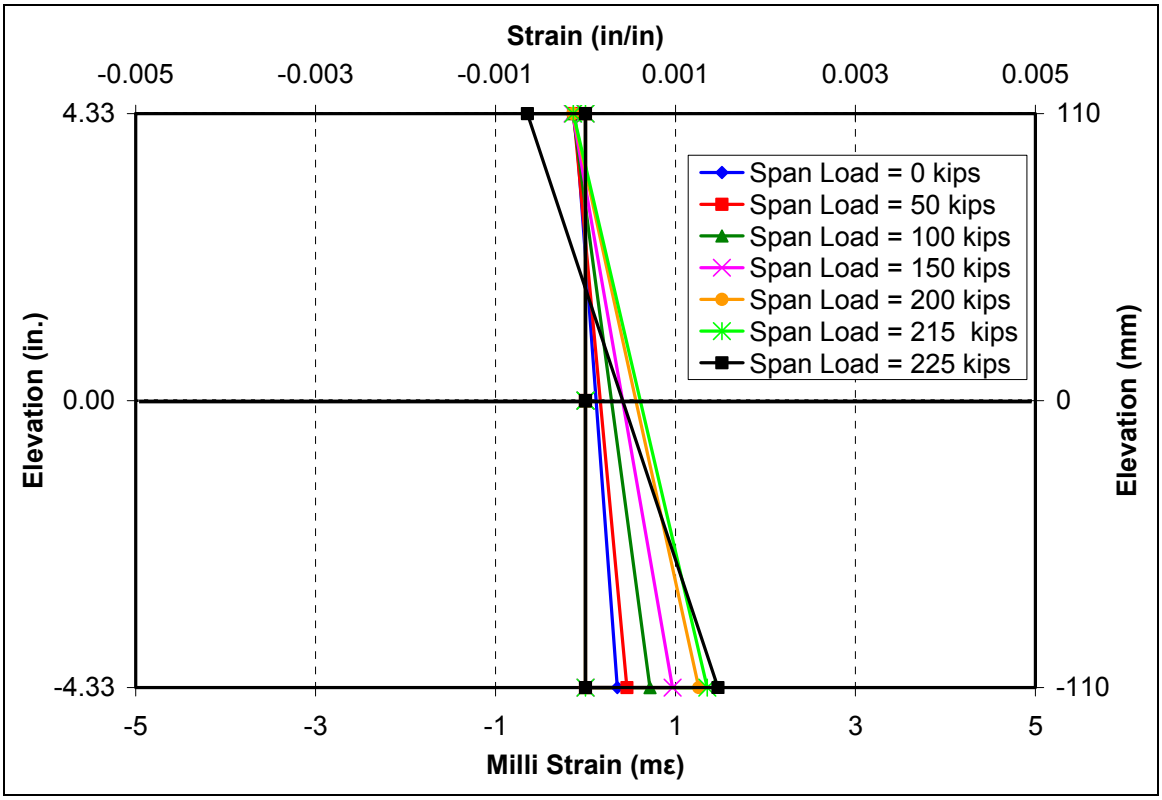

Figure 7-2: Strain Profiles from PI Gages T1 and B1 First Deck

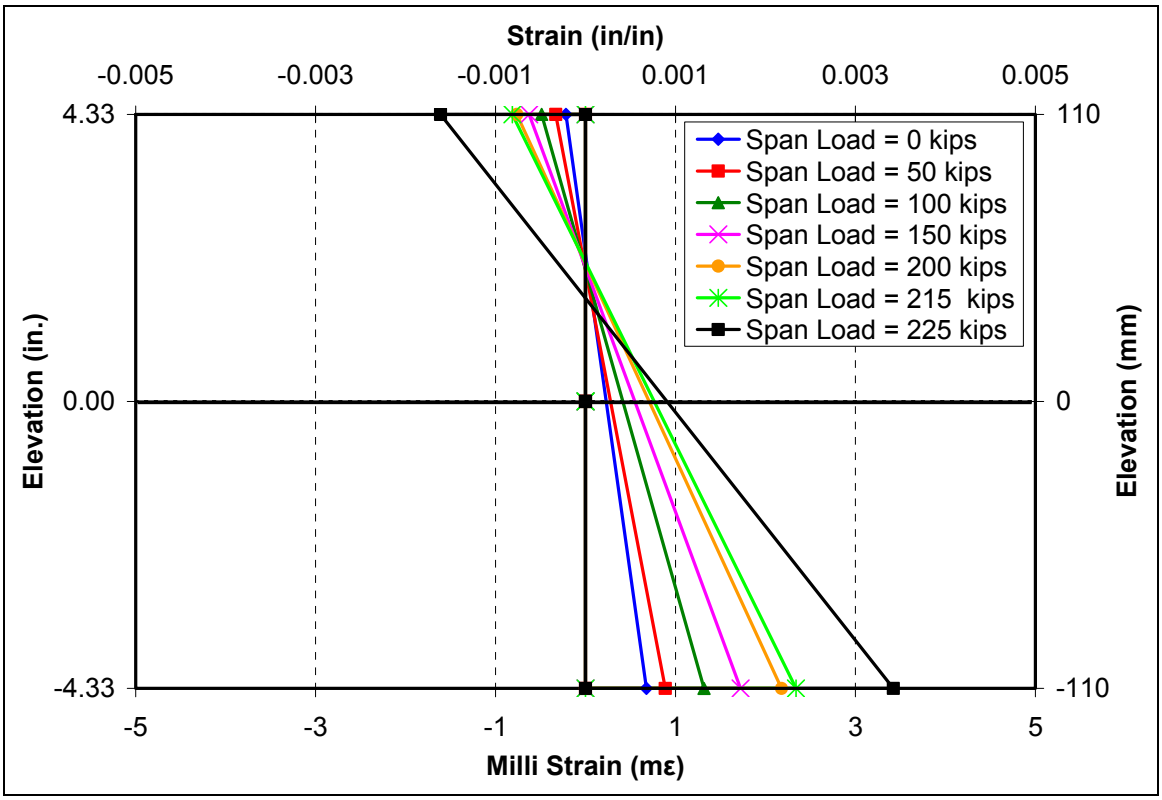

Figure 7-3: Strain Profiles from PI Gages T2 and B2 First Deck

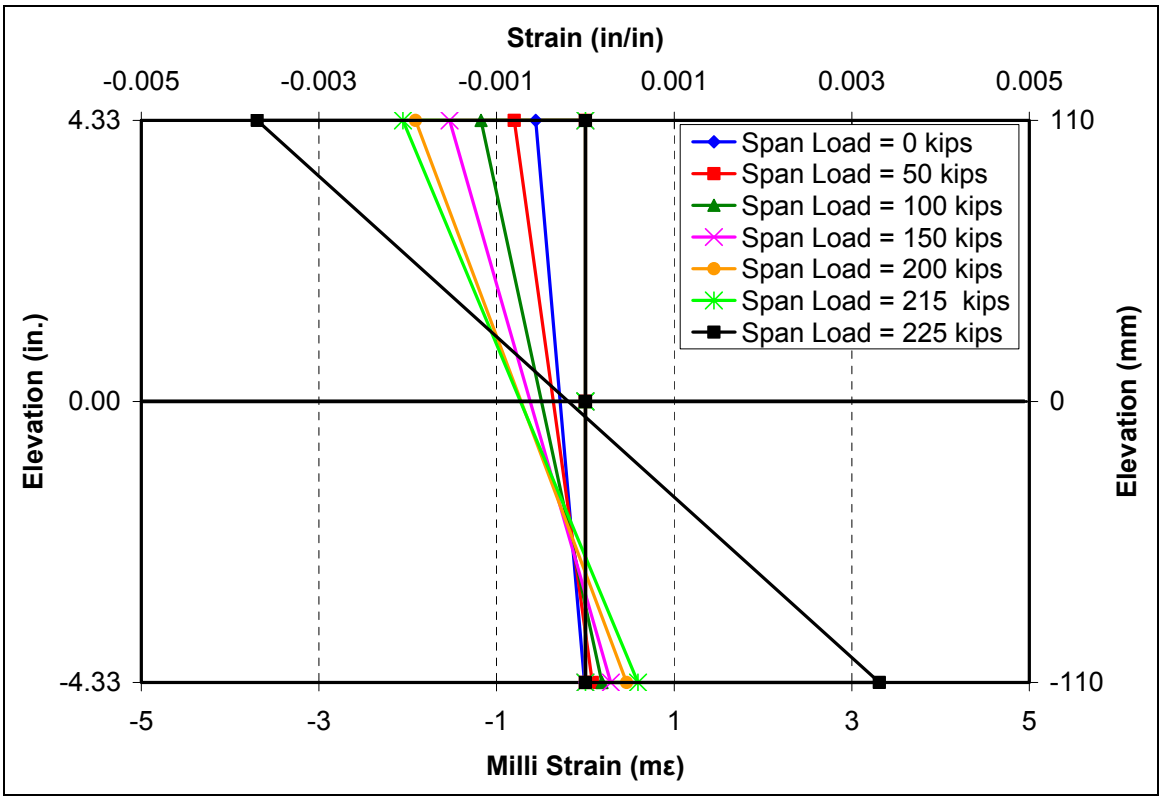

Figure 7-4: Strain Profiles from PI Gages T3 and B3 First Deck

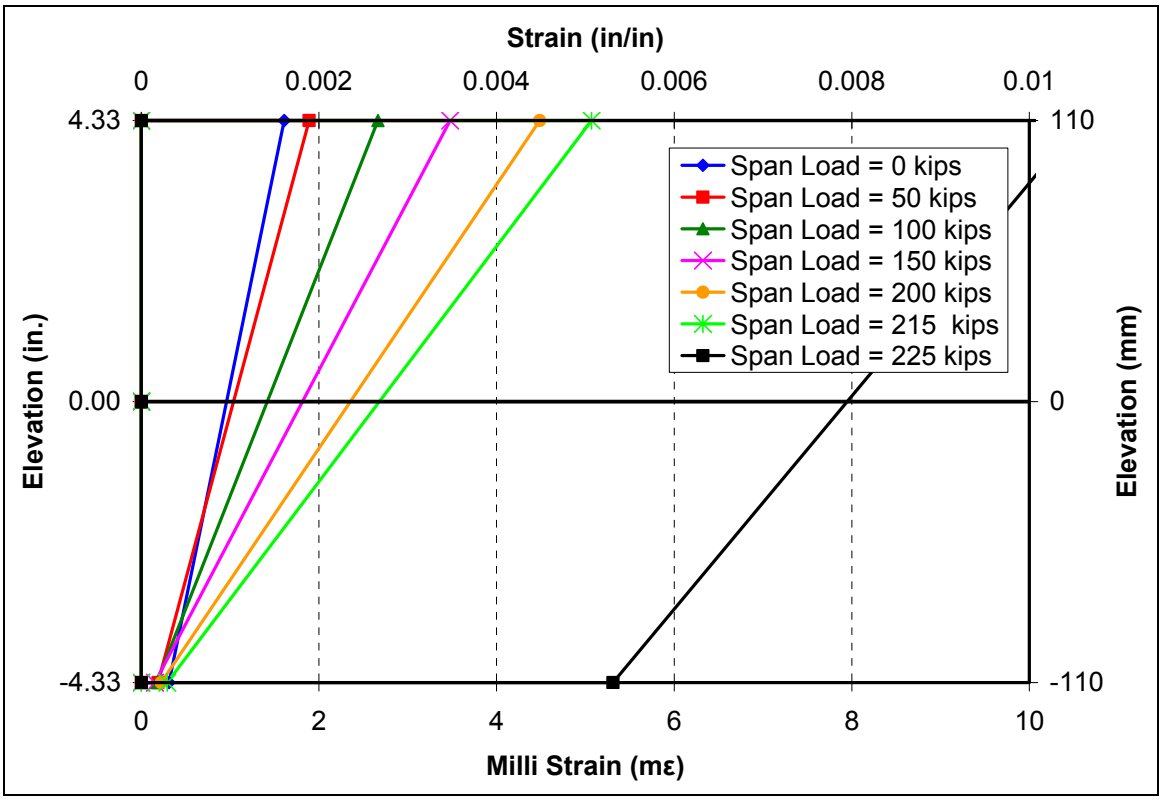

Figure 7-5: Strain Profiles from PI Gages T4 and B6 First Deck

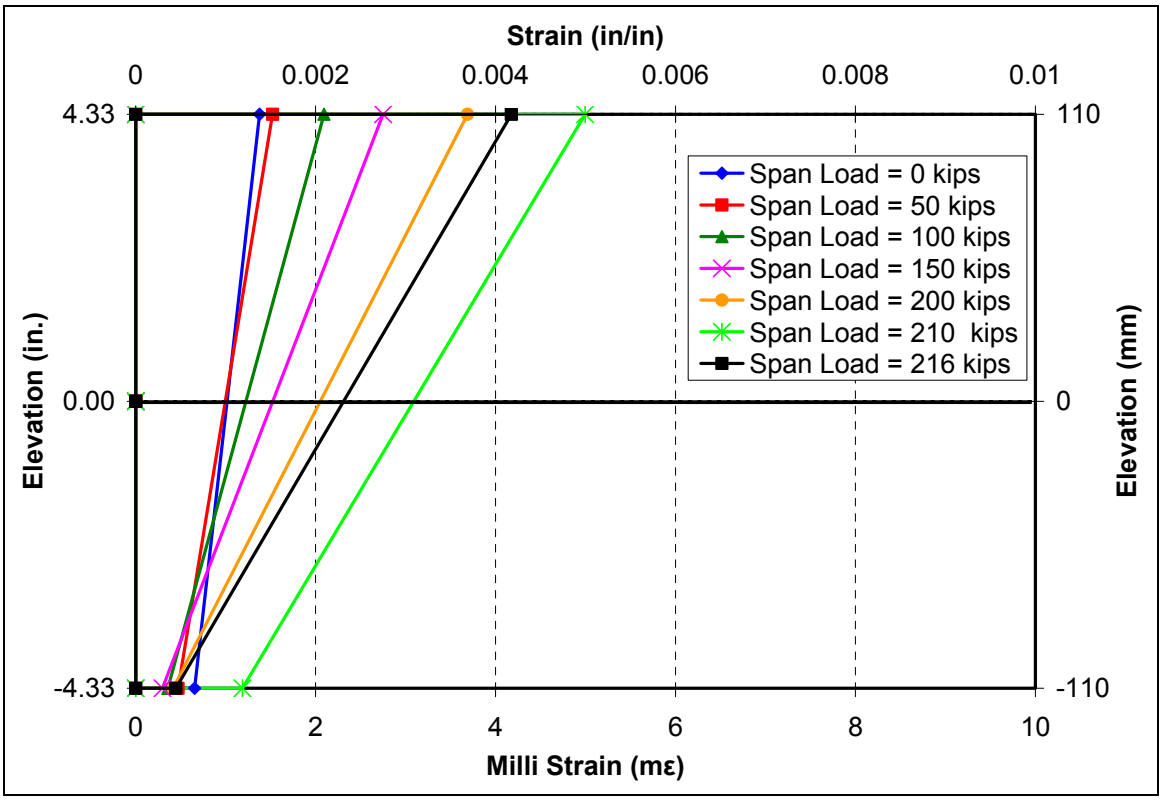

Figure 7-6: Strain Profiles from PI Gages T5 and B7 First Deck

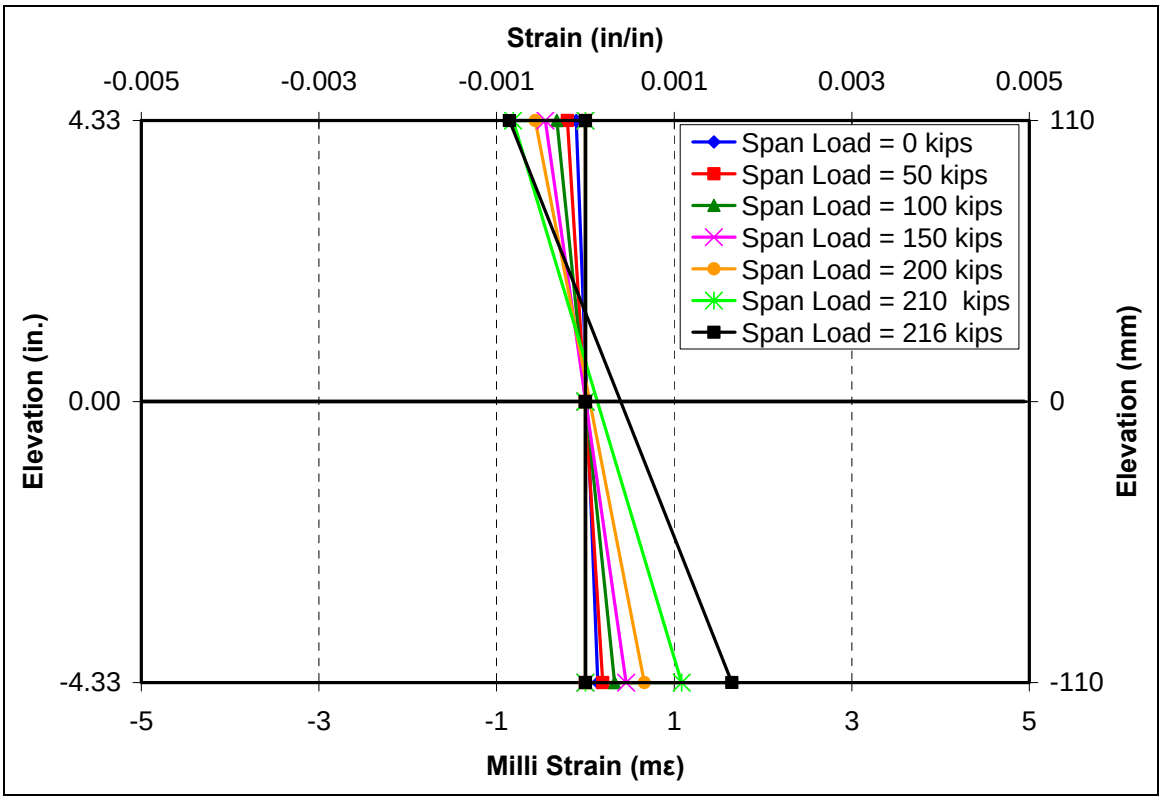

Figure 7-7: Strain Profiles from PI Gages T7 and B11 First Deck

Second Bridge Deck

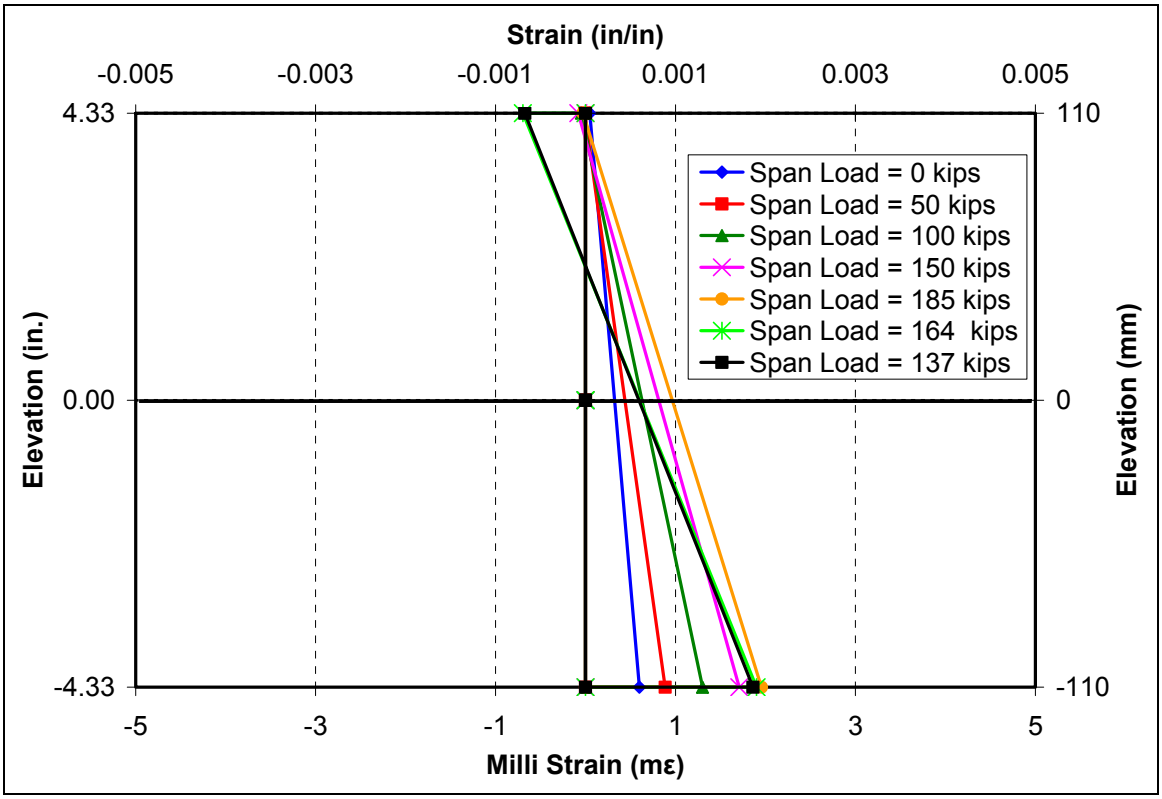

Figure 7-8: Strain Profiles from PI Gages T1 and B1 Second Deck

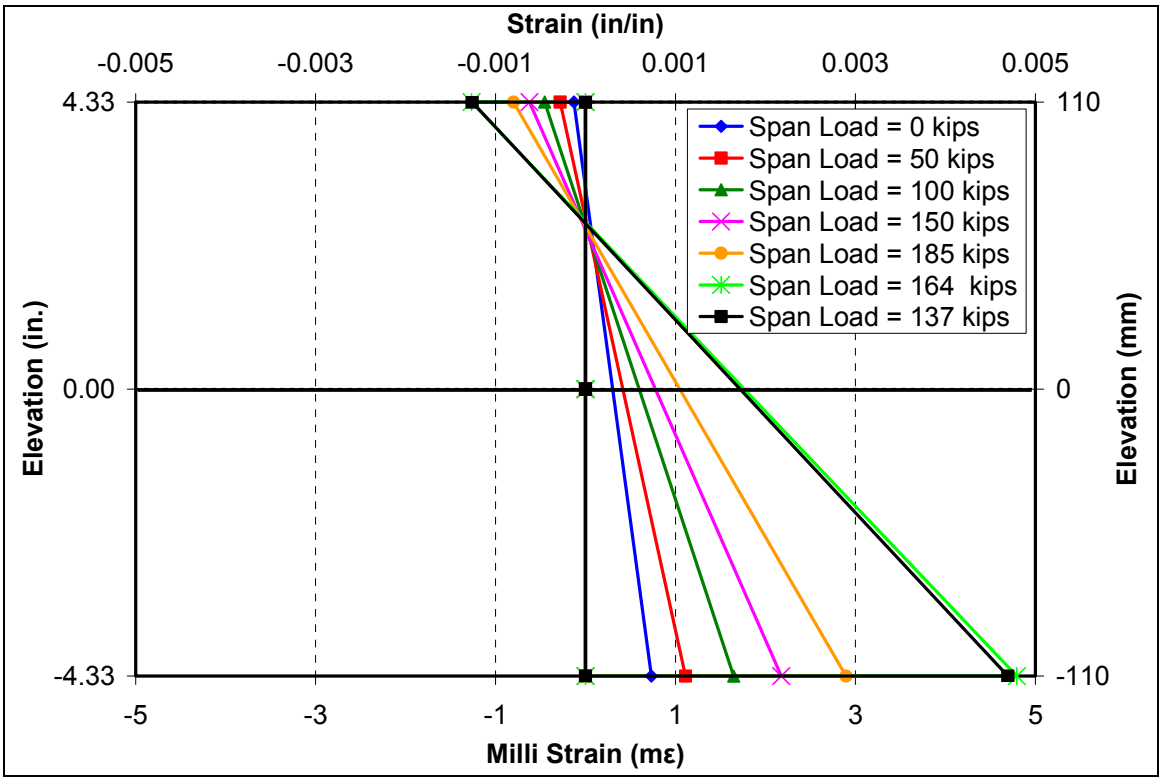

Figure 7-9: Strain Profiles from PI Gages T2 and B2 Second Deck

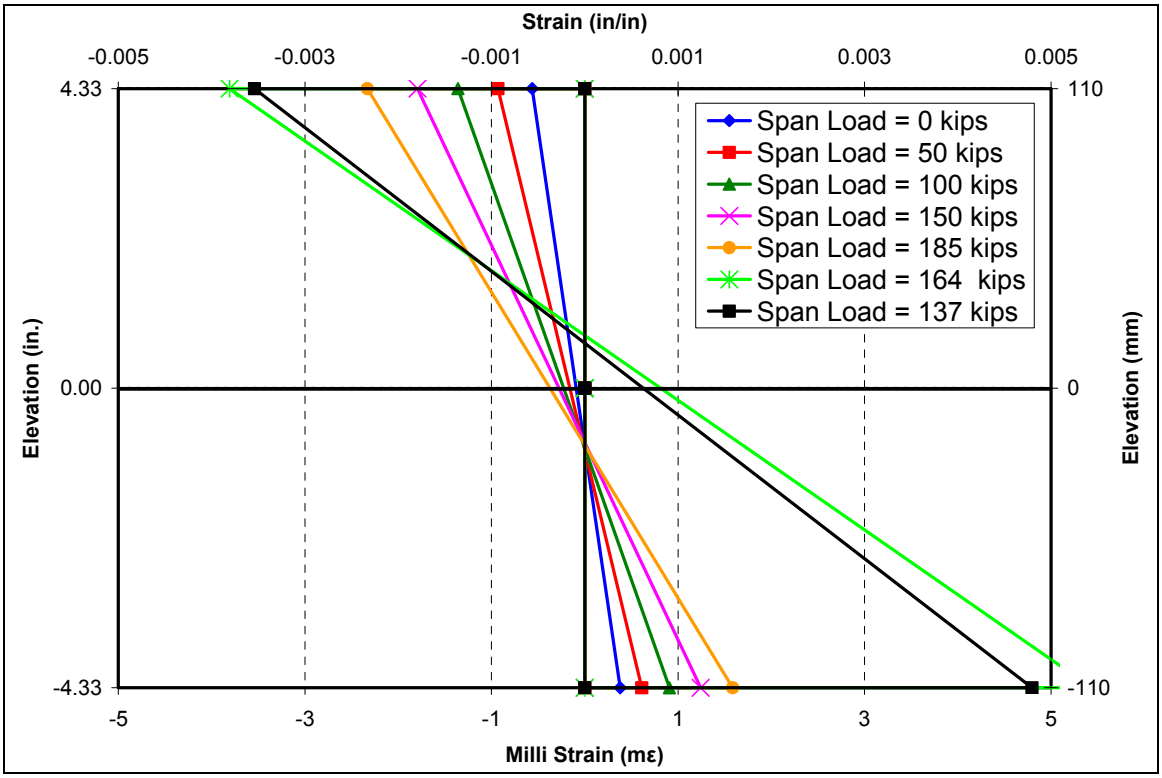

Figure 7-10: Strain Profiles from PI Gages T3 and B3 Second Deck

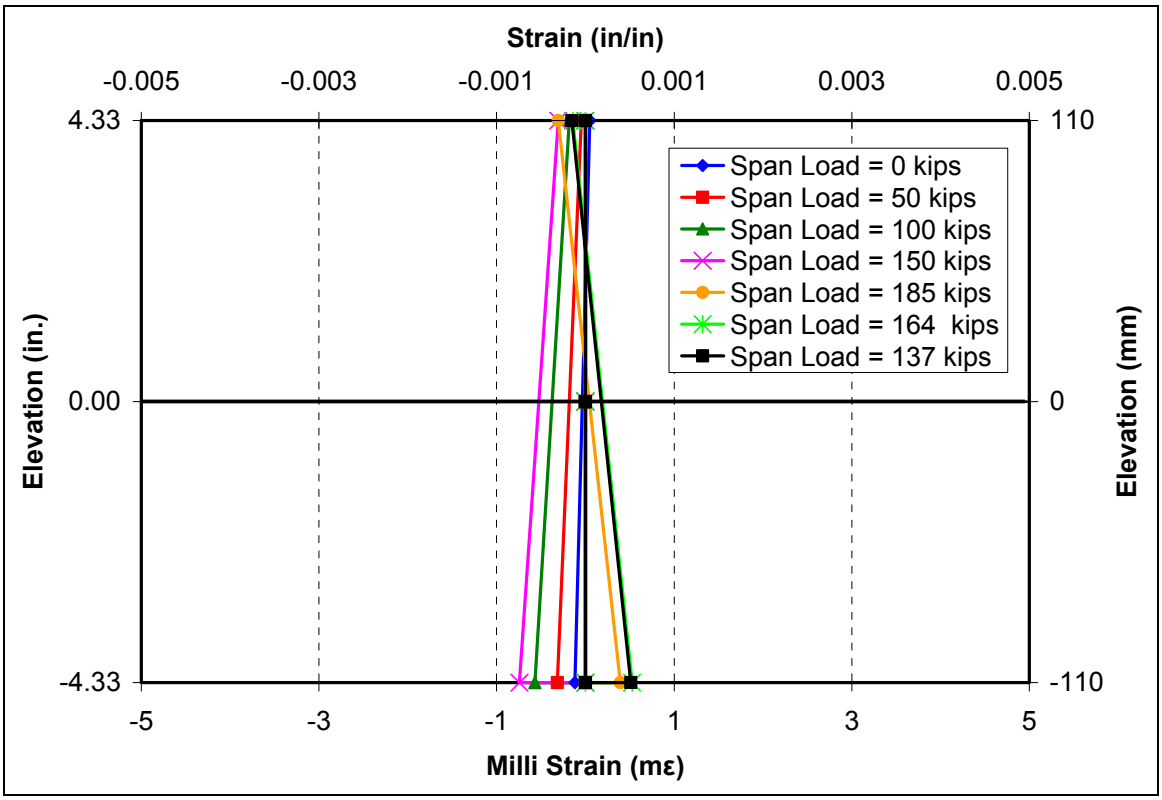

Figure 7-11: Strain Profiles from PI Gages T4 and B6 Second Deck

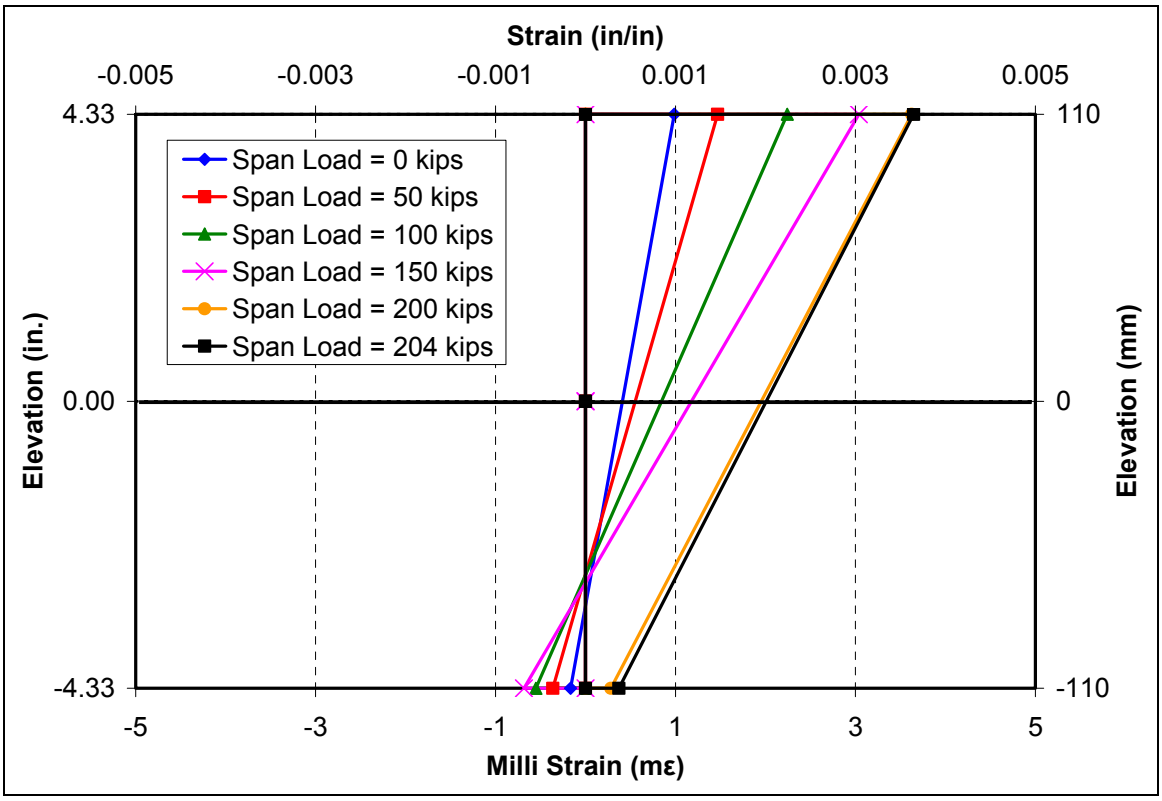

Figure 7-12: Strain Profiles from PI Gages T5 and B7 Second Deck

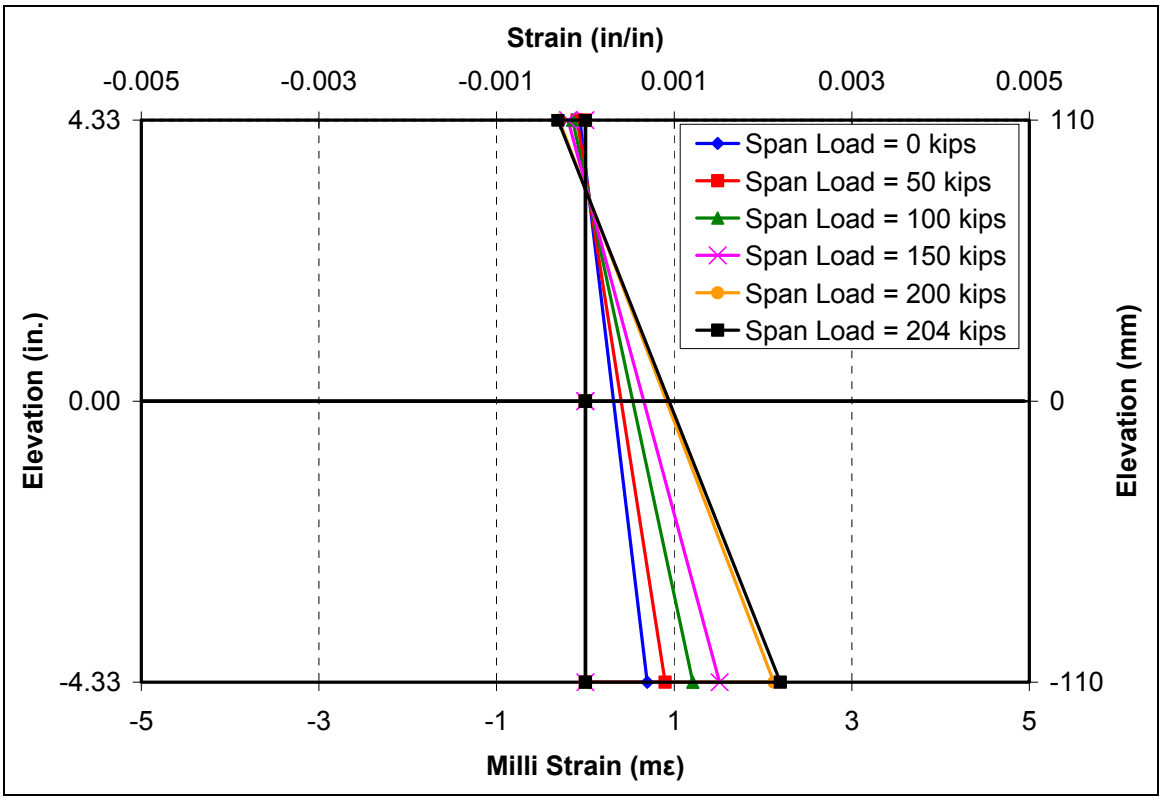

Figure 7-13: Strain Profiles from PI Gages T7 and B11 Second Deck

Third Bridge Deck

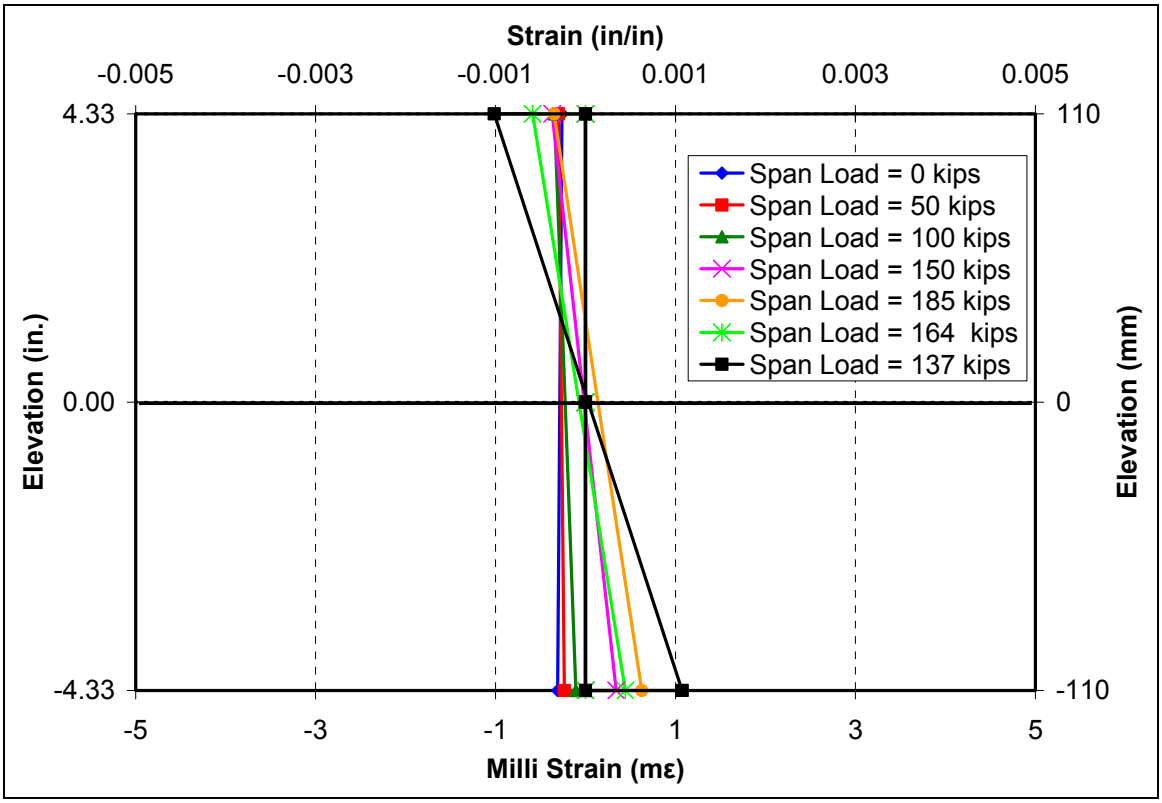

Figure 7-14: Strain Profiles from PI Gages T1 and B1 Third Deck

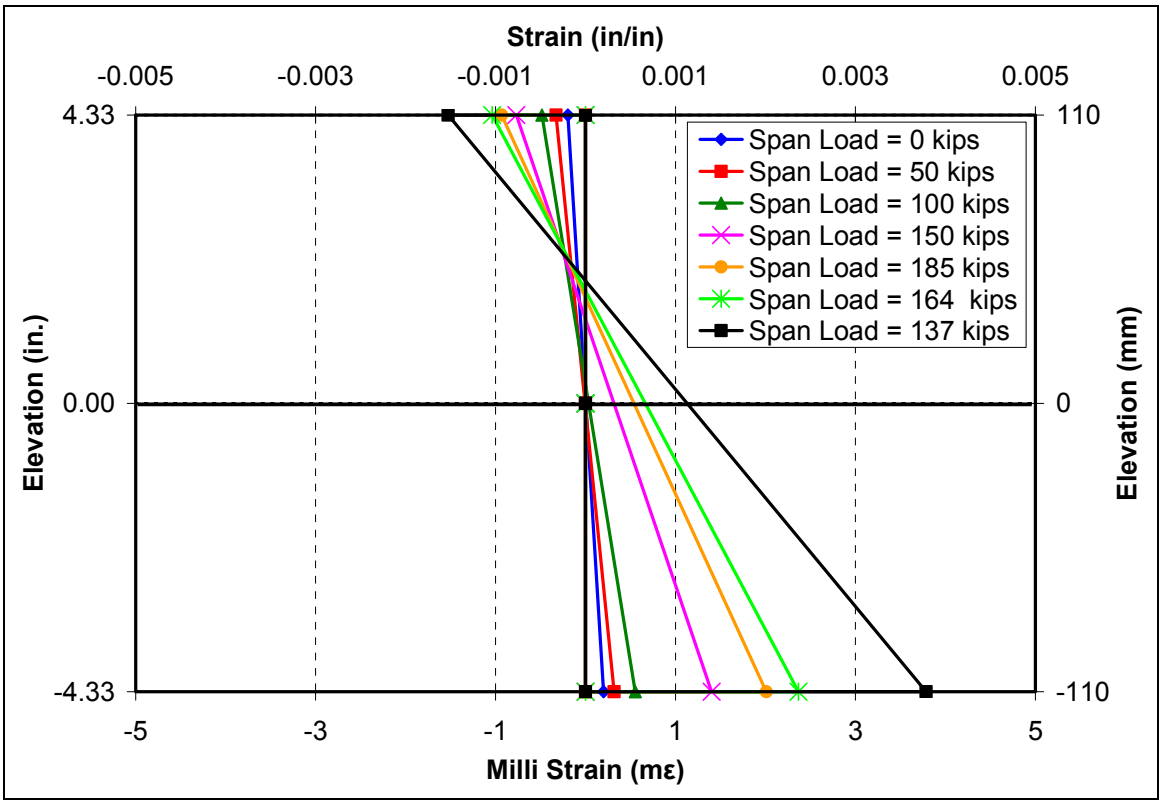

Figure 7-15: Strain Profiles from PI Gages T2 and B2 Third Deck

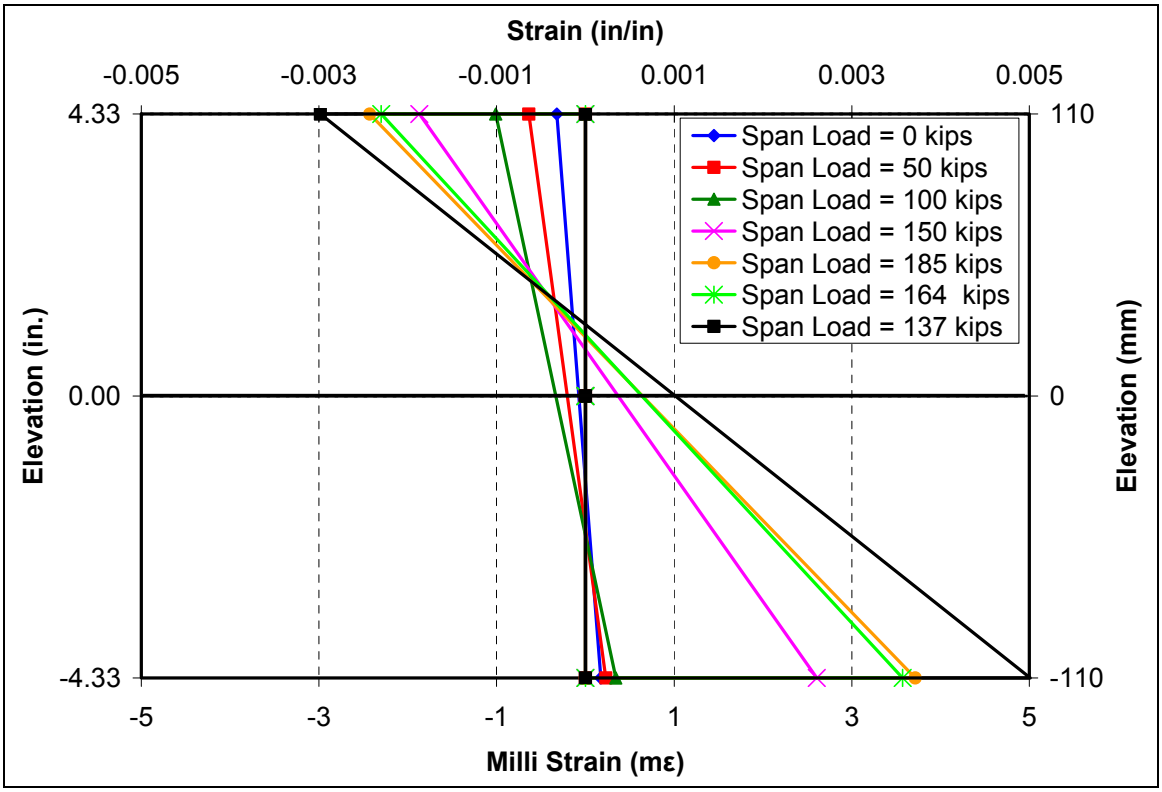

Figure 7-16: Strain Profiles from PI Gages T3 and B3 Third Deck

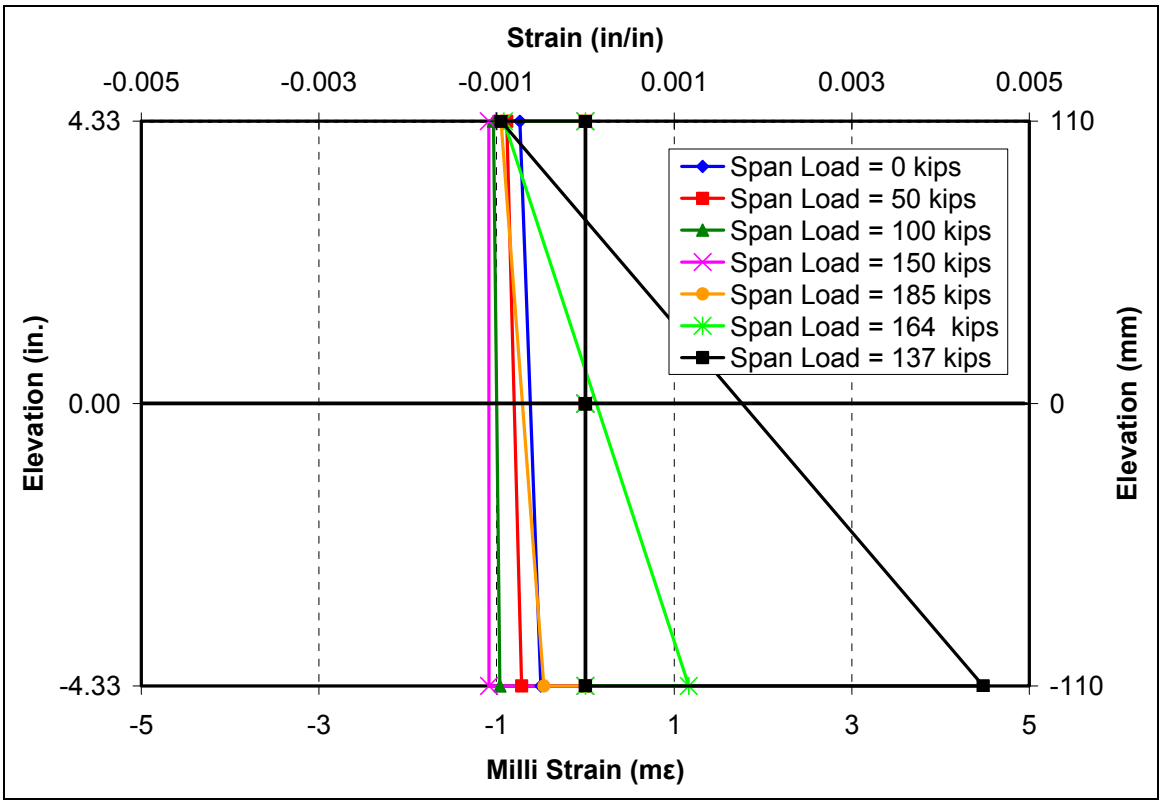

Figure 7-17: Strain Profiles from PI Gages T4 and B6 Third Deck

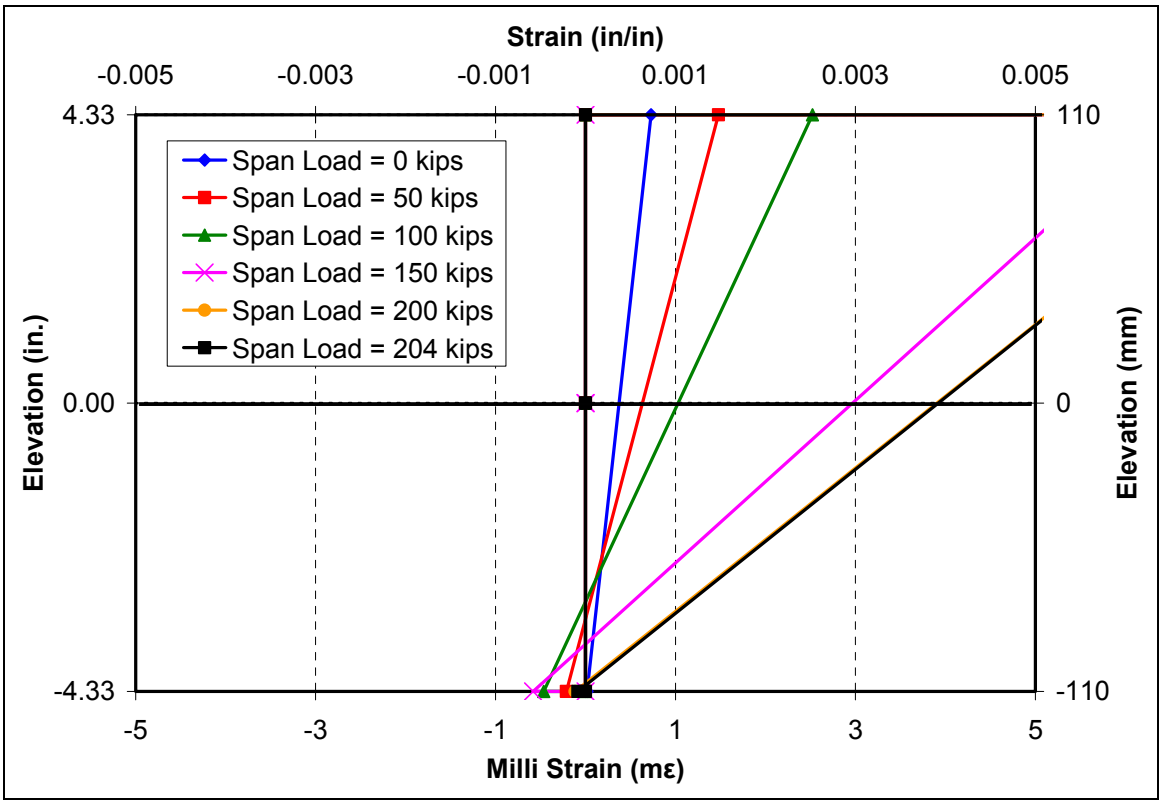

Figure 7-18: Strain Profiles from PI Gages T5 and B7 Third Deck

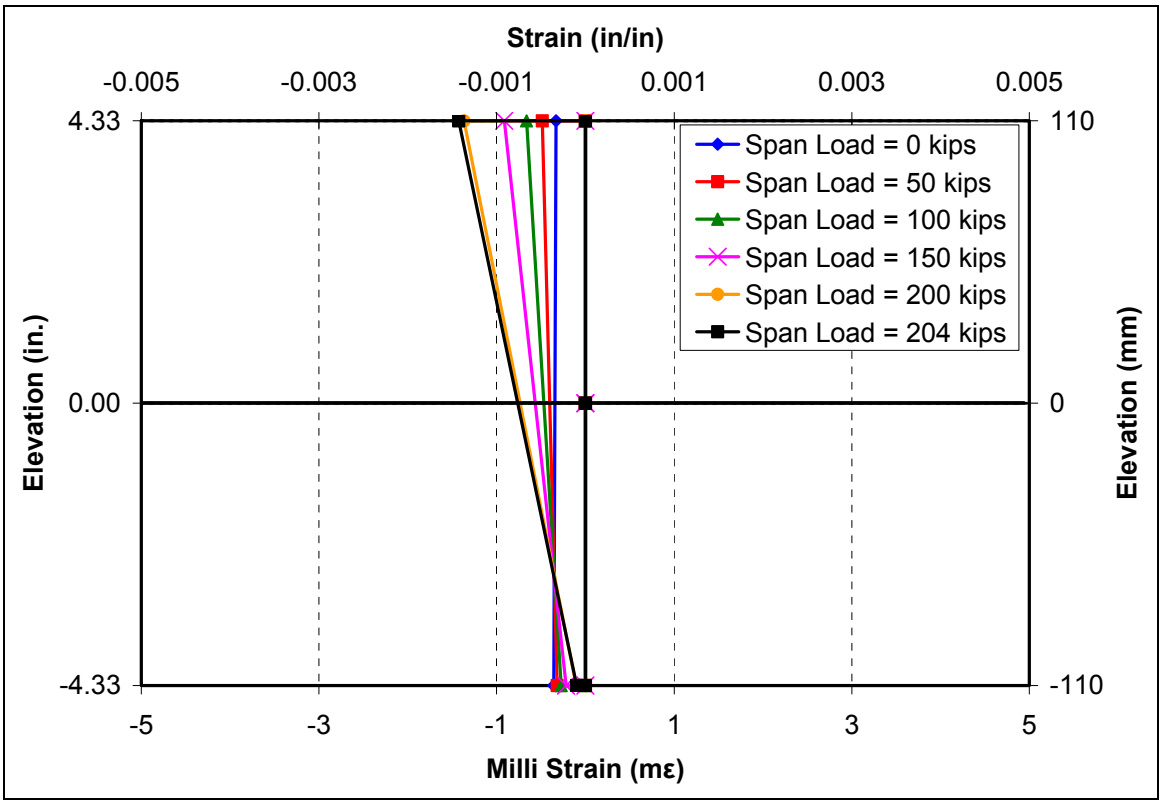

Figure 7-19: Strain Profiles from PI Gages T7 and B11 Third Deck

8. Appendix B: Strain Gage Data

Strain data is plotted by gage location in the following figures for each of the three bridge decks. See Section 3 for detailed information on exact gage locations.

Left Spans Lower Transverse

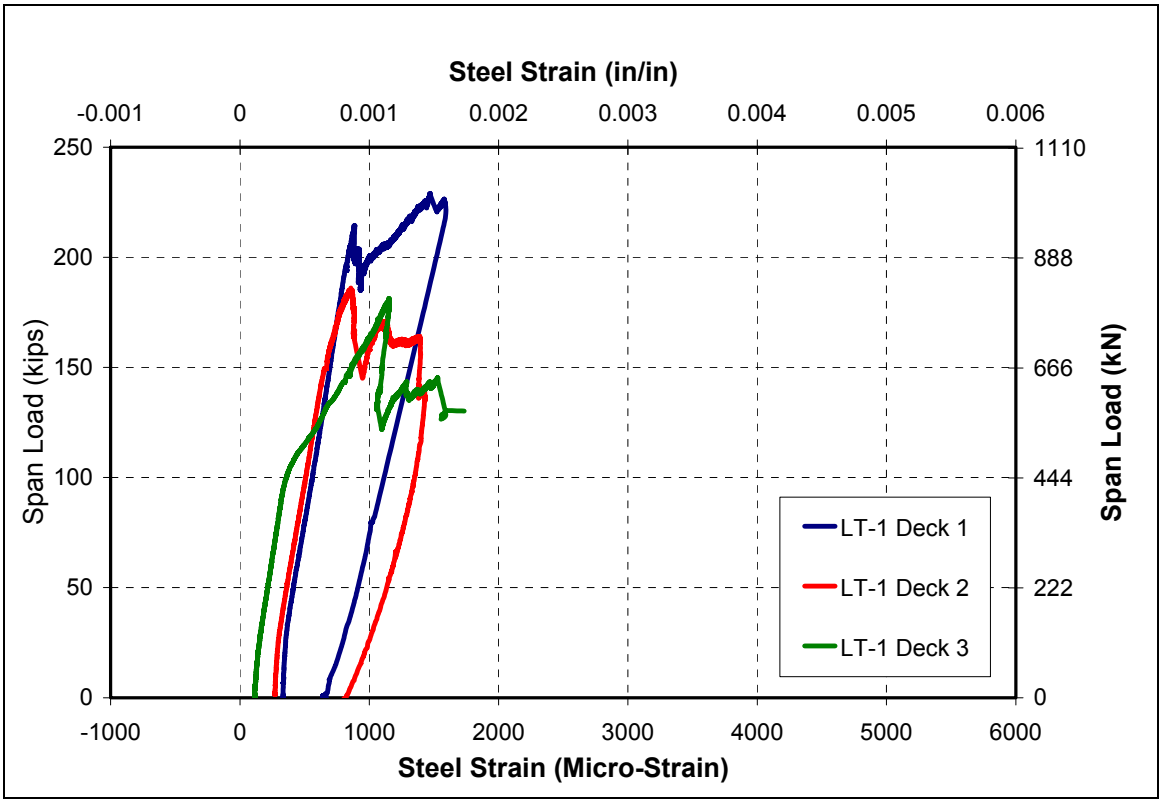

Figure 8-1: Strain Data from Gages at Location LT-1

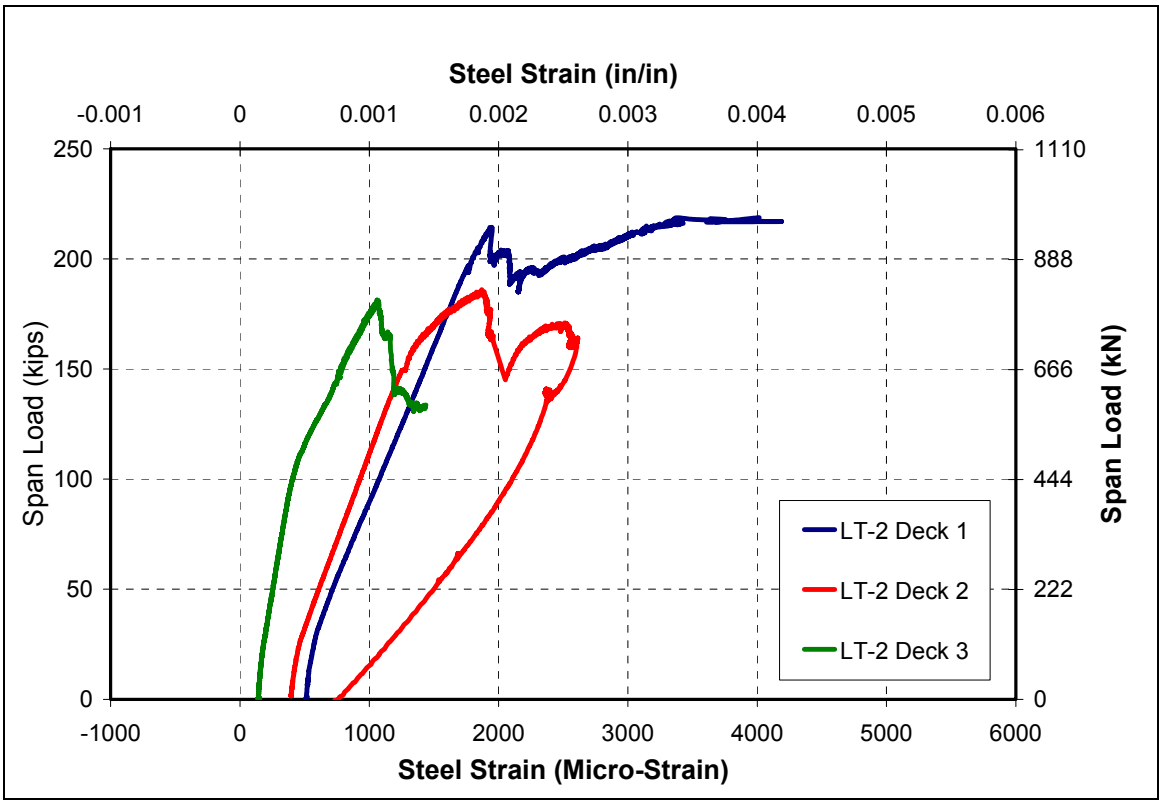

Figure 8-2: Strain Data from Gages at Location LT-2

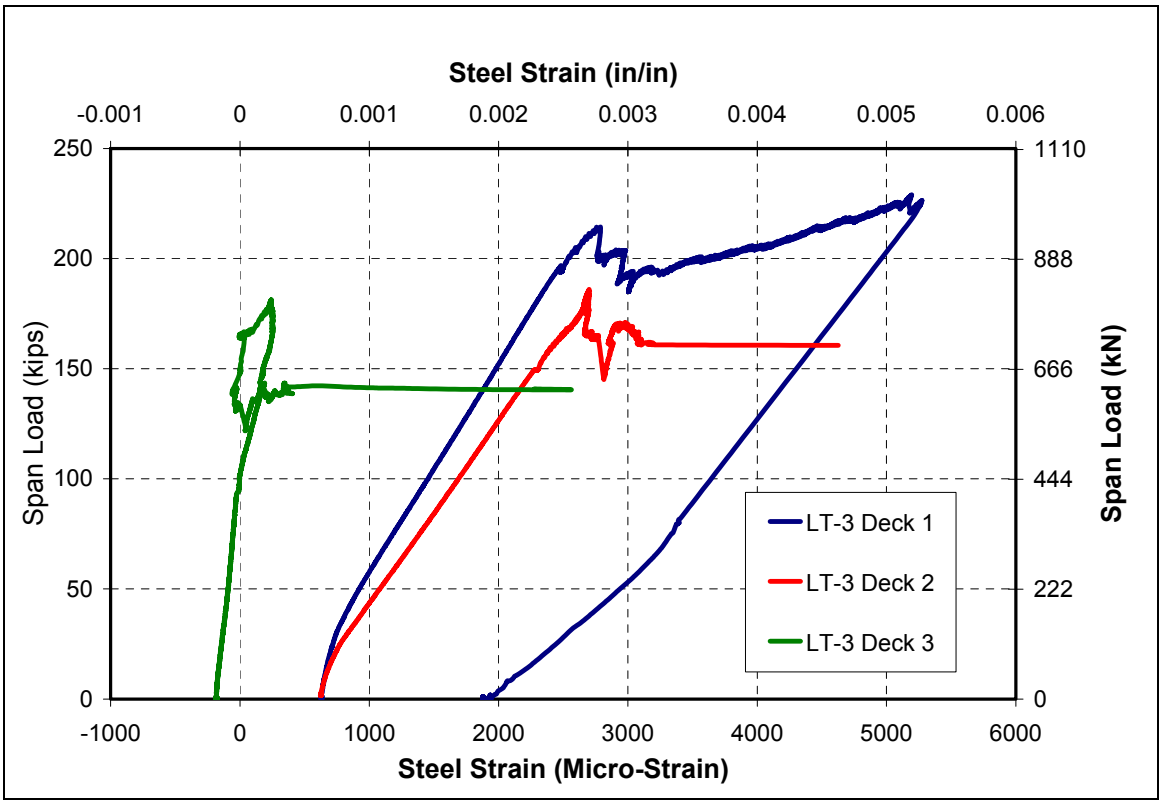

Figure 8-3: Strain Data from Gages at Location LT-3

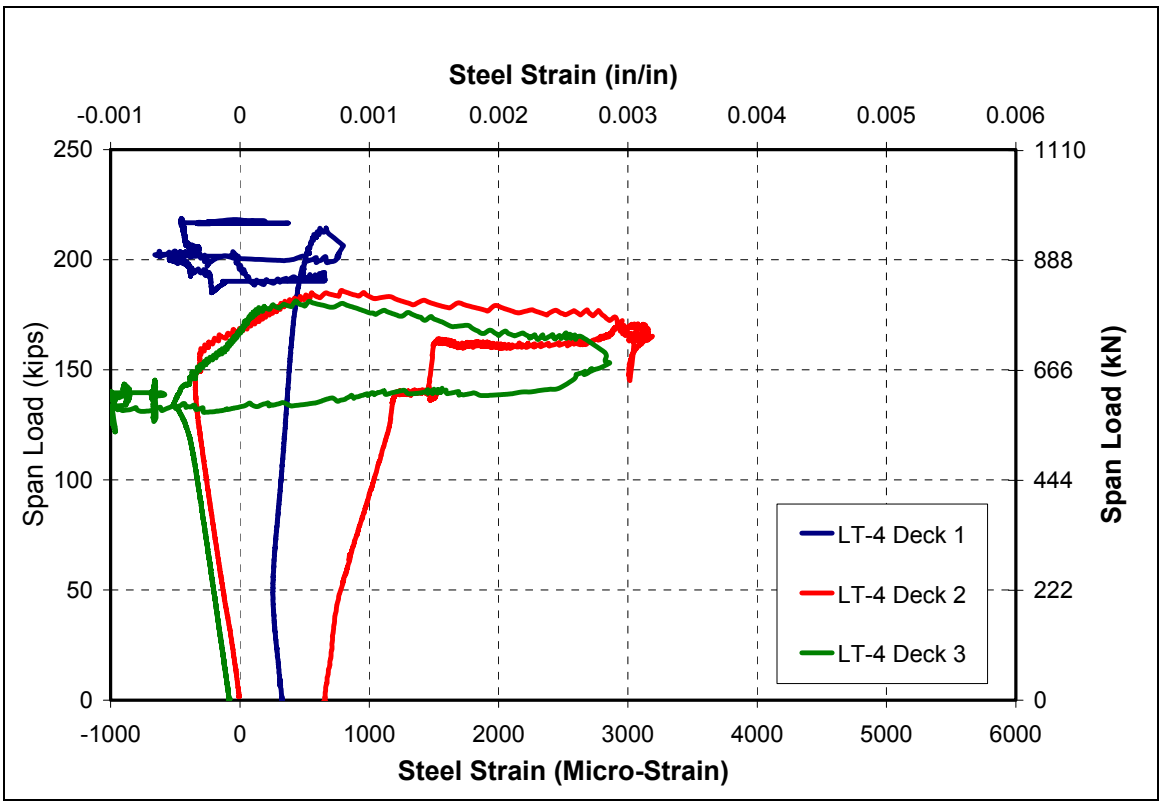

Figure 8-4: Strain Data from Gages at Location LT-4

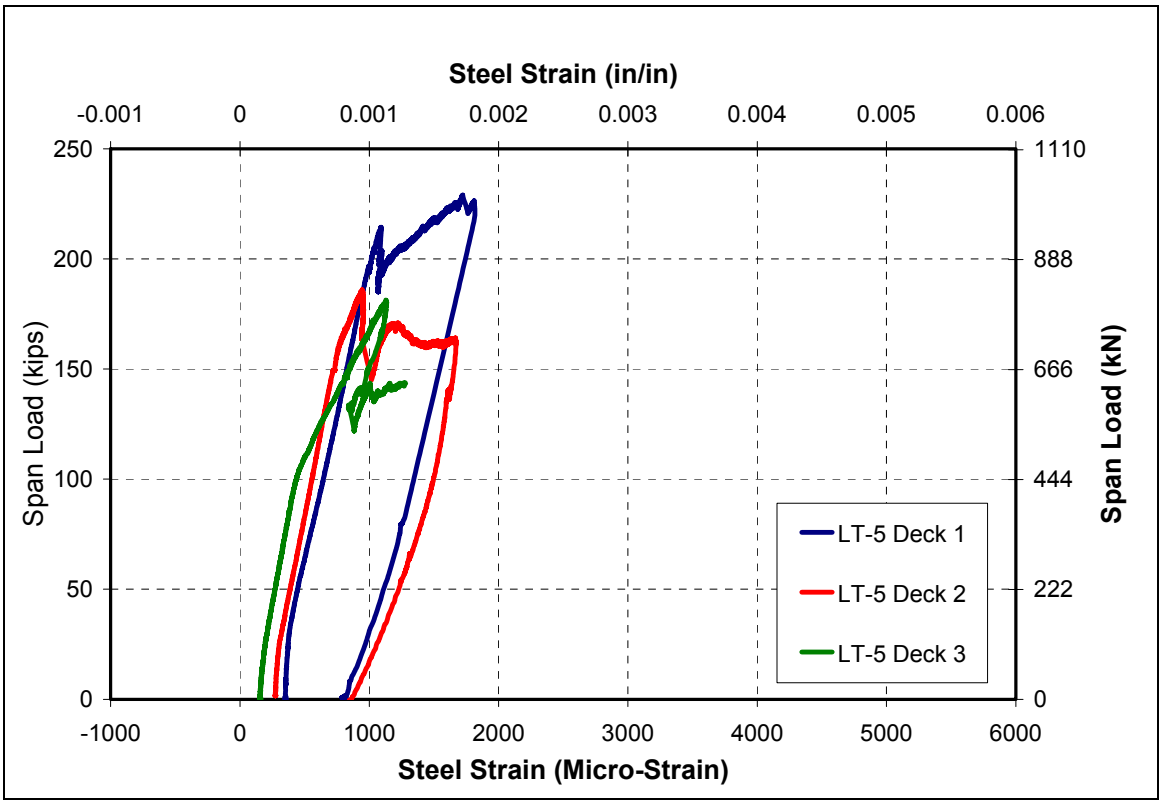

Figure 8-5: Strain Data from Gages at Location LT-5

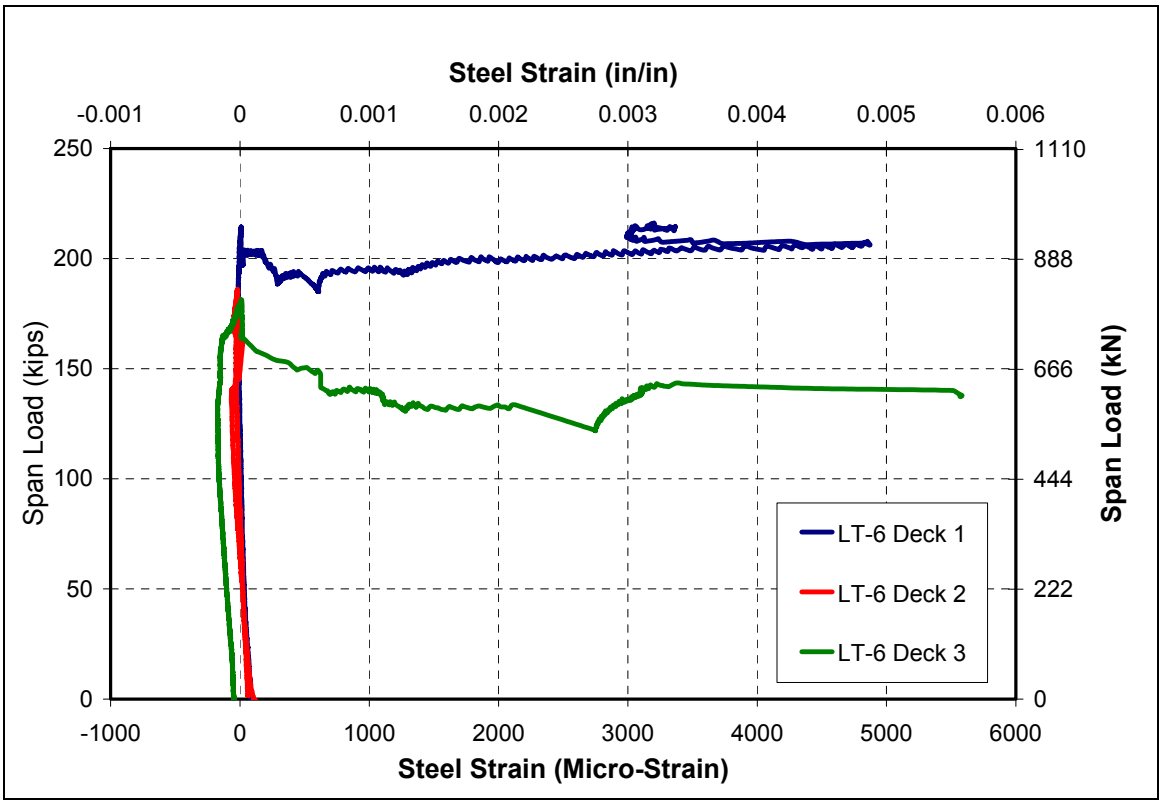

Figure 8-6: Strain Data from Gages at Location LT-6

Right Spans Lower Transverse

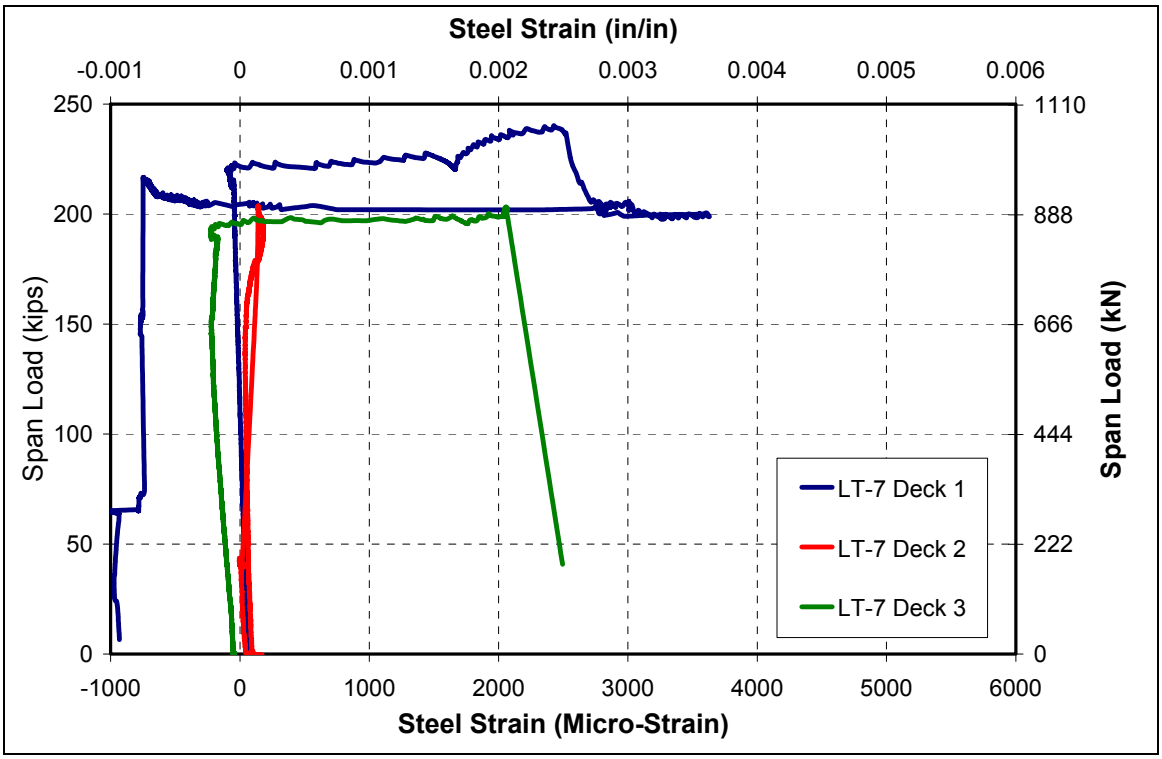

Figure 8-7: Strain Data from Gages at Location LT-7

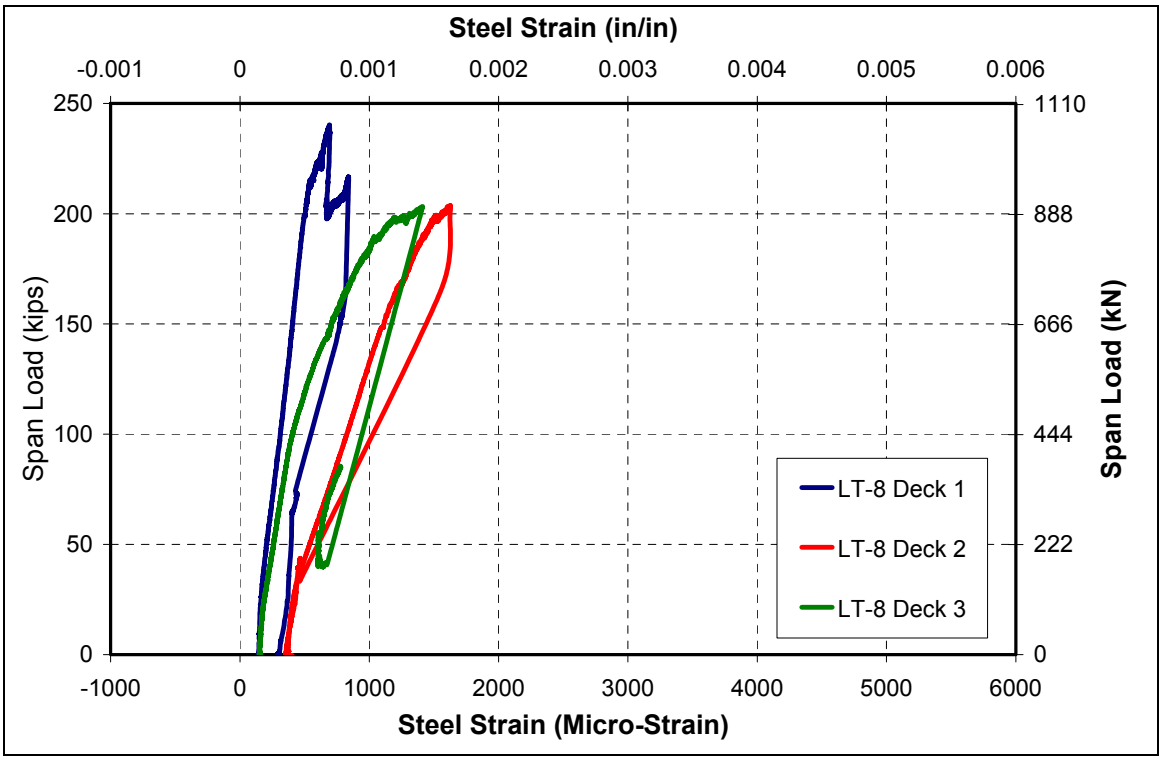

Figure 8-8: Strain Data from Gages at Location LT-8

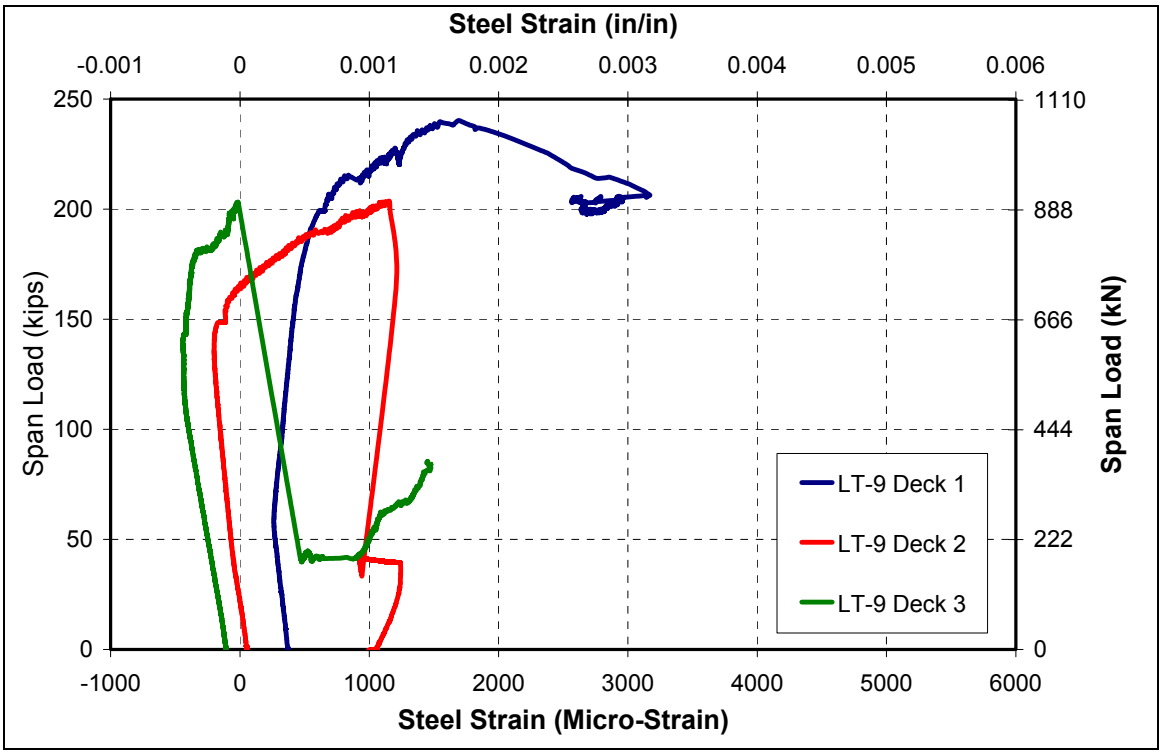

Figure 8-9: Strain Data from Gages at Location LT-9

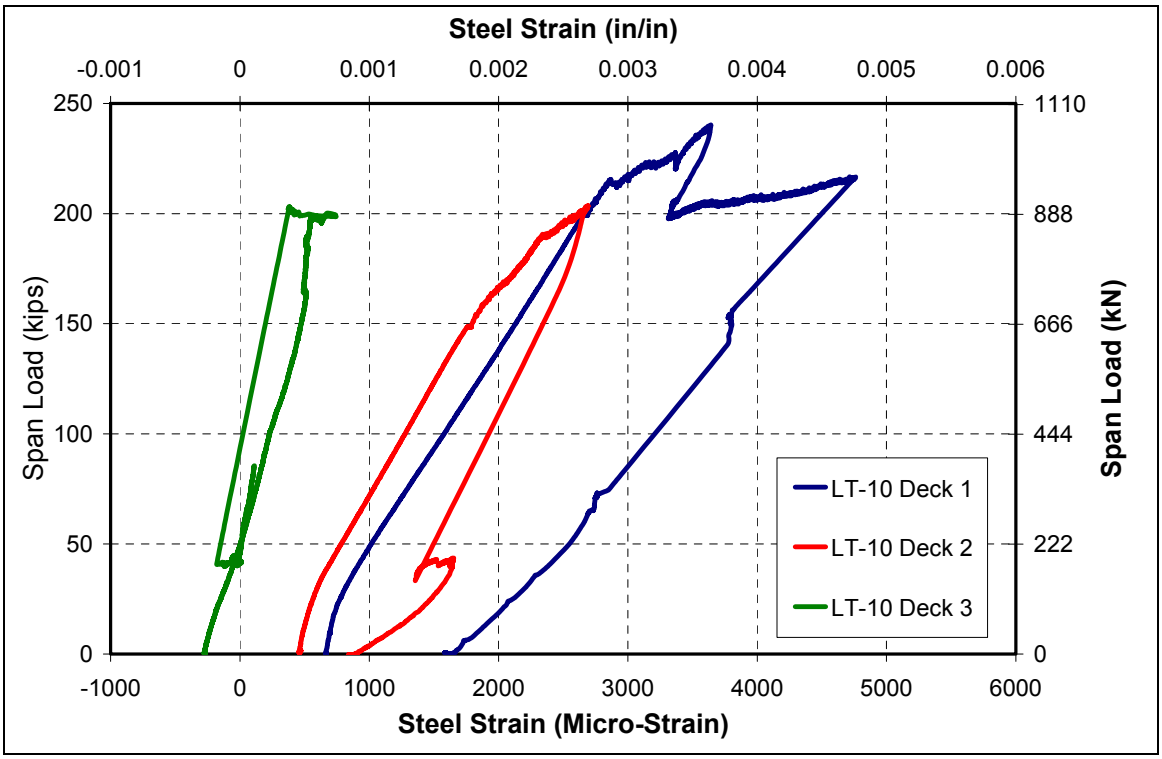

Figure 8-10: Strain Data from Gages at Location LT-10

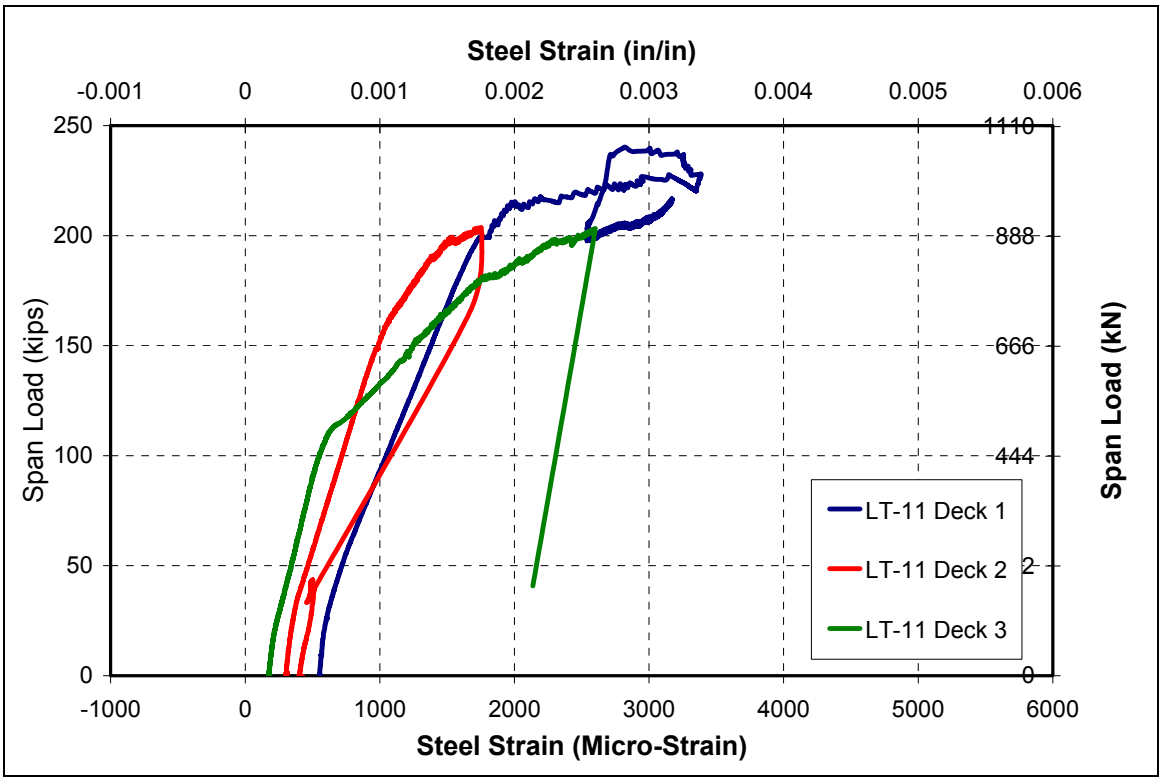

Figure 8-11: Strain Data from Gages at Location LT-11

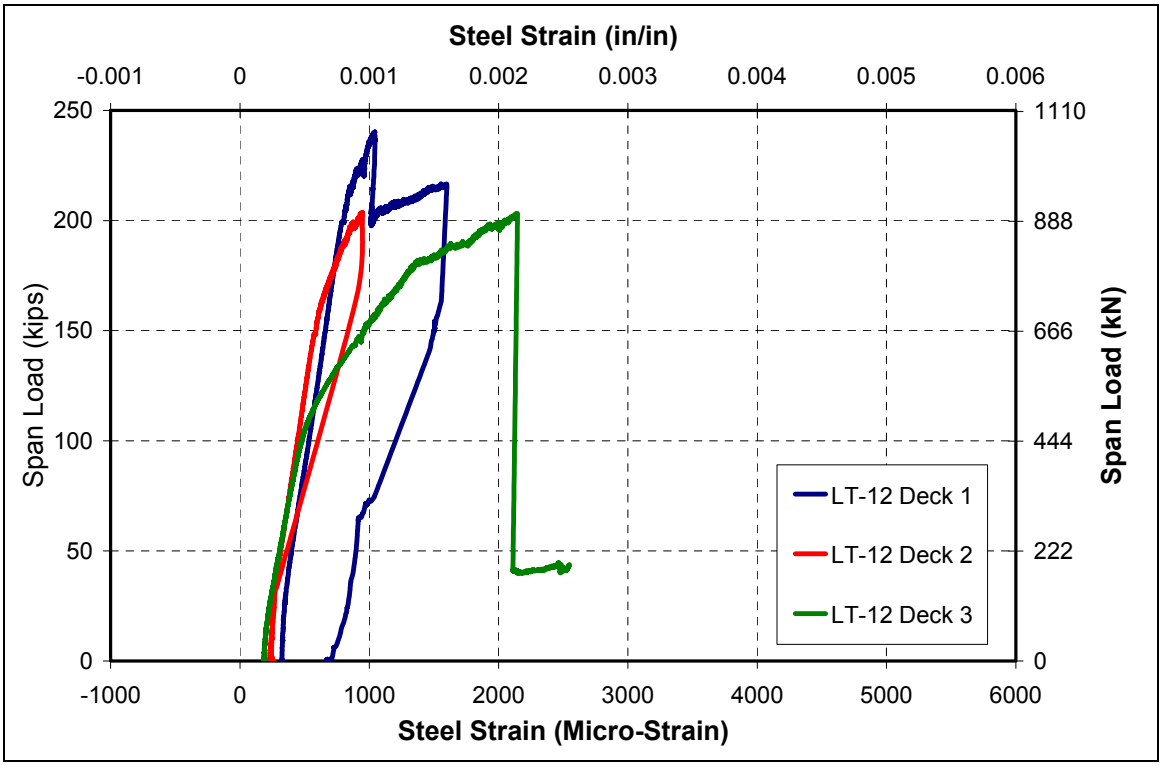

Figure 8-12: Strain Data from Gages at Location LT-12

Left Spans Upper Transverse

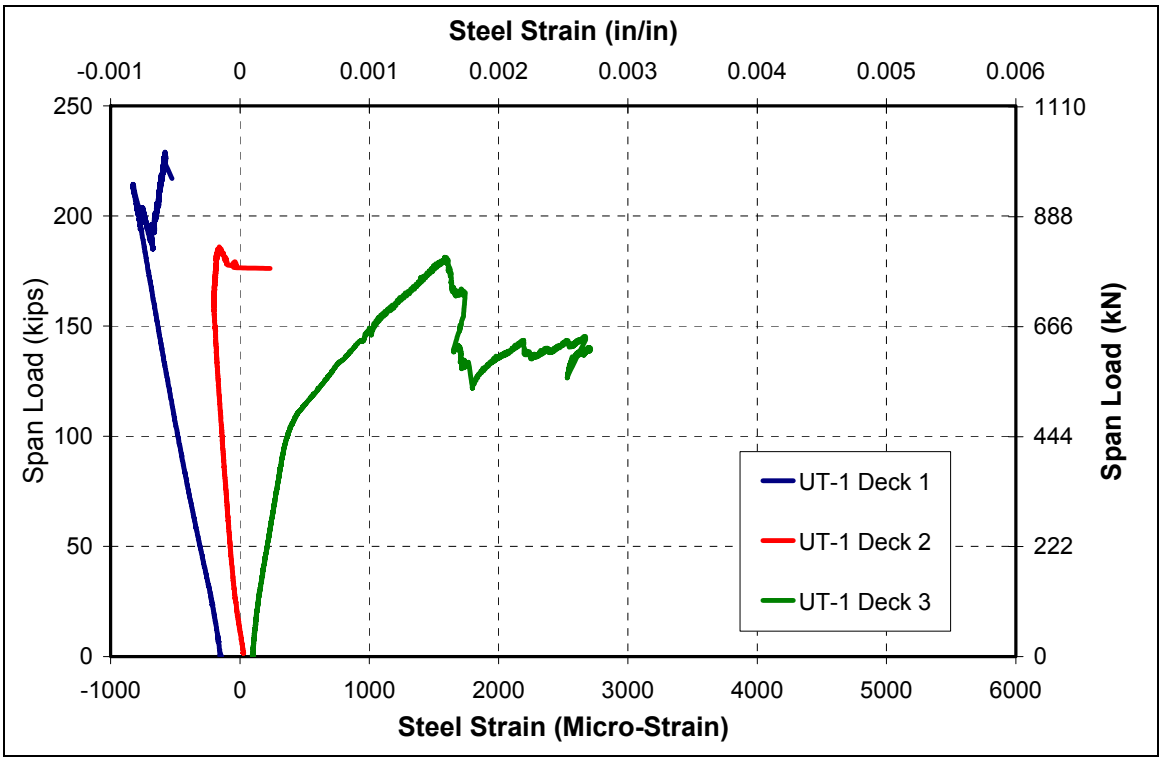

Figure 8-13: Strain Data from Gages at Location UT-1

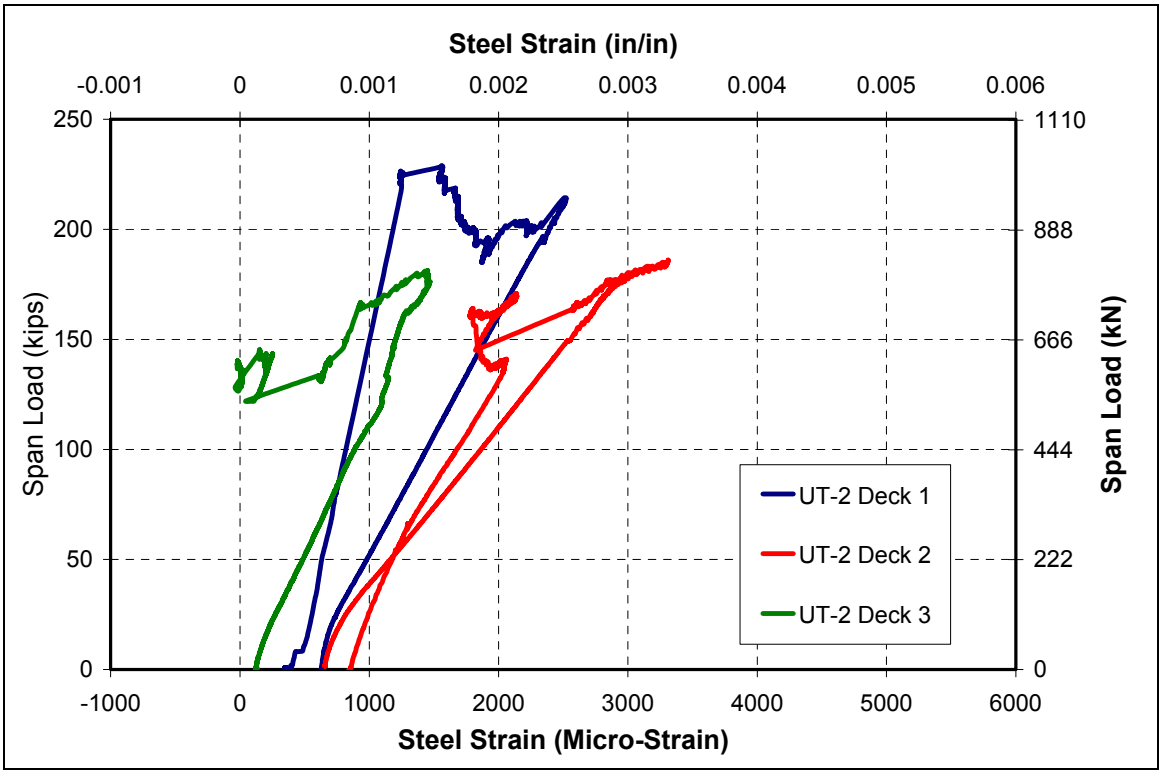

Figure 8-14: Strain Data from Gages at Location UT-2

Right Spans Upper Transverse

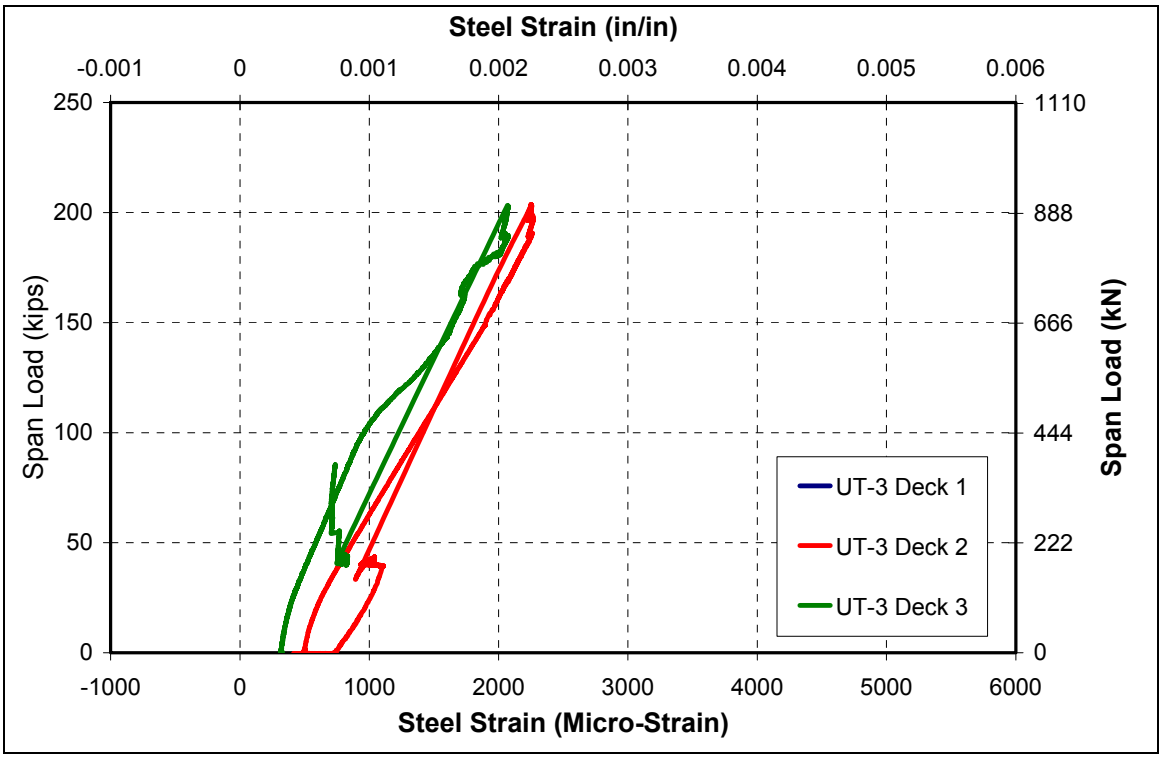

Figure 8-15: Strain Data from Gages at Location UT-3

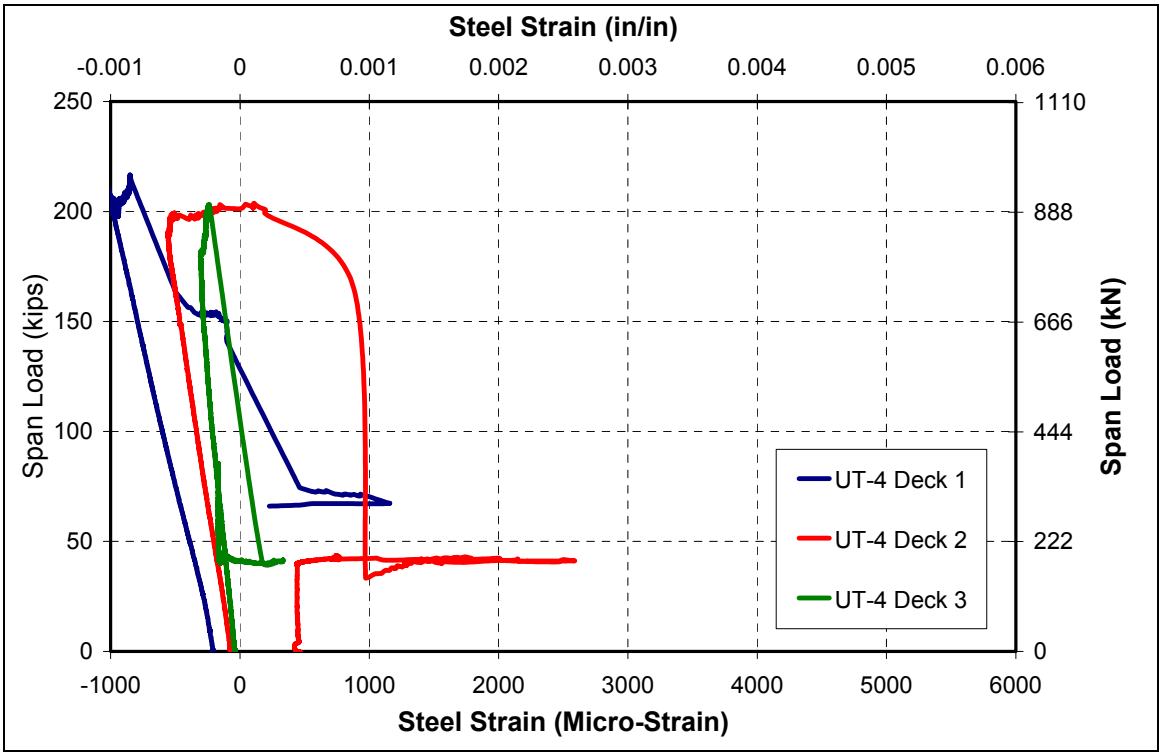

Figure 8-16: Strain Data from Gages at Location UT-4

Left Spans Lower Longitudinal

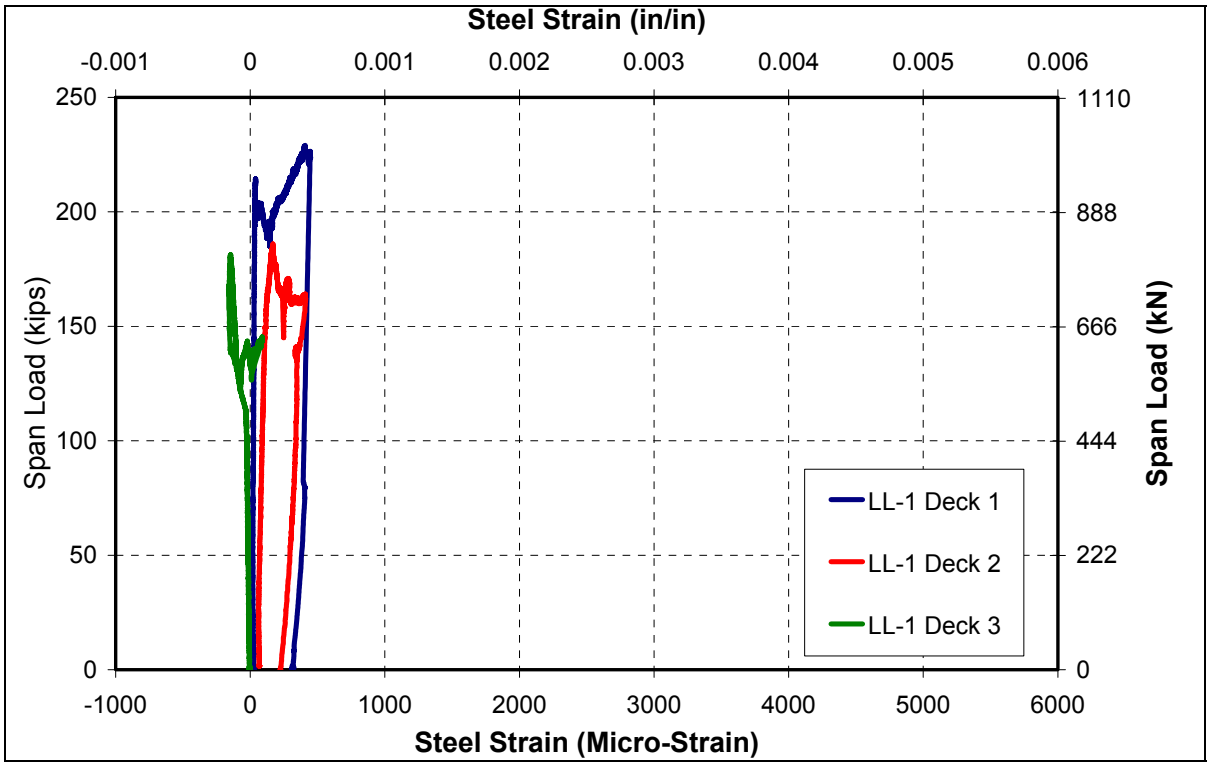

Figure 8-17: Strain Data from Gages at Location LL-1

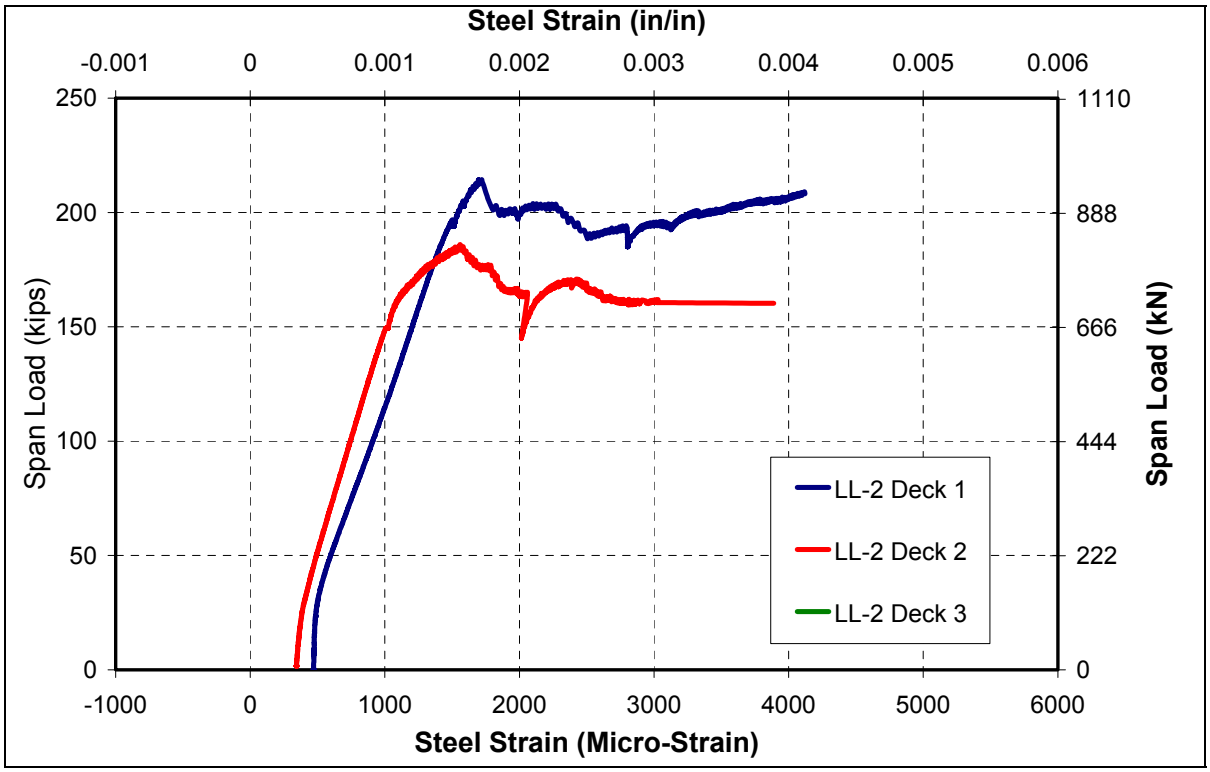

Figure 8-18: Strain Data from Gages at Location LL-2

Right Spans Lower Longitudinal

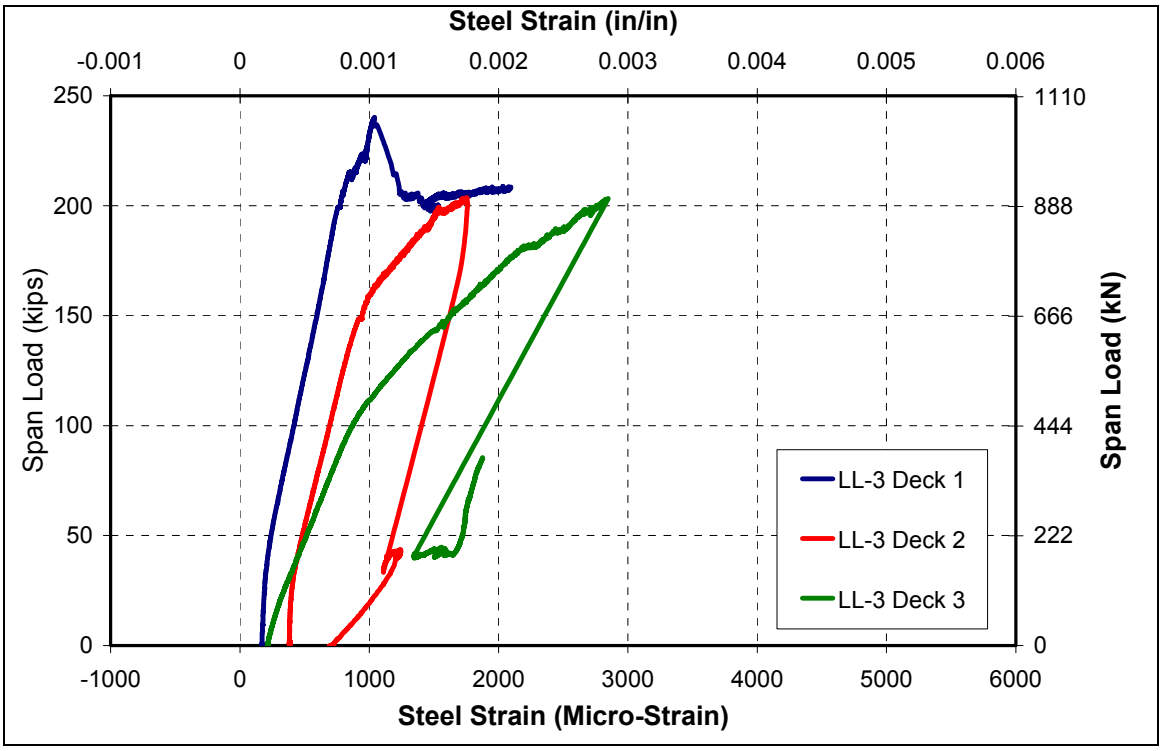

Figure 8-19: Strain Data from Gages at Location LL-3

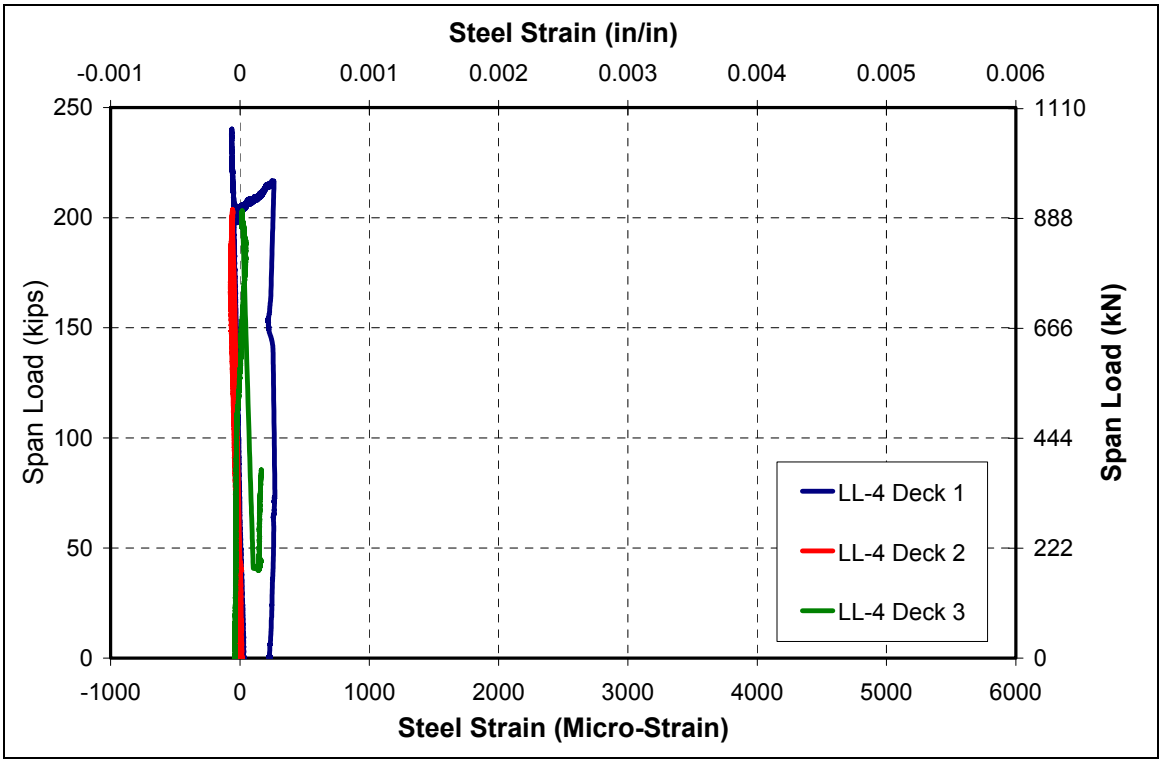

Figure 8-20: Strain Data from Gages at Location LL-4

9. Appendix C: Johnston County Bridge

Figure 9-1: East Abutment

Figure 9-2: Bridge Pier Forms

Figure 9-3: Double Bent Bridge Pier

Figure 9-4: Steel Girders After Erection

Figure 9-5: Transverse Cross-Bracing

Figure 9-6: Stay-in-Place Forms After Installation

Figure 9-7: MMFX Steel at the Site

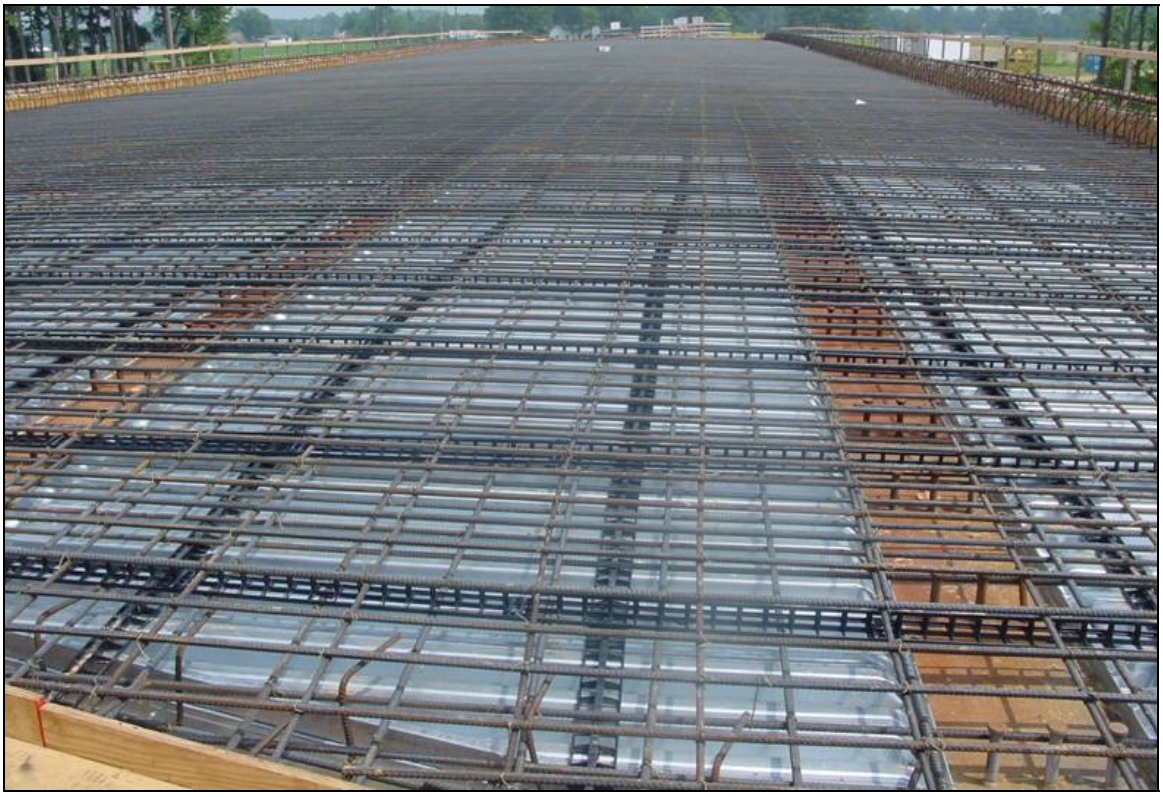

Figure 9-8: Bridge Deck Prior to Casting Concrete

Figure 9-9: NCDOT and NCSU Teams at the Bridge Site

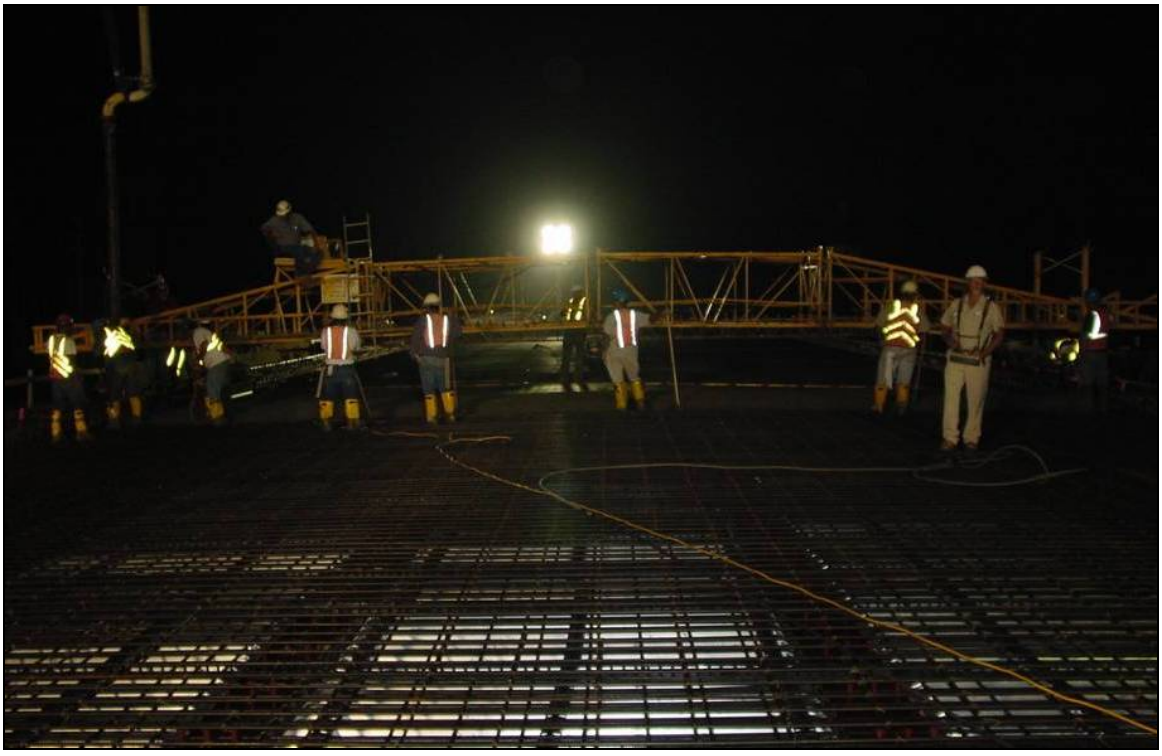

Figure 9-10: Placing the Concrete Deck Early in the Morning

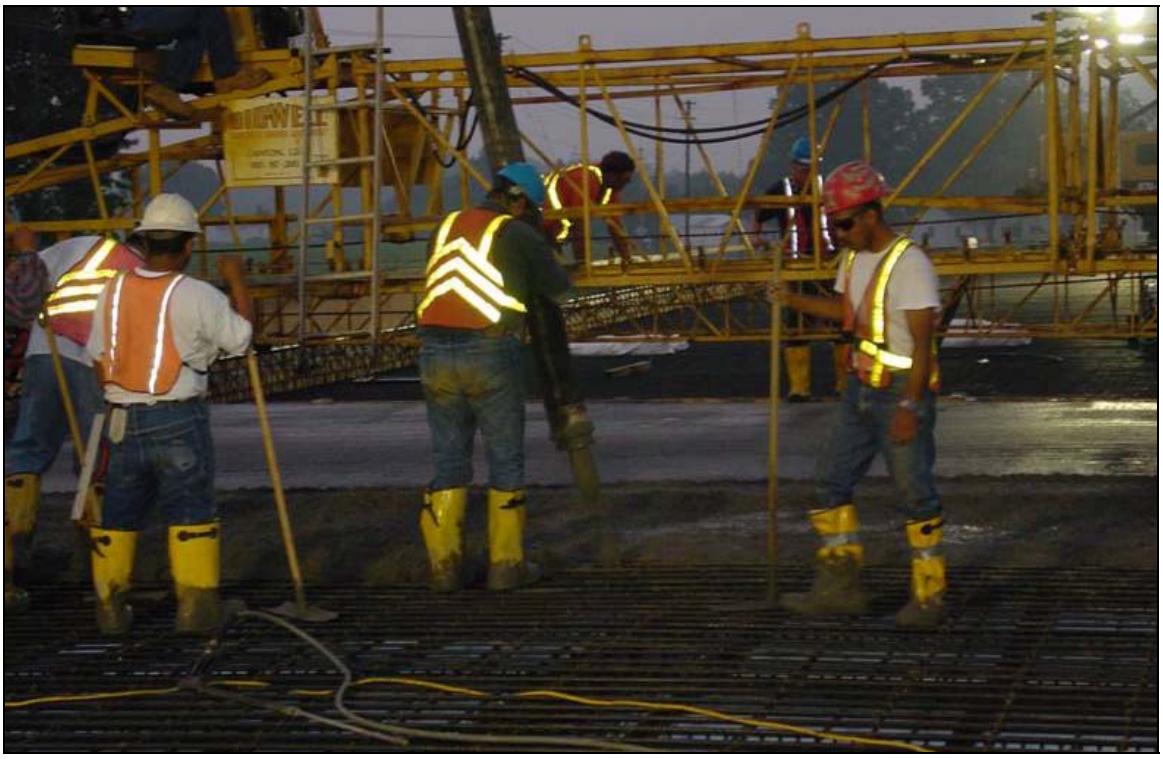

Figure 9-11: Near the End of Concrete Placement

Figure 9-12: Completed Johnston County Bridge